Cool Roofs in Smart Cities

Implications for Urban Heat Island Mitigation and Building Energy Efficiency in Different Climate Zones

Master Thesis in Renewable Energy

Global Energy and Climate Development

Author: Anja Lindgaard Molnes

Supervisor: Asgeir Sorteberg

University of Bergen

Geophysical Institute

June 2018

ABSTRACT

As climate change contributes to elevate urban temperatures, undesirable consequences like increased energy consumption, reduced air and water quality and elevated levels of thermal stress for the population continue to threaten the urban environment. It is paramount to address issues related to urban sustainability, environmental performance and energy demand as climate change intensifies and the urban population rapidly continues to grow. Smart city strategies to promote urban sustainability and efficiency are emerging, and mitigation of the urban heat island (UHI) effect through implementation of cool roofs can contribute to reduce these adverse effects by lowering urban temperatures and reducing the cooling loads of buildings and the associated GHG emissions. Through the use of a 1-D bulk urban canopy model combined with an atmospheric layer model, this thesis aims to build a framework for assessing the cool roof mitigation potential on the UHI effect and the associated response in cooling energy demand for the cities of Cairo, Chicago, Delhi, Rome and Singapore. The resulting change in cooling energy demand for space cooling were calculated using degree-days. The results displayed a general reduction in temperature after cool roofs were implemented for all cities, indicating a significant UHI mitigation potential. The magnitude of the UHI effect was reduced by 23-31% after the large-scale introduction of cool roofs, while the temperature-dependent energy demand during the summer period was also reduced, ranging from 10-33% between the different cities.

ACKNOWLEDGEMENTS

LIST OF CONTENTS

LIST OF FIGURES

LIST OF TABLES

LIST OF EQUATIONS

x

ABBREVIATIONS

ABBREVIATION	MEANING
AHE	Anthropogenic heat emissions
AUHI	Atmospheric urban heat island
BLUHI	Boundary layer urban heat island
BPT	Balance point temperature
BTU	British thermal units
BUCM	Bulk urban canopy model
CDD	Cooling degree-days
CDR	Carbon dioxide removal
CLUHI	Canopy layer urban heat island
COP	Coefficient of performance
CRP	Cool roof paint
DBT	Dry bulb temperature
GHG	Greenhouse gas
IR	Infrared radiation
JJA	June, July, August
LCZ	Local climate zone
LW	Longwave (radiation)
OLR	Outgoing longwave radiation
RT15	Relaxation time of 15 minutes
RT45	Relaxation time of 45 minutes
SDG	Sustainable development goal
SRI	Solar reflectance index
SRM	Solar radiation management
SUHI	Surface urban heat island
SURY	Semi-empirical urban canopy parametrization
SVF	Sky view factor
SW	Shortwave (radiation)
TLC	Temperature-load curve
UHI	Urban heat island
UN	United Nations
UTC	Coordinated universal time

1. Introduction

The sustainable development goal (SDG) number seven set by the United Nations (UN) states that we need to "ensure access to affordable, reliable and sustainable and modern energy for all". According to the UN, more than 1.3 billion people live without access to electricity, and the expected global population increase will put a heavy strain on the future energy demand. At the same time, we need to reduce greenhouse gas emissions in order to address the pressing environmental issues of climate change.

Climate change and the environmental impacts of fossil fuels impose challenges on both the natural environment and cities. Improvement of environmental performance and energy efficiency will be crucial for the future development of urban sustainability. Although cities occupy only 2% of the Earth's surface, they are responsible for approximately 80% of global greenhouse gas emissions (Morvaj et al., 2011). Every aspect of urban life will be affected by climate change, and these issues will become increasingly concentrated in urban areas. Consequently, addressing urban sustainability issues and high urbanization rates have become increasingly important in order to prepare cities for the challenges ahead. A growing number of smart city solutions have emerged across the globe over the past years in order to achieve sustainability targets. As stated by Townsend (2014), "smart cities are fixes for the dumb designs of the last century to prepare them for the challenges of the next, a new industrial revolution to deal with the unintended consequences of the first one".

Urban development and changes in the radiative and thermal properties cause cities to experience elevated temperatures compared to the surrounding rural areas. This is known as the *urban heat island* (UHI) *effect*, which can bring about a number of undesirable consequences for the urban environment, like increased energy demand, reduced air and water quality and elevated levels of thermal stress for the population. Additionally, buildings are the largest energy consuming sector in the world, accounting for over on third of total final energy consumption (IEA, 2013). As building rooftops comprise a substantial fraction of the urban surface area, their physical properties are important determinants of the urban environment. Cool roof technology has the potential be an effective and affordable solution to mitigate the adverse effects of the UHI and increase energy efficiency in order to meet future energy targets.

The intent of this thesis is to build a framework for assessing the UHI mitigation potential of a city-scale cool roof implementation and the associated response in cooling energy demand. Northern hemisphere cities of different climate zones during the summer months of June, July and August were selected for evaluation. I will focus on a smart city perspective, and whether or not the passive cool roof strategy possesses the desired qualities to be part of a smart city scheme.

2. BACKGROUND

2.1 GLOBAL URBANIZATION TRENDS

On a global scale, more than half the world's population of 7.6 billion people now resides in urban areas. The urbanization trend continues to grow, and the coming decades will bring about profound changes to the size and spatial distribution of the world's population. By 2050 projections indicate an increase of the global population to 9 billion people, and population growth is expected to add 2.5 billion people to the world's urban population over the same time period. Additionally, regions all over the world are expected to further urbanize over the coming years, and cities in Africa and Asia are experiencing the most rapid urban expansion (United Nations: Department of Economic and Social Affairs, 2014).
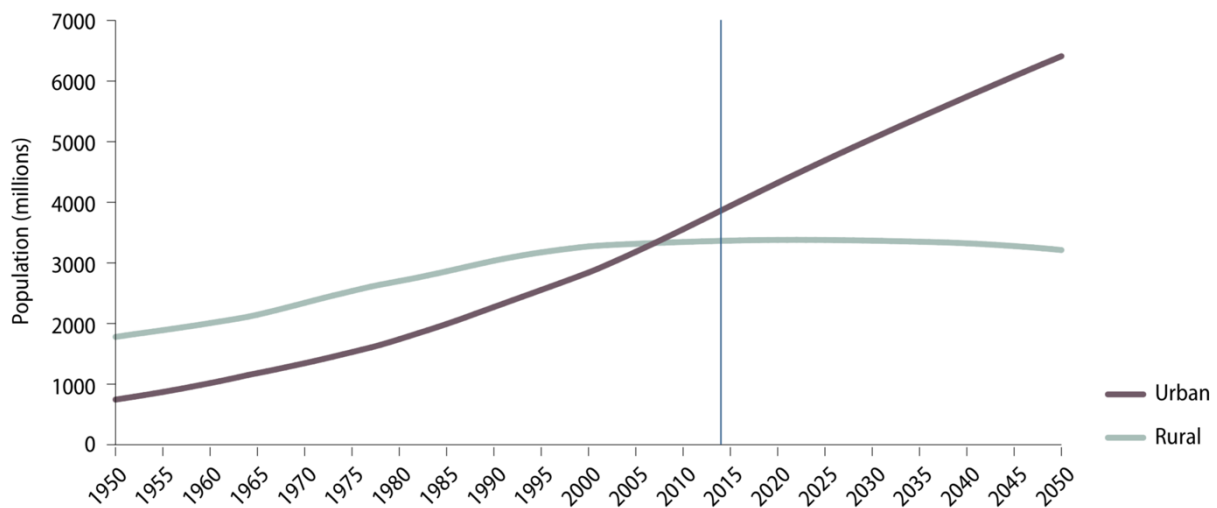
Figure 2-1: The urban and rural population of the world, 1950-2050 (United Nations: Department of Economic and Social Affairs, 2014).

As the world population continues to increase while a strong and swift urbanization is taking place, sustainable development and energy related challenges will be increasingly concentrated in cities. Finding smart and efficient solutions for urban development will be paramount in order to reduce the energy demand and associated greenhouse gas (GHG) emissions of a growing urban population.

2.2 SMART AND SUSTAINABLE CITIES

As stated by Kim (2017), the low-carbon, smart city intends to systematically incorporate mitigation and adaptation measures to enable cities to respond to climate change through a well-planned and designed urban environment. Sustainable smart city projects should include strategies like application plans for reducing urban heat islands and limit the urban energy consumption by utilizing energy standards for different types of buildings.

2

Today, there are no universally acknowledged definition of a smart city. As pointed out by Haarstad (2017), asking what a smart city is might be the wrong question; the more relevant question is what a smart city – or rather the smart city framing – does. This means that we understand it as a strategy, and according to a definition by Morvaj et al. (2011), "a smart city is a city that combines information and communications technology (ICT) with its physical infrastructure to improve conveniences, facilitate mobility, add efficiencies, conserve energy, improve the quality of air and water, identify any problems in the operation of city systems and fix them quickly, recover rapidly from disasters, collect data to make better decisions and deploy resources effectively and efficiently".

There exist a large variety of perspectives on what constitutes a smart city, ranging from purely ecological to technological, and from economic to societal; the ecological smart city perspective focuses on the commitment of local governments, businesses and communities to reducing GHG emissions, reversing urban sprawling, increasing urban density and green urban areas; the technological perspective targets the utilization of smart urban technology solutions to improve livability of communities and sustainability of cities; the economic perspective points to generating an innovation economy through smart technology solution development; and the societal perspective focuses on establishing socio-economic equality and public participation in the smart city planning and initiatives (Yigitcanlar and Kamruzzaman, 2018).

In order to achieve sustainable outcomes, careful city planning will be crucial for adopting sustainable urban development principles, particularly by promoting such planning at the local level. Kim (2017) argues that resilient, low-carbon smart cities also incorporate climate mitigation and adaptation policies at each stage of the planning process. This will likely contribute to generate ecological sustainability, which is considered a critical element of smart cities (Yigitcanlar and Kamruzzaman, 2018).

However, according to Haarstad (2017), given that there currently exist no prevalent definitional boundaries of the term 'smart city', it is difficult to measure whether or not smart city projects actually make any contributions to urban sustainability. Even though a number of cities claim to be smart, evidence that a smart city can provide sustainable solutions to the complex problems of future cities is currently non-existent (Anthopoulos, 2017). According to Mora et al. (2017), "the knowledge necessary to understand the process of building effective smart cities in the real world has not yet been produced, neither have the tools for supporting the actors involved in this activity".

2.2.1 SMART CITY PLANNING

According to UNs sustainable development goal (SDG) number 11, sufficient urban planning and management are needed to make the world's urban spaces more inclusive, safe, resilient and sustainable. Kim (2017) argues that we are on the eve of a new era of climatic-responsive urban planning. The climate crisis of the twenty-first century is a direct result of nineteenth century industrialization, the land-use planning and urban design solutions of the twentieth century. He argues that humans have strained the equilibrium between us and nature to the breaking point, and it will be important to use the next generation of city building and planning as an opportunity to restore this equilibrium in order to prevent further climatic and ecological disaster. Research in smart cities is often characterized by different needs; decreasing pollution and emissions, improvement of energy efficiency and optimization of production and consumption of energy are the main actions required (Dispenza et al., 2017). The energy efficiency is the ratio between the useful output and the energy input. The increasing number of urban responses to climate change emphasize the need for carbon-centered comprehensive smart planning models that can incorporate climate change mitigation and adaptation policies at each stage of the process (Kim, 2017).

As climate change continues to be a major threat to the urban environment, smart climate urbanism has emerged as a new tenet of climate change for cities: it aims to reform all aspects from sustainability, efficiency, connectivity, circularity and resiliency perspectives. It involves new development, urban retrofits and suburban infill. Smart climate urbanism supports urban planning for urban development, climate change mitigation and adaptation planning. It also contributes to the development of green infrastructure; it can reduce GHG emissions, increase circularity and resilience of vulnerable cities and thereby ensure urban sustainability; and it covers issues like energy, transport, industries, land use, livelihoods, health, food and water, infrastructure and ecosystems in a connected manner (Kim, 2017).

2.3 URBAN CLIMATOLOGY

Generally, urban climates are characterized by the balance between the absorption of insolation and heat losses from longwave radiation from walls, roofs and ground. Convective heat exchange between urban surfaces and the atmosphere also plays a central part, in addition to heat generation within the city itself. Furthermore, urban areas tend to experience an overall reduction in wind speed, mainly due to the increased friction associated with the roughness of urban landscapes (Wilkinson and Dixon, 2016). Urban advection, the horizontal transport of heat by wind, is often reduced as it depends heavily on the geometry of the urban surface, surface moisture and roughness, thermal admittance and mean wind velocity (Jacobson and Hoeve, 2012).

2.3.1 GEOMETRY OF THE URBAN CANYON

Urban geometry is the physical characteristics and configuration of a city (Wilkinson and Dixon, 2016). As more inhabitants are continually added to the urban jungle, cities are experiencing a rapid expansion and densification. This contributes to the creation of urban street canyons, the basic urban unit of analysis, particularly at the micro ($>10^2$ m) and local ($>10^2$-10^3 m) scales. These canyons are defined as the space above the street and between buildings. Here, heat is trapped during daytime, which has a significant impact on the urban heat island effect (Wilkinson and Dixon, 2016).
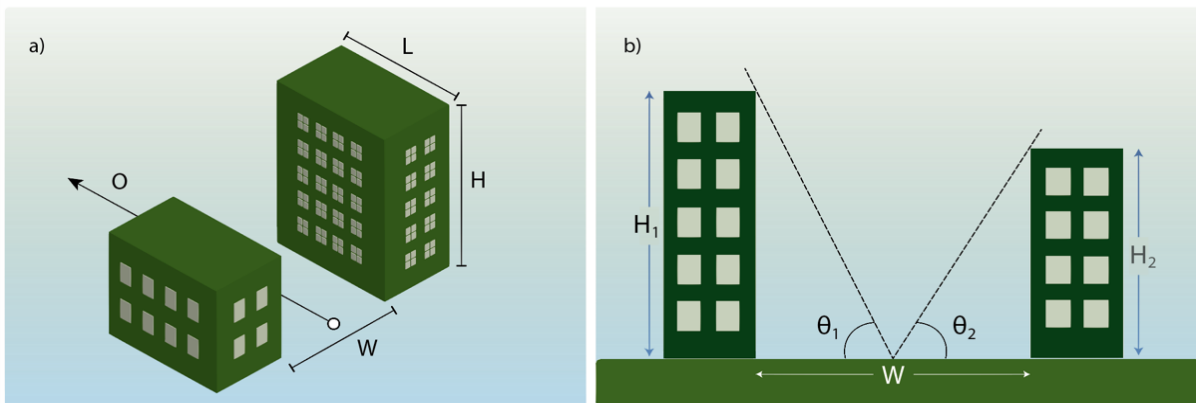
Figure 2-2: *Urban canyon schematics where **a)** displays the width and orientation of the canyon, height and length of buildings. (Redrawn from (Wilkinson and Dixon, 2016)).* **b)** Geometry of an asymmetric urban canyon between two buildings. (Redrawn from (Oke, 1988)).

The four main parameters that constitute the urban canyon are mean building height, canyon width, length and orientation of the canyon, as depicted in Figure 2-2a. The height-to-width-ratio is called the aspect ratio. The sky view factor is the ratio between incoming radiation received by a planar surface and that of the entire hemispheric radiating environment. It can be directly related to the height-to-width ratio, and Figure 2-2b illustrates how the geometry of an asymmetric canyon affects the radiation received by the surface (Oke, 1988).

These geometric properties affect several microclimatic factors; solar exposure of buildings and open space, wind speed and direction, pollution dispersion and the presence and intensity of heat island phenomena, which is further described in section 2.3. The geometric parameters also have an impact on building energy demand for heating, cooling and lighting, and the associated greenhouse gas emissions. Additionally, they can have an influence on outdoor comfort levels, which in turn affect the health and wellbeing of citizens. As the building density increases in large cities, the radiatively active surfaces move upwards from street level to roof tops. Therefore, in densely built cities, roofs absorb, reflect and emit a substantial amount of the radiation received by the city surface (Wilkinson and Dixon, 2016).

2.3.2 URBAN BOUNDARIES

The atmospheric boundary layer is the lowest part of the troposphere, where wind, temperatures and humidity are strongly influenced by the surface. Fluxes of heat, momentum and moisture by small-scale turbulent motions in the boundary layer are critical to climate (Hartmann, 2016). The urban boundary layer extends from the rooftop level to a point where urban landscapes no longer have an impact on the atmosphere. This region is typically no higher than 1.5 km from the surface. The urban canopy layer is defined as the layer of air where people live. It stretches from the ground and up to about the mean roof level – the rough surface of the city, as shown in Figure 2-3. Additionally, the rural boundary layer, located outside the urban core, also extends to a point where the landscape no longer affects the atmosphere, but the rural boundary is usually much closer to the ground than the urban core (EPA, 2008).
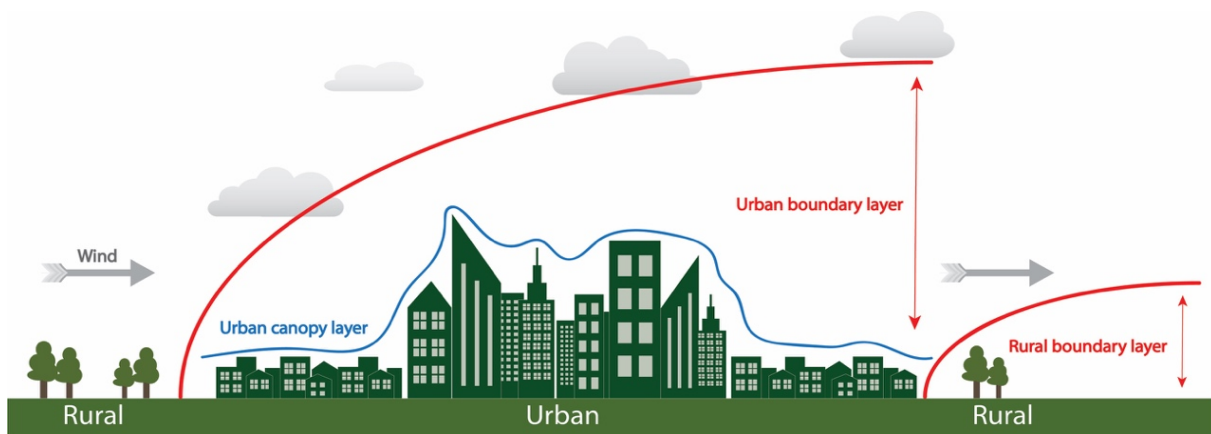
Figure 2-3*: Schematic of the different layers and boundaries that makes up the urban atmosphere: The urban boundary layer stretches from the rooftops to about a maximum of 1.5 km from ground level. The rural boundary layer is usually lower than the urban, but also extends to a point where the landscape no longer affects the atmosphere above. The canopy layer stretches from the top of buildings and down to ground level (Redrawn from Figure 8.6 in Oke (1987).*

2.3.3 THE URBAN SURFACE ENERGY BUDGET

The energy budget of the surface can be expressed in terms of energy flux per unit area passing vertically through the air-surface interface and is measured in watts per square meter. The surface energy budget determines the amount of energy available to evaporate surface water and to raise or lower the temperature of the surface. Furthermore, the energy budget is highly complex, as it considers fluxes of energy by conduction and convection of heat and moisture, in addition to radiation. The local surface energy budget depends on the insolation, surface characteristics like wetness, vegetative cover and albedo, and the characteristics of the atmosphere above (Hartmann, 2016). Figure 2-4 depicts the energy budget of the surface in an urban area.
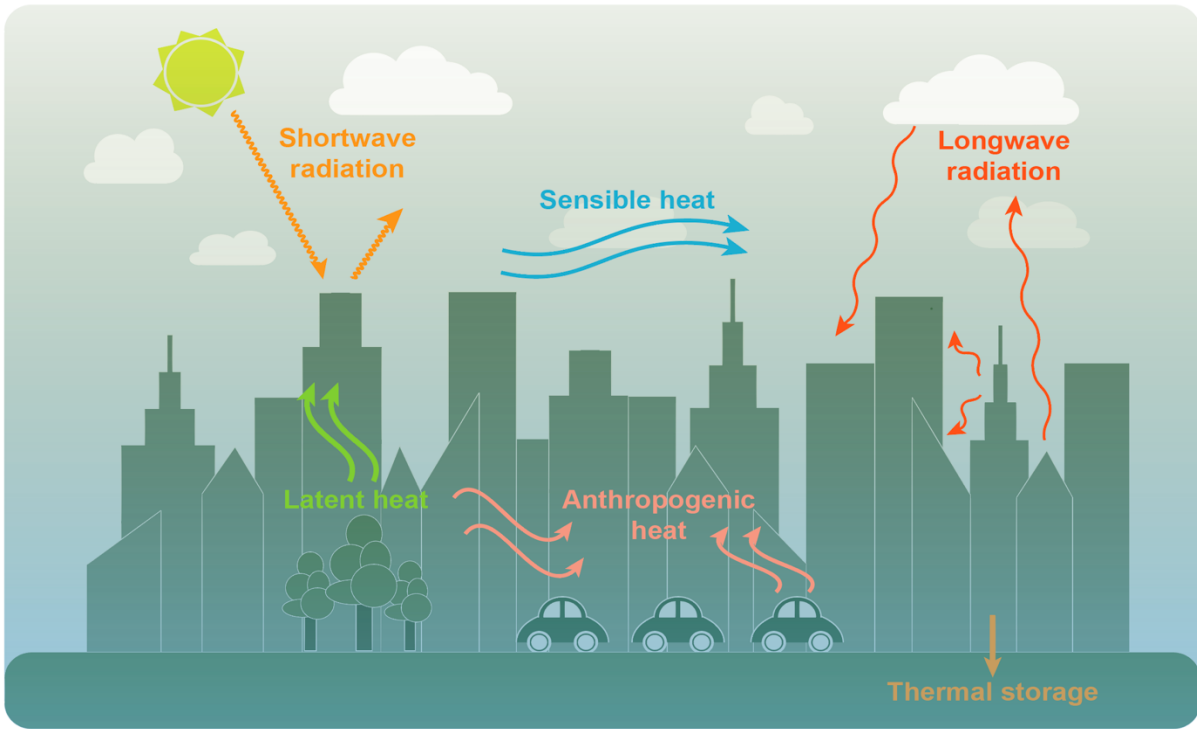
Figure 2-4*: The energy budget of the urban surface, which is characterized by the incoming and reflected shortwave radiation, outgoing and incoming longwave radiation, thermal storage and latent, sensible and anthropogenic heat release (Redrawn from EPA (2008)).*

SHORTWAVE AND LONGWAVE RADIATION

The surface radiation balance is mainly determined by shortwave and longwave radiative transfer. Shortwave radiation (SW) is radiant energy with wavelengths corresponding to the visible, ultraviolet and near-infrared spectra of the sun. The Earth receives a daily amount of insolation, which is the amount of downward solar radiation energy incident on a plane surface. Seasonal and latitudinal variations in temperature are driven primarily by variations of insolation and the average solar zenith angle, which depends on latitude, season and time of the day. Averaged over the entire planet, roughly 340 W/m^2 of energy from the Sun reaches the surface. About one third of this energy is reflected back into space, and the remaining 240 W/m^2 is absorbed by land, ocean, and atmosphere (Hartmann, 2016).

Terrestrial longwave radiation (LW), is electromagnetic radiation in the infrared part of the spectrum, mainly wavelengths between 4 μm and 100 μm. Heat absorbed by the surface from shortwave radiation during daytime is released as longwave thermal radiation. The emitted outgoing longwave radiation (OLR) is the Earth's primary means of losing energy to space, and the emitted terrestrial radiation is about 396 W/m^2, 239 W/m^2 of which is released to space at the top of the atmosphere. The higher the temperature of the surface, the greater the OLR. This balance between the incoming shortwave and outgoing longwave radiation largely determines the heating and cooling of the Earth system. Additionally, the strong downward emission of terrestrial radiation of about 345 W/m^2 from the

atmosphere is essential in order to maintain the relatively small diurnal variations in land surface temperatures. (Hartmann, 2016).

<center>SENSIBLE AND LATENT HEAT FLUXES</center>

Under most conditions, radiation heats the land surface and latent while sensible heat fluxes cool it, and turbulent fluid motions in the boundary layer produce sensible and latent heat fluxes from the surface. Sensible heat is caused by conduction and convection, and represents the energy required to change the temperature of a substance, like air, without a phase transition. The global average of sensible heat fluxes is approximately 20 W/m^2, and the temperature change originates from absorption of sunlight by the surface or the air itself. For a warm surface and a cooler urban atmosphere, heat will be conducted into the atmosphere and then convection will move the heat higher up.

Latent heat, on the other hand, is the energy absorbed or released by a substance during a phase change: evaporating water into vapor requires energy, while the process of condensation results in the release of energy (latent heat). Consequently, the energy budget of the urban surface is highly related to the hydrologic cycle, since evaporation from the surface is a key component in the budgets of both energy and water. Latent heat is also a great temperature moderator as it helps cool hot urban surfaces at a global average of 88 W/m^2 (Hartmann, 2016). The latent heat flux of cities is characterized by a number of highly complex processes due to the impervious surfaces of developed areas, like pavements, walls and roofs. The urban evaporation originates from the part of the urban canopy occupied by water-permeable surfaces like soil, vegetation and water. As cities expand, and vegetated areas are replaced by pavements and buildings, less incoming solar energy is used for latent cooling and more goes into sensible heat – which has an undesirable warming effect on the urban air.

The causes and effects of urban climates are complex, and evapotranspiration (evaporation and transpiration) from soil-vegetation systems is an effective moderator of near-surface climates. Under favorable conditions, evapotranspiration can create cooler 'oases' with temperatures of 2-8 °C below their urban surroundings. Under extreme conditions, the latent heat flux can become so high that it causes the sensible heat flux to take on negative values (Taha, 1997). Both sensible and latent heat fluxes respond to temperature differences between the surface and the air; when cold air flows across the warm urban surfaces, strong sensible and latent heat fluxes warm and moisten the air, and turbulent motions mix the air upwards in a convective manner.

The atmosphere is transparent to shortwave radiation and opaque to longwave radiation, meaning that the shortwave radiation easily passes through the atmosphere and warms the surface, while the outgoing longwave radiation is partly absorbed by the atmosphere's greenhouse gases. Water vapor, carbon dioxide, methane and other trace gases are the major contributors to the natural greenhouse effect, as these gas molecules absorb thermal radiation that heats the atmosphere. Much of the OLR that is absorbed by the greenhouse gases will be re-emitted back to the Earth's surface, a process often referred to as back radiation. Without the natural greenhouse effect, the temperature of the Earth would be about -18°C on average, and life as we know it would not exist (Hartmann, 2016).

The average global temperature increased by 0.85°C from 1880 to 2012 as global emissions of carbon dioxide (CO_2) have increased by almost 50% since 1990. The emissions continue to rise due to the large-scale burning of fossil fuels, the UN have taken several measures to address the human-induced climate change; the 2015 Paris Agreement within the United Nations Framework Convention on Climate Change (UNFCCC) is currently signed by 195 member countries (June 2018). The overall purpose of the agreement is to limit the global temperature rise to well below 2°C, and all countries are obligated to promote measures and strategies to help achieve this goal. In order to accomplish this, the concentration of CO_2 in the atmosphere cannot exceed 450 ppm, as compared to the pre-industrial levels of 280 ppm (UN-SDG, 2018).

Human activity produces heat from a variety of sources, like energy demand for heating and cooling, transportation and industrial processes. The amount of heat released peaks during wintertime in both rural and urban areas and depends on many factors such as the spatial and temporal variation of the energy consumption, density of population, industrial activity, prevailing climatic conditions, transportation characteristics and geographical location (EPA, 2008). Anthropogenic heat emission (AHE) can be an important contributor to the thermal environment of cities, especially during winter when the anthropogenic heat output peaks. According to (Yang et al., 2017), numerical simulations of the urban temperature regime indicate that anthropogenic heat can contribute to increased urban temperatures of up to 3 °C during winter time, and ranges between 0.8-1.5 °C.

Additionally, AHE has large implications for the urban temperature and will consequently impact the energy demand of buildings. The release of anthropogenic heat can be said to cause a positive feedback loop during summer; buildings with low energy efficiency and high cooling loads uses more energy to keep indoor climates at comfort temperatures – the associated heat release contributes to increase to a warming of the urban air, which in turn increases the cooling loads. By making buildings more energy

efficient and reducing the energy demand for cooling during summer, the anthropogenic heat release will decline, which in turn can contribute to a reduction of the urban heat island phenomenon.

THERMAL STORAGE

Energy storage in the surface is very important for the diurnal cycle over land and ocean. Energy storage strongly depends on the heat capacity, which is determined by the properties of the surface materials. The depth of the surface layer that exchanges heat with the atmosphere is also important, and the first few meters of soil respond to seasonal forcing most rapidly. Urban materials tend to have higher heat capacities than vegetated rural areas, and an increase in heat capacity can also have a warming effect on the surface and atmosphere. Materials with low heat storage capacity are therefore desirable to counteract the adverse warming effects. Additionally, cities have more thermal mass as opposed to the rurals, which further contribute to the warming of urban air (Hartmann, 2016).

2.4 THE URBAN HEAT ISLAND EFFECT

Urban areas are generally warmer than the rural, vegetated surroundings, as urban surfaces reduce evapotranspiration and have sufficiently different heat capacities, thermal conductivities, albedos, and emissivities to enhance urban warming. Consequently, a common characteristic of urban and suburban areas is that they tend to have higher temperatures compared to areas surrounding the city; this temperature difference is what is called the urban heat island (UHI) effect (Jacobson and Hoeve, 2012). The UHI effect is characterized by an important spatial and temporal variation related mainly to climate, topography, physical properties and short-term weather conditions, while its intensity is determined by the thermal balance of the urban region (Yang et al., 2017).

The urban heat island effect is a result of differences between urban and rural energy balances, and the magnitude of the UHI effect is indicated by the temperature differences between the urban and rural areas (Stewart and Oke, 2012). The Merriam-Webster Dictionary defines urban areas as "relating to, characteristic of or constituting a city", whereas rural areas are characterized as an "agricultural or pastoral area, characteristic of the country or country life". Furthermore, Stewart and Oke (2012) interpret 'rural landscapes to be less populated than cities, with fewer built structures and more abundant natural space for agricultural use, whereas urban landscapes have significantly more built structures and larger populations. By extension, suburban landscapes are those lying immediately outside or adjacent to a town or city, and that have natural and developed spaces with population densities lower than cities but higher than the country'.

The magnitude of the UHIs tend to reach peak values in the late afternoon, when the solar radiation has heated the urban surfaces throughout the day, as can be seen in Figure 2-5. However, the largest measured temperature differences occurred on still winter nights, with recorded temperatures of 10-12 °C higher than surrounding areas. Additionally, the difference between urban and rural temperatures (ΔT_{u-r}) is generally greater at higher latitudes (Fallmann2015). Several data analysis studies have estimated that the globally averaged UHI may have contributed ≤0.1 K to global temperature changes since the preindustrial era, and the urban heat island (UHI) effect may contribute to 2-4% of gross global warming. The Intergovernmental Panel on Climate Change (IPCC) Fourth Assessment Report concluded that the UHI may have increased temperatures of ~0.065 K over land and ~0.022 K globally from 1900 to 2008. However, these studies cannot distinguish urban temperature changes in due to the UHI effect from those due to greenhouse gases, cooling or warming aerosol particles, transmission or use of electricity, stationary or mobile combustion, or human respiration (Jacobson and Hoeve, 2012).

The major large-scale feedback of the UHI appears to be the increase in energy and decrease in moisture flux from urban areas to the surrounding region as a response to a lower evapotranspiration from the urban surface (as will be explained later). Locally and on region-scale, these changes decreased the relative humidity and cloudiness, contributing to an increase in surface solar radiation. Furthermore, greater local convection over cities also increased precipitation downwind of many urban areas (Jacobson and Hoeve, 2012).
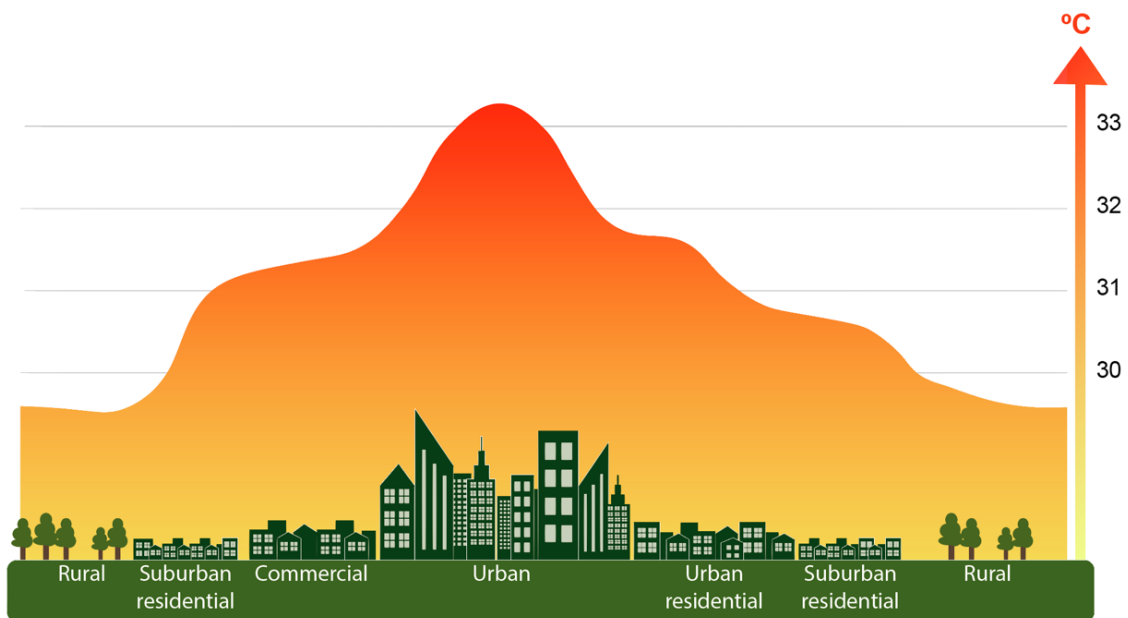
Figure 2-5: Urban heat islands tend to reach the highest temperatures in the late afternoon, with a peak temperature over the city core, as this is the area that is least affected by the surrounding areas (Redrawn from Stewart (2017)

UHIs mainly depend on the modification of energy balance that occurs within urban areas, which is caused by several factors: the formation of urban canyons, thermal properties of building materials, substitution of green areas with impervious surfaces with limited potential for evapotranspiration and a general decrease in albedo associated with urban surfaces (Susca et al., 2011). The following excessive warming of the surface, along with heat generated by anthropogenic activities like burning of fossil fuels and air conditioning, result in large urban areas that are significantly warmer than the surrounding rural areas (Fallman et al., 2015). The result of this warming is an annual mean urban temperature of about 1-3 °C higher than the rural areas surrounding the city (Oke, 1982). However, research has indicated that the properties of the rural areas have significant impacts on the development of the temperature differences between the urban and rural sites. According to Zhao et al. (2014), energy redistribution through convection between the surface and the atmospheric boundary layer can either increase or reduce the temperature differences. This energy redistribution depends on whether the efficiency of convection over urban land is large or small relative to the adjacent rural land.

To identify urban heat islands today, scientists use both direct and indirect methods, numerical modelling and estimates based on empirical models. Remote sensing is a frequently used indirect measurement technique to estimate surface temperatures (EPA, 2008).

2.4.1 ATMOSPHERIC AND SURFACE URBAN HEAT ISLANDS

We distinguish between two main types of urban heat islands; atmospheric and surface UHIs, and Table 2-1 provides an overview of the basic characteristics of the two types of UHIs.

Table 2-1: Basic characteristics of the surface and atmospheric heat islands, which are the two main categories of UHIs.

FEATURE	SURFACE UHI	ATMOSPHERIC UHI
Temporal development	• Present at all times of the day and night • Most intense during the day and in the summer	• May be small or non-existent during the day • Most intense at night or predawn and in the winter

Peak intensity (most intense UHI conditions)	• More spatial and temporal variation:
	   o Day: 10 to 15 °C
	   o Night: 5 to 10 °C
		• Less spatial and temporal variation:
		   o Day: -1 to 3 °C
		   o Night: 7 to 12 °C

ATMOSPHERIC URBAN HEAT ISLAND

The atmospheric urban heat island (AUHI) is defined as an excessive warming of the urban atmosphere compared to the cooler air of surrounding rural areas. The atmospheric UHIs can be divided into two subcategories; canopy layer (CLUHI) and boundary layer (BLUHI) urban heat islands. The distinction between these layers was previously illustrated in Figure 2-3, section 2.3. CLUHIs are the most frequently observed and are the ones most often referred to by the general term 'atmospheric urban heat islands'. Atmospheric UHIs are often weak throughout the day and become more prominent after sunset because of the slow release of heat from urban infrastructure. The time of the peak temperature of the atmospheric UHI depends on the properties of both the urban and rural surfaces, season and prevailing weather conditions (EPA, 2008).

SURFACE URBAN HEAT ISLAND

Surface urban heat islands (SUHI) are characterized by the warming of dark urban surfaces like roofs, walls and pavements. On hot summer days, the sun can warm up dry, exposed urban surfaces to temperatures 27-50 °C hotter than the air. Shaded, vegetated or moist surfaces typically found in rural areas tend to remain closer to air temperatures, as the latent cooling rate is higher. The daytime surface temperature differences between urban and rural areas averages at 10 to 15 °C; night-time temperature differences are generally smaller, at 5 to 10 °C. The magnitude of the SUHI varies with season because of changes in the intensity of the sun, as well as weather and ground cover. Because of this, SUHIs are typically greatest in the summer (EPA, 2008).

RELATIONSHIP BETWEEN ATMOSPHERIC AND SURFACE UHIS

According to Voogt and Oke (2003), the relation between surface and air temperature is empirical and no simple general connection exists between the two, even if their correlation improved at night when microscale advection is reduced. In the canopy layer, surface temperatures have an indirect, but significant impact on air temperatures. Because of atmospheric mixing, the relationship between surface and air temperatures are not constant, and Figure 2-6 illustrates that air temperatures vary less than surface temperatures. Additionally, the figure shows a larger difference between surface temperatures during daytime than at night, when temperatures level out to a much greater extent (EPA, 2008).
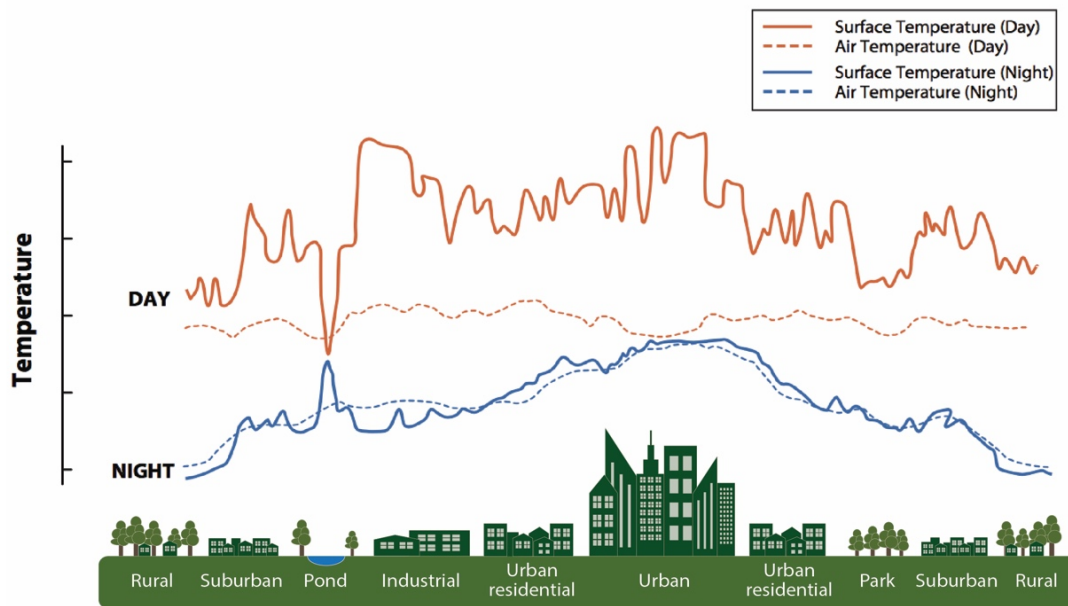
Figure 2-6*: Variation of surface and air temperatures during daytime and night-time over urban and rural areas. There is a significant temperature difference between the surface and air temperatures during the day, while these differences tend to level out at night* (Redrawn from EPA (2008)).

2.4.2 FORMATION MECHANISMS OF URBAN HEAT ISLANDS

Beside the development and changes in the radiative and thermal properties, which are the main causes of the UHI formation, buildings also have an impact on local microclimates, and especially tall buildings can reduce the urban cool-off rate at night. Heat islands are influenced by a number of factors, like geographic location, local weather patterns and their daily and seasonal intensity variation. Local climate change due to UHIs is fundamentally different from global climate change; the effect of UHIs are limited to local scale and decrease with distance from the source, i.e. the city. Global climate change, on the other hand, is caused by large-scale factors such as increase in the sun's intensity or greenhouse gas emissions and are not confined to local or regional scale. Impacts from urban heat islands and global climate change are often similar, and both can contribute to increase in energy demand and the associated issues of air pollution and further greenhouse gas emissions. Solar reflectance, thermal emissivity and heat capacity are properties of urban materials that largely contribute to influence the formation of heat islands. Materials determine how radiation is absorbed, reflected and emitted, and hence the amount of heat that is absorbed by the city (EPA, 2008)

THE URBAN ALBEDO

Shortwave radiation is the primary driver of Earth's climate and weather. The amount of radiation absorbed locally depends on the reflectivity of the atmosphere and the surface, also known as the planetary albedo (Carlowicz, 2014). The albedo is a reflection coefficient, where 1 being the maximum

where all incoming radiation is reflected by the surface, and 0 being the minimum where all radiation is absorbed by the surface. As a substantial part of the sun's energy is found within the visible wavelengths of the spectrum, the albedo of a material strongly correlates with its colour. Consequently, light surfaces tend to have high albedos and a cooling effect on the surroundings, while dark-coloured surfaces have a low albedo warming effect on the climate (EPA, 2008).

Because the solar zenith angle, cloud cover and ice/snow cover all increase with latitude, so does the albedo. Consequently, a smaller fraction of the shortwave radiation is absorbed at the poles than near the equator. Changes in ice/snow cover, cloudiness, airborne pollution, or land cover have subtle effects on the global albedo. Estimations based on accumulated satellite measurements dated back to the 1970's have approximated an average global albedo at 0.29. These estimations accommodate both the cloud and surface albedo contributions. The remaining 0.71 of all incoming solar radiation is absorbed by the climate system. Urban areas generally have lower albedos than the global average, and Table 2-2 lists the typical albedos of some selected urban materials. Urban surface materials include asphalt, concrete, window glass and vegetation and the canopy floor, which includes roads, pavements and courtyards (Sugawara, 2014).

Table 2-2: *Albedos for various surfaces. Albedos selected from table 4.2 (Hartmann, 2016).*

SURFACE TYPE	RANGE	TYPICAL VALUE
Deep water (low wind)	0.05-0.2	0.7
Asphalt pavement	0.05-0.1	0.07
Concrete pavement	0.15-0.35	0.2
Dry light sand	0.3-0.4	0.35
Vegetation	0.1-0.3	0.2
Fresh snow	0.7-0.9	0.8

The construction materials most commonly used in cities have a lower albedo than rural areas and significantly contribute to the development of urban heat islands by altering the surface radiative properties. As the mean daytime insolation in a mid-latitude city is approximately 500 W/m^2, the fraction of sunlight absorbed is higher for lower albedos; the average effective urban albedo is about 0.15, whereas the typical rural albedo measures about 0.25 (Taha et al., 1992). As a result, cities absorb more radiation, contributing to a rise in surface and atmospheric temperature and the associated formation of surface and atmospheric heat islands (EPA, 2008).

The urban surface albedo, which is the ratio of incoming to outgoing shortwave irradiance above the building canopy, is a key factor for determining the urban heat budget. According to Sugawara and Takamura (2014), in determining the urban albedo, building structure and surface materials are the two key components: building structure has shown to have a large impact on the urban albedo, which in turn depends on the geometric structure of buildings. In addition, it has been found that urban albedo decreases with lower street width and increasing building height.

THERMAL EMITTANCE AND HEAT CAPACITY OF MATERIALS

Thermal emittance is a measure of the ability of a surface to emit thermal infrared radiation (IR), i.e. to release heat to its surroundings. Therefore, surfaces with high emittance values tend to stay cooler. A material's heat capacity is also an important property and can be explained by a material's ability to store heat. Traditional building materials like steel and stone have higher heat capacity than many materials found elsewhere, like vegetation and soil. Cities that have high densities of materials with great heat capacities, will consequently have an increased contribution to the UHI effect as the city will store heat more effectively. In fact, urban areas can absorb and store twice the heat amount of rural areas during the daytime (EPA, 2008).

URBAN GEOMETRY

The formation of urban heat islands is also influenced by urban geometry, which has an impact on wind flow patterns, energy absorption and thermal emittance. Especially at night, the air above cities is warmer than surrounding areas due to tall buildings and large structures that obstruct the thermal emittance of other urban surfaces. Urban canyons are urban structures that largely influence the development of heat islands. During daytime, canyons have competing effects: tall buildings provide shade, which allows surfaces and air to cool off; when sunlight reaches the canyon surface, parts of this sunlight will be reflected on to building walls where it is absorbed. This contributes to a further lowering of the total urban albedo (the net reflectance from the surface albedo plus urban geometry) and can increase city temperatures as they slow down cooling during night-time (EPA, 2008).

The effects of urban geometry on heat islands are often described by the sky view factor (SVF), which constitutes the visible area of the sky from a given point on the surface. For instance, the SVF of an open field with a panoramic view will be large, while densely built cities with tall structures will have a low SVF (EPA, 2008).

VEGETATION AND LATENT HEAT / EVAPOTRANSPIRATION

Vegetation and open land typically dominate rural areas. In addition to the shade provided by trees and shrubs, vegetation and soil can reduce air temperatures by evapotranspiration; the release of water to the surrounding air. In contrast, the ground cover in cities consists mostly of dry, impervious surfaces with less shade and moisture to keep the urban areas cool. Additionally, cooling by latent heat absorption during evaporation is an important process for cooling the surface. As less evaporation occurs in urban areas, more energy goes into sensible heat, which in turn elevates surface and air temperatures (EPA, 2008).

ANTHROPOGENIC HEAT

A large contributor to the urban heat island development is anthropogenic heat. Although the average anthropogenic heat flux is small compared to the daytime incoming solar radiation during summer, waste heat from urban anthropogenic activities might have a significant impact on the formation and magnitude of the urban heat island phenomenon. Many experimental and modelling studies have documented that waste heat from urban energy and infrastructure systems contribute to intensification of heat islands (Yang et al., 2017). Furthermore, anthropogenic heat largely affects the surface temperature of urban areas, and numerical simulations have shown that it contributes up to 29.6% to the development of the UHI and could result in a 0.5–1.0 °C increase in surface temperature at night (Yang et al., 2017).

GEOGRAPHIC LOCATION AND WEATHER

The two primary weather components that contribute to the development of UHIs are wind and cloud cover. In general, urban heat islands are most prominent on calm and clear days; absorption of insolation by urban surfaces reaches a maximum under these conditions, and winds minimize the convection of heat away from the surface. In contrary, heavy clouds will block out solar radiation and reduce the daytime warming, and strong winds will carry heat away from the urban surfaces. The geographic location of the city will also influence the development of UHIs, as it partly determines the climate and topography of the area. For instance, proximity to large water bodies can help moderate temperatures and generate winds. Additionally, mountainous terrain will have an impact on local weather patterns and can either block out winds or generate winds that provides ventilation to the city (EPA, 2008).

2.4.3 IMPACTS AND CHALLENGES OF URBAN HEAT ISLANDS

The ramification of urban heat islands extends to more than just an increase in temperatures and the environment – it also influences the quality of life, society and the economy. Impacts include heat-related deaths, illness and discomfort, air pollution, increase in electricity and water consumption and the associated emission of greenhouse gases (Wilkinson and Dixon, 2016).

ENERGY DEMAND

Energy demand is the volume of power required by an electrical system or device at any given point of time. An increase in energy demand for cooling due to elevated summer temperatures adds pressure to the electricity grid during peak periods of demand, which increases by 1.5 to 2 percent for every 0,6 °C increase in summertime temperature. This means that 5 to 10 percent of the urban electricity demand is used to compensate for the urban heat island effect. The energy demand during periods of extremely high temperatures can result in a system overload and power outages (EPA, 2008).

GREENHOUSE GAS EMISSIONS AND POLLUTANTS

In many cities across the globe, fossil fuels are commonly used to generate electricity. Higher demands for energy during summer tend to cause higher levels of pollution and greenhouse gas emissions. Besides the emissions of greenhouse gases like carbon dioxide (CO_2), toxic pollutants like sulphur dioxide (SO_2), nitrogen oxides (NO_x), carbon monoxide (CO), particulate matter (PM) and mercury (Hg) are also released during the process of burning fossil fuels. These are harmful to human health and contribute to massive problems related to air quality and global climate change. Another side effect of elevated urban temperatures is an increase in the formation of ground-level ozone (O_3). This is not emitted directly into the air but created by chemical reactions between nitrogen oxides (NO_x) and volatile organic compounds (VOC) in the presence of sunlight (EPA, 2008).

HEAT WAVES AND THERMAL STRESS

An anticipated consequence of global warming is an increase in frequency and intensity of heat waves. The increase in the UHI magnitude is predicted to exacerbate climate-induced heat waves and can cause serious health implications for urban residents. Besides general discomfort, issues like respiratory problems, heat cramps, exhaustion, heat stroke and heat-related mortality are expected to become more common as the urban climate deteriorates (EPA, 2008). Particular groups at risk are the elderly, children and the poor in rapidly urbanizing regions of the tropics and subtropics (Wilkinson and Dixon, 2016).

Thermal pollution contributes to a degradation of water quality. As city surfaces warm during daytime, part of this excessive heat is transferred to storm water. When pavement temperatures have been measured to 11-19°C above air temperature, runoff water from urban areas have been measured at temperatures 11-17°C hotter than runoff from nearby rural areas. This heated storm water is then released into streams, rivers, ponds and lakes, and can have a significant impact on aquatic life. Rapid changes in temperatures in can be both stressful and harmful for aquatic ecosystems, and the metabolism and reproduction systems in many species are particularly vulnerable to temperature changes (EPA, 2008).

However, there are a few positive impacts that follow the effects of urban heat islands. During wintertime, many cities can benefit from a reduced heating demand because of higher outdoor temperatures in the city. It can also help melt snow and ice in the streets, as well as provide the urban vegetation with a prolonged growing season – which in turn has many more benefits to counteract the negative effects of the UHI (EPA, 2008).

2.5 BUILDINGS AND ENERGY

2.5.1 ENERGY DEMAND

Cities produce over 70% of the global greenhouse gas emissions, and 70-80% of these emissions are attributed to buildings. Buildings can be considered as the basic unit of observation when considering urban infrastructure systems. Additionally, the percentage of building-related emissions is growing compared to the total of the city. Buildings are therefore in the front line of the battle against climate change (Roaf et al., 2009). Given improvements in economic development and living standards of the growing population, energy use in the buildings sector is predicted to rise significantly, putting an additional strain on the energy system (IEA, 2013).

The SDG target number 7.3 states that by 2030, the global rate of improvement in energy efficiency should be doubled. As buildings are the largest energy consuming sector in the world, the potential savings are substantial; the buildings sector accounts for one third of all energy use and the associated greenhouse gas emissions in western countries (IEA, 2012, IEA, 2015). According to IEA (2015), the energy consumption worldwide is predicted to increase by 48% by 2040, resulting in higher greenhouse gas emissions, climate change and poor urban air quality. Building-related CO_2-emissions have

increased by about 1% annually since 2010. Furthermore, the worldwide energy intensity of the buildings sector measured by final energy per square meter was reduced by 1.3% per year between 2010 and 2014. This reduction was mainly caused by the adoption and enforcement of building energy codes and efficiency standards.

The energy demand per capita has remained nearly constant at 5 MWh per person per year since 1990. In order to meet the 2 degrees-target set by the UN, the average building energy use per capita needs to be reduced by at least 10% to less than 4.5 MWh by 2025. Currently, policies and investments related to the energy efficiency of buildings is not on track to meet this target; about two-thirds of all countries do not have any existing building codes for energy regulation and consumption. However, as stated by the IEA (2013), technologies and measures that allow the buildings sector to be more energy efficient and sustainable already exist and will play an important part in transforming the energy sector. Unlocking the potential of energy efficiency, particularly in the buildings sector should be a priority for all countries. According to Ürge-Vorsatz et al. (2015), in 2010 the building sector used approximately 115 EJ (exajoules) globally, accounting for 32% of global final energy demand (24% for residential and 8% for commercial) and 30% of energy-related CO_2 emissions. Furthermore, the building sector used 23% of the global primary energy and 30% of the global electricity, and the predicted 85% increase in building energy use towards 2050 will likely come from urban areas. Understanding the underlying trends in drivers and past energy use will be of great importance for future projections, modeling activities and policy design aimed at addressing environmental and social problems related to energy use in buildings (Ürge-Vorsatz et al., 2015).

While appliances, lighting, electronics and computing reduce heating requirements in cold climates, they have an adverse effect on cooling requirements. According to Lam et al. (2008), internal heat loads such as these account for 75% of the total building annual cooling load: more energy efficient lighting and office equipment would help reduce the overall electricity demand, air conditioning included. A simple schematic of the indoor energy balance is shown in Figure 2-7. The cooling load of a building is the rate at which heat is removed from the conditioned space to maintain a constant space air temperature, while space heat gain is the rate at which heat enters a space, or heat generated within a space (City University).

The choice of location and technologies for buildings, the form and fabric of the built environment and the lifestyles we adopt in them deeply affect quality of life of urban dwellers (Roaf et al., 2009). In order to achieve carbon-neutrality targets in big cities worldwide, adaptation to reduce building-related energy consumption is strongly encouraged. Consequently, reducing the energy use in the building sector will be crucial when confronting the issues of global warming. Moreover, it has proven more cost effective and environmentally friendly to reduce the energy use than to extend the capacity of the energy supply

system (IPCC, 2007). The energy efficiency report from (IEA, 2017) claims that in order to limit the CO_2 concentration in the atmosphere to 450 ppm, two-thirds of the emission reductions will have to come from increases in energy efficiency.
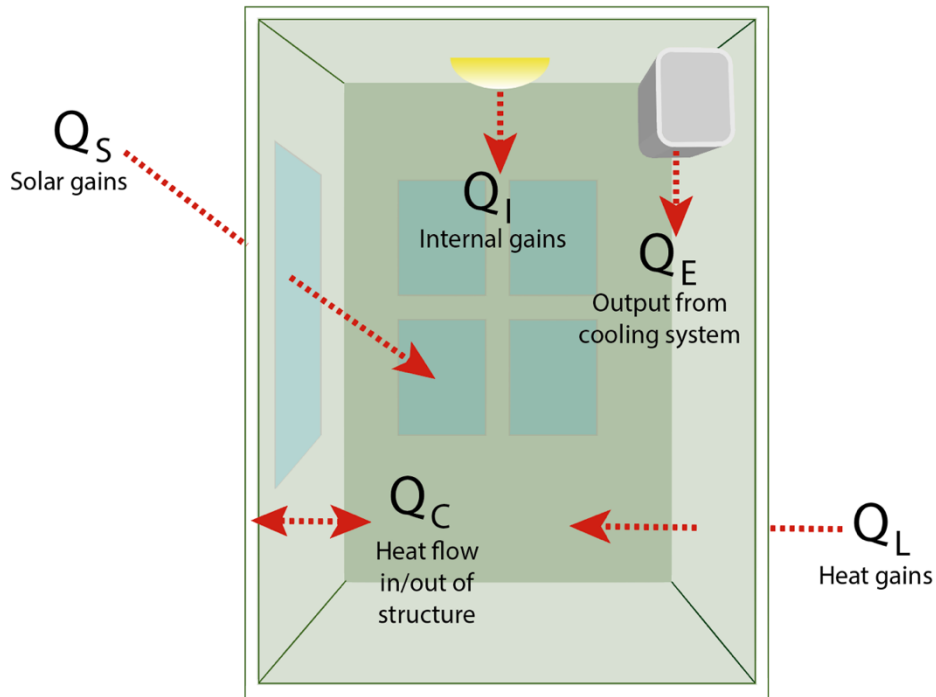
Figure 2-7*: The energy balance of an air-conditioned building, showing solar gains, internal gains, heat gains, output from cooling system and the heat flow in and out of the building structure. Redrawn from (CIBSE, 2006).*

2.5.2 GLOBAL TRENDS IN COOLING ENERGY

As the urban population numbers grow larger, living conditions improve and the economy continues to expand, an increase in energy demand associated with a growing number of households and businesses is inevitable. Energy consumption from space cooling in buildings increasing by nearly 60% between 2000 and 2010 and accounted for roughly 4% of total global buildings energy use in 2010. The cooling energy as a fraction of total energy demand of buildings is usually higher in OECD-countries (Organization for Economic Cooperation and Development) than non-OECD. The amount of cooling energy also depends on climate: in warmer climates, cooling accounted for as much as 10% of total energy use, while the cooling energy use in colder areas is typically less than 3%.

According to Waite et al. (2017), in a review of ten international cities, roughly half of building energy-related GHG emissions is associated with electricity generation to serve urban areas. Cooling energy use is also dependent on regional climates: in warmer climates, cooling accounted for as much as 10%

of total buildings energy use, while in cooler regions with greater heating demand, cooling is typically less than 3% of buildings energy consumption (IEA, 2013).

At the city-scale, heating, ventilation and air-conditioning (HVAC) may be of even greater significance as building energy use tends to dominate in urban areas. Cities generally have more limited opportunities for power generation. This energy demand may be intensified due to the urban heat island effect and tendency towards service-economy (the service sector will become increasingly important to the future economy of industrialized countries), which increases the relative share of air-conditioned commercial buildings (Waite et al., 2017). For example, in the United States, it has been shown that increases in air temperature can explain 5 – 10% of urban peak electric demand, with a typical rise of 2 – 4% for every 1 °C rise in daily maximum temperature over 15–20°C, and the use of air conditioning systems is expected to increase significantly in the near future (Antunes et al., 2015).

As the economy of developing countries and population incomes increase, urban households are predicted to consume more energy per capita, and trends point towards higher electricity usage (Waite et al., 2017). Regional climatology will also be a key driver in energy use, but subtle variations in consumption will be apparent depending on the availability of energy efficiency measures for passive cooling systems and building construction (Antunes et al., 2015).

Electricity demand in hot areas during summertime has shown to be more sensitive to temperature variations than the cooler urban areas. Leaky building envelopes, heat island effects and increasing urbanization will have large impacts on the peak electricity demands in emerging megacities. While the interrelated effects among these factors are complex, five structural variables that drive long-term building energy use have been identified: 1) population growth, 2) economic growth, 3) urbanization, 4) per-capita floor space, and 5) demand for building energy services. Furthermore, population, economy size and functions drive baseload electricity demand at annual to decadal timescales; climate drives seasonal variability; and human behavior, physiology and meteorology drive diurnal patterns (Waite et al., 2017).

A study performed by Waite et al. (2017) provided a baseline assessment of urban electricity demand for cooling and heating in 35 global cities in both OECD and non-OECD countries. Their results indicated a significant difference in cooling electricity requirements of OECD cities (35-90 W/°C/capita), as compared to non-OECD cities (2-9 W/°C/capita). However, the observed trends indicate the gradual (and in some cases rapid) adoption of air conditioning equipment in developing cities. Furthermore, non-OECD cities in cooling climates likely exhibit lower cooling electricity response than OECD cities because of low penetration of cooling equipment. Some non-OECD cities

are further along the development spectrum, and cities that experience very high temperatures already have high electricity demands for cooling (and heating). According to Waite et al. (2017), these cities are likely to experience significant increases in both annual electricity usage and peak electricity demands for thermal comfort in the future.

As stated by Antunes et al. (2015), the temperature associated shift of energy requirements from heating to cooling can bring about a series of challenges; oil and gas are traditionally used for heating, whereas electricity is used for cooling. As electricity has a tendency to be less efficient, and therefore more expensive, current estimates indicate that additional expenditure of energy on cooling in summer can outweigh winter energy savings. Furthermore, electricity also has higher CO_2 emissions per unit of consumption, meaning that the shift from heating to cooling could potentially further exacerbate climate change and global warming. However, if renewable energy continues to replace fossil fuels in the electricity mix, the CO_2 emissions per unit of consumption will be significantly reduced.

ELECTRICITY COSTS

Globally, space cooling is typically produced using electricity, although some regions use natural gas cooling equipment.
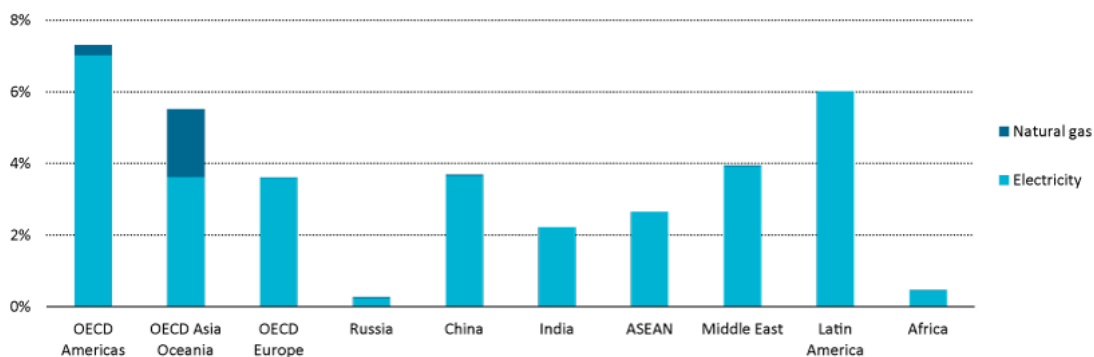
Figure 2-8*: Space cooling energy consumption in different global regions as a share of total building energy use in 2010 (IEA, 2013)*

Electricity costs will vary from country to country and also from one location to another within the countries. Costs also vary throughout the day; when the demand is high, the associated fuel demand increases. Consequently, fuel prices go up, resulting in higher costs to generate electricity. The cost related to the supply of electricity can change by the minute and will also vary among the different consumer groups; residential electricity prices are usually higher than for commercial and industrial consumers. Prices are determined by a number of factors, like cost of power generation in power plants, government subsidies, transmission and distribution infrastructure and industry regulation. Weather conditions will also affect the prices; rain and snow provide water for low-cost hydropower generation,

23

sunny conditions will increase productivity of photovoltaics and wind can provide cheap power generation from wind turbines when wind speeds are favorable. The selection of fuels to generate electricity is a main driver for electricity prices globally, and a country's electricity mix can consist of natural gas, renewable energy, petroleum products and coal. Additionally, CO_2 prices have increased significantly in recent years, and are likely to continue to rise in the near future. Extreme temperatures can also increase the demand for electricity for space cooling, and high demand can drive prices up. Moreover, electricity prices are usually highest during summer, when total demand is high because more expensive generation sources are added to meet the increased demand (EIA, 2018).

2.5.3 CHALLENGES OF MODERN BUILDINGS

Buildings inherently occupy two main climates: the land and the sky. The land climate has a relatively steady temperature that gradually fluctuates over the year following the annual temperature variations. The sky climate varies from one moment to another depending on the weather conditions, generally following the daytime and night-time temperatures determined by latitude, altitude, continental location and the sun. Because of this, buildings have evolved to take advantage of both climates to varying extent depending on location and the population's comfort requirements (Roaf et al., 2009).

One of the key climatic design problems of 'modern' buildings is that they are lightweight, thin, tight-skinned and air-conditioned, which makes buildings extremely vulnerable. Architectural design has turned away from the traditionally robust walls with reasonably sized windows, to glass-covered façades or thin cladding, which increases the vulnerability of building occupants to the external climate by an order of magnitude. As stated by (Roaf et al., 2009), "we have known for nearly 50 years that there is a problem with overglazed façades, and these problems will be exacerbated in a warming climate". Furthermore, (Roaf et al., 2009) explains that glass buildings with little or no shading have the potential to cause severe overheating, and this problem will become more severe as the climate gets hotter. The lack of insulation and thermal mass in these lightweight buildings will also impose huge energy penalties on building owners, as heating and cooling loads increases.

Another important design problem to consider is the height of the building: the taller the building, the more exposed it is to the sky climate. Wind speeds increase with height and more wind pressure on the envelope will extract heat from the structure. Also, the building will be more exposed to the sun during daytime, and the risk of overheating is high, especially for the heavily glazed façades. The height also largely affects the building's internal microclimate, and the natural buoyancy of hot air will cause the heat from the lower floors to rise. Consequently, the higher the building, the greater the problem of thermal stratification, which in turn increases the heating and cooling loads of buildings, especially in

the upper floors (Roaf et al., 2009). Moreover, high-rise buildings constitute a large part of the energy security problem, as their energy demand puts a heavy strain on the power grid and can threaten the energy supply of surrounding buildings, particularly in areas with weak power infrastructure.

2.5.4 PLANNING FOR ENERGY EFFICIENT BUILDINGS

Each year, 1-2 % of new buildings are added to the existing stock worldwide. Consequently, 87% of all the buildings in the world will have already been built by 2050 (Wilkinson and Dixon, 2016). In order to reduce GHG emissions from the building sector, the primary focus should be directed towards retrofitting and refurbishing existing buildings rather than constructing new ones (Hestnes and Eik-Nes, 2017). Many methods for increasing energy efficiency and reducing energy demand have been developed, and lately the concept of "zero emission buildings" have been brought to the agenda by researchers across the globe. According to (Roaf et al., 2009), the fabric of the building envelope (the physical separator between the inside and outside of a building) is the single most important part of the of low-energy building design. Furthermore, by looking at heat gains and losses, solar gain, windows, ventilation, temperature, humidity, wind speed, thermal mass, insulation, fabric performance and internal gains, buildings proved capable of being sensibly modified to remain habitable in a warmer future. In order to achieve the performance goals, buildings should have an appropriate form, have thermal mass, be naturally ventilated and shaded from the summer sun, and generate much of their own energy.

As previously stated, the low-carbon smart city intends to incorporate mitigation and adaptation measures to enable the city to respond to climate change through a well-planned and designed urban environment (Kim, 2017). An increasingly important aspect of the development of smart cities is the transition from single-function to multi-function infrastructure. Refurbishment can be hugely expensive, and some buildings are incapable of cost-effective demolition and should never have been built. Buildings should be designed with life cycle-thinking in mind, so that sustainability is considered in all phases of the buildings lifetime; planning, construction, operation and eventually demolition. Therefore, calculating the performance of buildings for future climates will become increasingly important. By developing climate models for buildings to test them against future climates, we can make decisions about planning and construction to best prepare the building performance for the future (Roaf et al., 2009).

2.5.5 ESTIMATING ENERGY USE: DEGREE-DAYS

Higher outdoor ambient temperatures will significantly influence energy consumption by increasing the demand for air conditioning. By definition, *degree-days* are based on the principle that energy balance is achieved when heat inputs into a building are equal to overall heat loss, resulting in no latent load (CIBSE, 2006). It is a measurement designed to quantify the weather-related energy demand for heating or cooling a building. The method is applied to new buildings as well as retrofitted/refurbished buildings and is used for energy monitoring and analysis based on historical data (Antunes et al., 2015).

Heat loss from buildings is directly proportional to the indoor-to-outdoor temperature difference. Therefore, the associated energy consumption of a heated building is closely related to the sum of these temperature differences over a given time period (usually 24 hours). The difference in temperature is between the outdoor air temperature and an indoor reference temperature, which is also referred to as the base temperature. The base temperature is based on the balance point temperature (BPT) – the outdoor temperature at which buildings can maintain comfort conditions without the use of heating or cooling systems.

As degree-days account for fluctuations in the outdoor temperature, the method eliminates periods when heating or cooling systems do not need to operate. Both magnitude and duration of extreme cold or warm events is considered, and consequently, the estimation of energy consumption is more reliable than mean temperature approaches. The degree-day approach assumes that all of the incidental gains can be averaged out over time to give some representative indoor temperature which relates to the cooling system contribution (CIBSE, 2006).
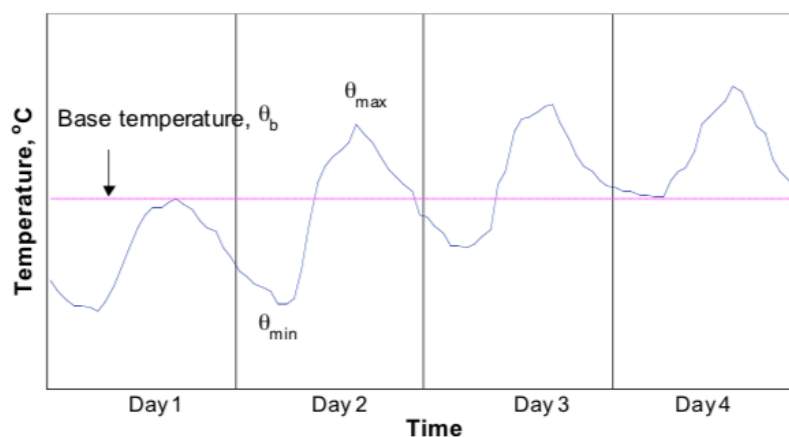
Figure 2-9*: In the case of cooling degree days, the maximum diurnal temperature (θ_{max}) is higher than the base temperature, which is the case for day 2 through 4 in the figure above (CIBSE, 2006).*

Degree-days are the integral of differences between outdoor temperatures and a specifically defined base temperature, denoted θ_b. For the case of cooling degree-days (CDD), the maximum diurnal temperature (θ_{max}) is higher than the base temperature, in which case the cooling degree-days is given by the total area between the two temperature curves. For heating degree-days, θ_{max} is less than the base temperature, as illustrated in Figure 2-9, and the calculation of degree-days needs to be able to handle situations for both heating and cooling (CIBSE, 2006).

DEFINING THE BASE TEMPERATURE

The base temperature for CDD is considered the outdoor temperature below which a building needs no cooling, and the base temperature depends on factors like the thermal properties of the building, cooling schedule and external influences like solar gains. Buildings have a lot of internal heat gains, which can provide a few degrees of additional heating to the building (Bromley, 2009). Base temperatures are calculated from the balance point temperature (BPT) and take into account building size, configuration and available cooling technology for the region in question. Consequently, in order to compensate for the use of outdoor temperature data in the analysis, base temperatures are often several degrees lower than the expected balance point. Furthermore, a range of comfortable temperatures exist, and for uninsulated buildings in the United States, the CDD have traditionally been calculated using a base temperature of 22 °C (Antunes et al., 2015).

2.5.6 COOLING TECHNOLOGY

Conventional space cooling technologies like air conditioners and chillers are standardized products in the residential sector throughout the world, and air conditioners have a high-power consumption rate. The largest markets for air conditioning units can be found in the hot and humid regions of Asia and the Pacific, followed by OECD Americas and OECD Europe (IEA, 2013).
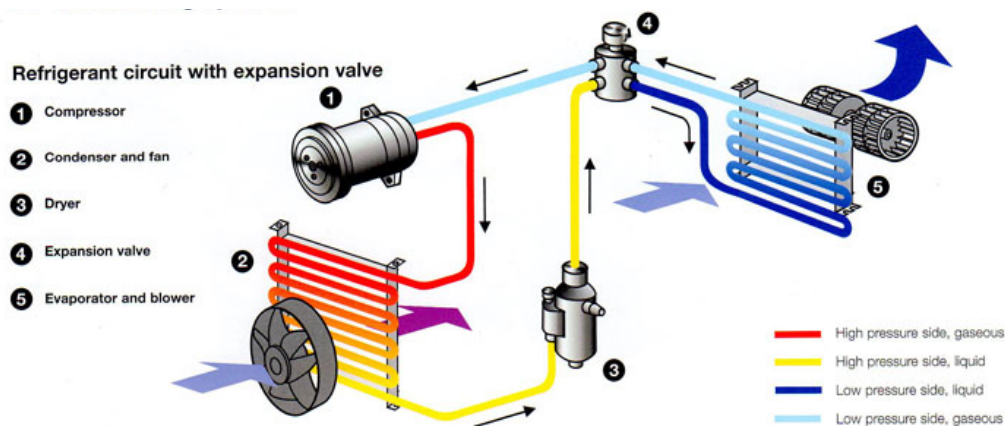
Figure 2.10: *Schematic of the vapor compression refrigeration cycle consisting of a compressor, condenser and fan, dryer, expansion valve and evaporator and blower (AutoInTheBox, 2017).*

The AC unit removes heat and moisture from the room where it is installed, and thereby improves the thermal comfort of residents. A vapor compression refrigeration cycle is the standard technology for air conditioning throughout the world. The four basic principles of the AC are compression, expansion, evaporation and condensation, and the AC system has specific components to employ the physical processes described in the schematic in Figure 2.10: 1) Low-pressure gas enters the high-pressure compressor, condensing it to a hot liquid. 2) The hot, high-pressure liquid is cooled by the fan (located outdoor), releasing excess heat. 3) The dryer extracts moisture from the refrigerant. 4) The expansion valve reduces the liquid pressure such that expansion occurs and rapidly reverts the liquid to vapor. Evaporation of the refrigerant cools the AC coils to extremely low temperatures. 5) A fan blows air across the coils, which contributes to lower the indoor air temperature (MeasureQUICK, 2017).

The required cooling capacity for a room air conditioner (AC) depends on the size of the room being cooled. Air conditioners generally have cooling capacities that range from 5,500 Btu/hour to 14,000 Btu/ hour. A common rating term for air conditioning size is the 'ton', which is 12,000 Btu/hour. Proper sizing is very important for efficient air conditioning. An oversized AC unit will cool the room(s) to the thermostat set-point before proper dehumidification occurs, making indoor climate uncomfortable for residents. A small unit running for an extended period operates more efficiently and is more effective at dehumidifying than a large unit. Based on size alone, an air conditioner generally needs about 70 Btu/h (or 23 W) for every square meter of living space. Other important factors to consider when selecting an air conditioner are room height, local climate, shading, and window size (Saver, 2018).

The efficiency of the air conditioning system depends on the coefficient of performance (COP), which is the efficiency ratio of the amount of cooling provided by a cooling unit to the energy consumed by the system. Air conditioner COPs usually range between 2.5 to 4.0 in most parts of the world, with COPs for small (2.2 kilowatt [kW] class) units approaching 6.0 in some countries. Today, most air conditioners operate at less than maximum efficiencies. Significant energy efficiency improvements can be accomplished through system optimization and design, as many systems are oversized due to a lack of detailed analysis of building cooling needs. Improved building design, correct sizing and optimal design of cooling systems will contribute to significant reductions in cooling energy demand (IEA, 2013).

2.6 COOL ROOFS

Promoting energy efficient technologies and initiatives as well as energy conservation in buildings is becoming one of the major concerns for the scientific community. In urban areas, building rooftops comprise a substantial fraction of the total land surface area, which means their physical properties are important determinants of the urban environment (Gaffin et al., 2006). As the transition from single-function to multi-function infrastructure becomes increasingly important to meet the future energy efficiency targets, building rooftops should also be exploited to serve several other purposes than their main function. One of the best and most cost-efficient passive solutions to reduce cooling loads in the building sector is cool roof technology (Anand et al., 2014). Cool roofs have a unique role to play in increasing the urban albedo and thereby improving the urban climate. Building integrated solutions related to lowering the cooling load of buildings are increasing in numbers, and a large-scale implementation of cool roofs offers an effective and affordable solution to some of the most important urban challenges we are faced with today. As many sustainable smart city strategies aims to reduce energy demand and increase urban sustainability through UHI mitigation, cool roofs could provide additional benefits to existing smart city schemes.

2.6.1 GEOENGINEERING

Geoengineering, sometimes referred to as climate engineering, describes deliberate and large-scale interventions in the Earth's climate system to counteract anthropogenic climate change (Shepherd et al., 2009). The term covers both solar radiation management (SRM), and carbon dioxide removal (CDR). Whereas the CDR methods aim to remove existing CO_2 from the atmosphere, the purpose of SRM methods is to reduce (and reverse) the climate changes resulting from a higher concentration of greenhouse gases (Caldeira et al., 2013). Solar radiation management (SRM) techniques aim to offset the warming caused by greenhouse gases and involves decreasing the amount of shortwave radiation absorbed by the Earth's surface by increasing the planetary albedo. Because SRM techniques act quickly, it would not take more than a few years to influence the local climate once deployed (Shepherd et al., 2009).

As the complexity of nature exceeds that of any human made climate model, it is important that the deliberate changes to manipulate the changing climate are sustainable, controllable and ultimately reversible in the case of unforeseen events. It should be noted that geoengineering is not a solution to continue the emissions according to the "business as usual"-model. Geoengineering should rather be considered an additional measure to reduce local temperatures on top of global-scale initiatives to reduce greenhouse gas emissions. Several methods of geoengineering have been suggested, like atmospheric

aerosol injections, space sunshades and marine cloud brightening, many of which are associated with controversy as the climatic and environmental consequences are currently unknown. Cool roofs, however, is considered a non-controversial and relatively harmless geoengineering method, and can be deployed in a sustainable, controllable and reversible manner. Brightening human structures, for instance by painting surfaces white, is now being recognized as an important passive strategy to mitigate urban climates.

2.6.2 THE COOL ROOF RETROFIT

Retrofitting buildings is now being recognized as an urban resilience strategy, and cool roofs create an adaptive capacity to deal with future environmental disturbances and climate change (Wilkinson and Dixon, 2016). As previously mentioned in section 2.3, the radiative surfaces move upwards from street level to roof tops when building density increases. Cities with vast areas of vacant roof tops offer good opportunities to mitigate climate change. The roof is the part of the building that experiences the maximum amount of solar radiation, and by exploiting the potential of these empty, dark-colored roof areas, we can implement cool roofs to moderate the temperature, reduce the urban heat island effect and increase the energy efficiency of buildings (Wilkinson and Dixon, 2016).
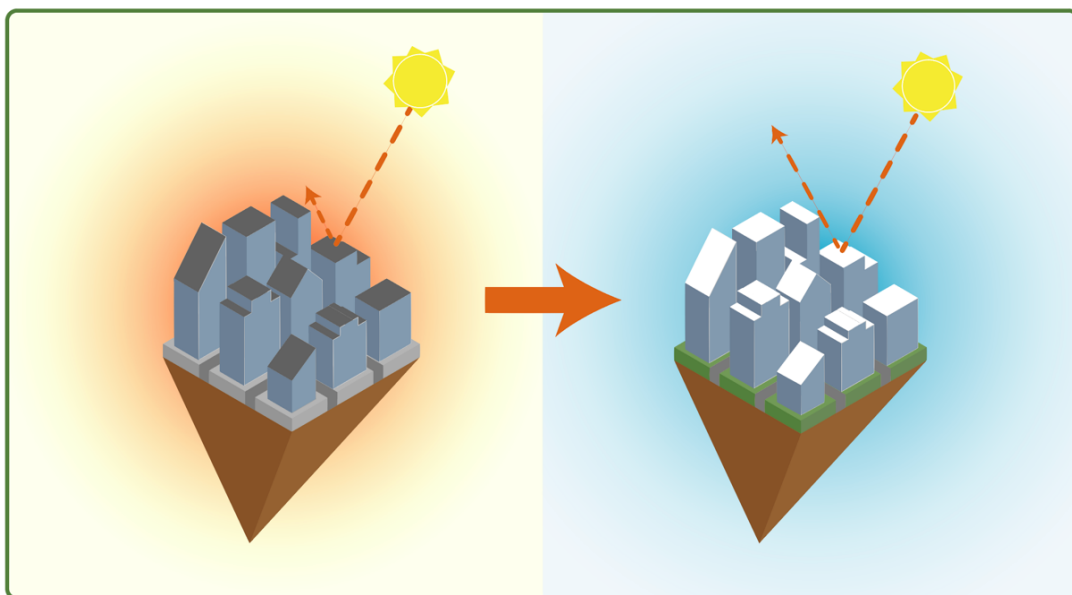
Figure 2-11*: The figure illustrates two urban scenarios: to the left is the conventional dark-colored city, with low-albedo rooftops that absorb the majority of solar radiation and heats the city. To the right is the retrofitted city, with a large-scale implementation of white roofs that has a cooling effect and contributes to increase the urban sustainability.*

In order to retrofit a building with a cool roof membrane, some technical and engineering considerations are needed prior to the installation, and urban cooling through roof retrofitting depends mainly on two factors: roof area as a proportion of a city's total horizontal surface area, and the proportion of roof

space available and suitable for retrofitting. Certain roof characteristics such as roof structure and overshadowing are important features to evaluate. Also, the orientation of the roof will deeply affect the amount of insolation on the roof surface; the more solar radiation the surface receives, the greater the decrease in temperature when covered with reflective materials.

A research project performed by Taha et al. (1992) indicated that high-albedo materials can potentially have a large impact on the temperatures of urban surfaces. On clear, sunny days, conventional roofing materials reached temperatures of about 40°C higher than the air, while the surface temperature of cool roofs were only about 5°C warmer. Furthermore, the researchers found that conventional roofing materials increased temperatures by an average of $0.055°C/(W/m^2)$, while cool roofs materials warm up by $0.015°C/(W/m^2)$ on average.

In order to design a full-scale research program for whitening cities, Taha et al. (1992) suggested that we need to understand the following key parameters:

- What is the typical urban albedo, and by how much can it be increased (from practical, visual, and climatic points of view)?
- What percentage of the urban surface is available for albedo modification?
- How much will albedos of light surfaces change because of weathering?
- What is the strength of the correlation between albedo modification and surface temperature changes?
- What are the related implementation issues such as cost, durability, maintenance, and public acceptability?

2.6.3 COOL ROOFS: FUNCTION AND BENEFITS

The main function of a cool roof is to provide a higher reflectivity and thermal emittance than that of conventional roofing. In addition to reducing the absorption and retention of heat, cool roofs offer a wide range of beneficial functions; they take on a temperature-moderating role, and ecosystem services that provide improved air quality and mitigation of the UHI effect. Other benefits, like improved energy savings, thermal comfort and aesthetics, and potentially increased property values can also be achieved by implementing white roofs (Wilkinson and Dixon, 2016).

In areas where the climate itself limits the opportunity of using vegetation as a temperature moderator, implementing white surfaces on the roof tops of buildings has proven to be an effective strategy for climate resilience and energy conservation. Conventional materials, like gravel, black synthetic rubber

and bituminous roofs contribute to excessive heating of buildings and surrounding air on hot sunny days (Wilkinson and Dixon, 2016). Thus, implementation of a cool roof membrane will reduce the surface temperature by reflecting more insolation. In return, many benefits are provided; lower exterior temperatures, reduced cooling loads and a more comfortable indoor environment, which can help reduce the need for power generation and lower GHG emissions associated with power production (Taha et al., 1992).

Whitening of external surfaces can prevent structural damage where conventional materials like asphalt has been used for roofing; asphalt tends to get very hot on sunny days, and white coatings can prevent it from melting and causing failure in the asphalt layer (Taha et al., 1992). The diurnal temperature cycles have clear implications for the durability and lifespan of the membrane. The conventional black membrane is undergoing enormous temperature variations, because of the extreme peak temperatures and extreme low night-time temperatures. These extreme and rapid diurnal temperature variations imply membrane expansions and contractions that are a major cause of rooftop deterioration over time. While the life expectancy of a conventional roof is about 20 years, the white membrane temperature cycle has a reduced amplitude which will likely contribute to membrane lifespan improvement (Gaffin et al., 2009).

By implementing reflective surfaces on roof tops of buildings, less energy is absorbed into the building envelope and cooling loads can be reduced. This has proven to be an effective energy conservation strategy, particularly in arid regions where soil conditions and water availability limit the potential for implementing vegetation to moderate temperatures and climate (Taha et al., 1992). Today, it is widely accepted that the higher reflectivity a roof has, the less solar energy is absorbed by the surface (Wilkinson and Dixon, 2016). Research suggests that high-albedo materials can save cooling energy by directly reducing the heat gain through the building surface (direct effect), and by reducing the temperature of the air surrounding the building (indirect effect). The combination of the direct and indirect effects of increasing roof top albedo suggest that city-wide applications of cool roofs can reduce peak cooling loads by $30-50$ %. Furthermore, by lowering the temperature of exterior building surfaces, a comfortable indoor environment can be achieved with a reduced cooling load. Consequently, the need for power generation goes down, with an associated reduction in emissions from power plants. A computer simulation done in Sacramento, CA, indicated that a change in overall urban albedo from an existing 0.25 to a white roof albedo of 0.40, can reduce peak cooling loads by 40 %. A similar study showed that a 1°C of air temperature reduction can result in electricity savings of 2-3% in most big mid-latitude cities (Taha et al., 1992).

According to Wilkinson and Dixon (2016) cool roofs will provide more benefits under some specific circumstances than others. For instance, energy savings are larger in older houses with little to no roof

insulation. Furthermore, research suggests that it is not the building type, but the cooling load of the building that determines the cooling potential of the roof; the larger the cooling load, the greater the benefit of the cool roof. Additionally, the potential for high-albedo roofing applications may be greater in arid cities, as vegetated areas are constrained by climatic limitations. Wilkinson and Dixon (2016) lists a number of circumstances in which cool roofs will be beneficial:

- In industrial buildings without heating or cooling.
- In buildings that mainly have a cooling load.
- In buildings with a large roof-to-total-surface area ratio.
- In buildings with roofs that are not overshadowed for more than 20% of the time.
- In buildings with roofs that have a pitch above 23° (mainly due to increased surface area).
- In buildings with solar photovoltaics (PVs): PVs are more efficient in a cold environment, and research indicates a 6.7% increase in electrical output of PV's when installed over a cool roof compared with an identical installation on a black roof.

By whitening other urban surfaces, for instance building walls and pavements, additional energy savings can be achieved from the reduced need for street lighting, as lighter surfaces require less illumination to make the visual environment comfortable at night (Taha et al., 1992).

2.6.4 COOL ROOF MEMBRANES

The passive cooling technology of cool roofs is now recognized as an effective and affordable method for mitigating the urban heat island effect and increasing energy efficiency of buildings. Although many different cool roof technologies exist today, the most commonly used are cool roof paints (CRPs) and highly reflective plies and membranes. This kind of treatment aims to reduce heat retention and the amount of heat transferred to the building below, which can result in a cooler and more constant temperature (Wilkinson and Dixon, 2016). Several studies have been conducted on reflective materials, and cool-colored roofing alternatives are developed with specially engineered pigments with a high reflectance of infrared wavelengths (EPA, 2008). However, substituting a conventional roof with a cool roof material involves a larger financial expense than does the CRP alternative when the roofing needs replacement (Wilkinson and Dixon, 2016). It is worth noting that CRP products need not necessarily be white, and even though some of them are dark-colored, they have albedos close to light-colored materials (EPA, 2008). With modern technology, cool roofs now come in a variety of colours and still provide a high solar reflectance because of the increased reflectivity in the infrared range of the spectrum. However, a dark-colored coating will never maintain the same amount of reflectance as a light-colored material (Wilkinson and Dixon, 2016).

The solar reflectance index (SRI) is often used in standards that specify cool roof requirements and incorporates both the solar reflectance and thermal emissivity of a roof membrane in one single value. The SRI determines how hot a surface would get relative to standard black and standard white surfaces: as such, SRI measures a material's ability to reject solar energy, based on a scale of 0 (standard black) to 100 (standard white) (Hao et al.). The EPA Energy Star Reflective Roof program have defined minimum performance standards for cool roofs, and a cool roof must have an initial solar reflectance value ≥0.65, and a three-year reflectance ≥0.50 as cool roofs deteriorate over time. Such cool roofs should also have a high thermal emissivity (≥0.90), but emissivity performance standards have not yet been defined (Gaffin, 2012).

Implementing white roofs is not a difficult task, and the entire building stock is expected to be refurbished within 65 years, with deep renovation occurring between 35 and 45 years in the life of a building (IEA, 2013). Moreover, as most buildings are painted or resurfaced about every ten years, it would be possible to paint them white or apply a coating/membrane when it is time for maintenance. This procedure should not require additional costs beyond the existing maintenance costs. For new buildings, the albedo of the roof tops could also be increased by incorporating highly reflective materials into the building codes (Taha et al., 1992).

2.6.5 MICRO-SCALE AND MESOSCALE EFFECTS

Although the effect of cool roofs on a global scale has proven limited, the potential for urban-scale implementation of high-albedo surfaces is great, as roof tops constitutes about 28% (global average) of the urban landscape (Jacobson and Hoeve, 2012). However, there are substantial differences in microscale and mesoscale benefits of implementing cool roofs on the urban heat island effect (Wilkinson and Dixon, 2016).

According to Wilkinson and Dixon (2016), a combination of green (vegetated) roofs and walls applied to a single urban block can create a "cool island" – a local area of lower surface and air temperatures. Yet applied to city scale, more general UHI mitigations benefits were achieved, as city-wide UHI results from a combination of heat production and/or retention at the micro and local scales. Although this was the case for green roofs, the study emphasizes an important difference between extreme variability of urban temperatures when measured at the microscale, and the relative consistency of these properties when averaged across the local neighborhood or the entire urban area. For these reasons, we cannot simply "scale up" findings at building or block resolution and draw conclusions about urban temperature reductions at city scale. According to Wilkinson and Dixon (2016), the simplifying assumptions

introduced to integrate scale-bound phenomena have been identified as the main cause of discrepancies in UHI results.

2.6.6 EFFECT ON BUILDING COOLING LOADS

Cool roofs have gained wide acceptance for their cooling potential: the higher the reflectivity of the roof, the lower the energy absorbed into the building and the lower the surface temperature of the roof (Wilkinson and Dixon, 2016). High-albedo materials can save energy used for cooling directly by reducing the heat gain through a building's envelope, but also indirectly by lowering the urban air temperature in the neighborhood of the building. Analyses of the direct and indirect effects have shown that major urban-scale changes in albedo can reduce peak cooling loads in many American cities by 30-50% (Taha et al., 1992). In a study by Konopacki and Akbari (2001), a cool roof-associated reduction in peak energy demand was calculated: compared with conventional black rubber membrane for roofing, a retrofitted white roof vinyl membrane produced an average decrease of 24°C in surface temperatures. An associated 11% reduction in energy consumption from aggregate air-conditioning was recorded, along with a 14 % drop in peak hour energy demand. In a similar study by Anand et al. (2014), cool roof membranes in residential buildings for various climatic conditions reduced the cooling loads by 18–93%, and peak cooling demand in air-conditioned buildings by 11–27%. Furthermore, an analytical quantification of cooling energy savings in commercial buildings indicated that cool roofs could potentially save energy ranging from 20-22 kWh/m^2 of cool roof area. This corresponds to a reduction in cooling loads of 14–26%.

2.6.7 LIMITATIONS AND CHALLENGES

EFFECT ON GLOBAL WARMING

Besides providing a number of beneficial functions, cool roofs can also present some environmental challenges. In a study performed by Jacobson and Hoeve (2012) on the local and global effect of cool roofs, they concluded that feedbacks of the local changes to the large scale resulted in a gross global warming of 0.07 K. However, the warming was smaller in magnitude than the UHI (temperature difference between urban and rural areas). A local ground cooling of cool roofs stabilizes the surface air, reducing vertical sensible and latent heat fluxes, reducing local cloudiness, increasing local surface solar radiation, which in turn offsets some of their local cooling benefits. A higher reflection from the urban surface increased air temperatures as a lot of the reflected radiation is absorbed by soot particles and dark pollutants in the atmosphere, resulting in a local cooling and global warming effect. However, the resulting feedback to temperature is minimal. Feedback effects of local changes to the global scale

is magnified at high latitudes over snow and sea ice, causing a net effect on globally averaged temperatures. Thus, white roofs may reduce temperatures locally but may or may not reduce overall global warming (Jacobson and Hoeve, 2012).

<center>PERFORMANCE DEGRADATION</center>

Over time, the performance of a cool roof will degrade due to accumulation of dust, pollution, biological growth and other substances that can change the overall albedo. Consequently, in order to ensure energy-savings over time, aged ratings are specified in policy programs. Recently, the cool roof strategy has included detailed roofing rating requirements that provide performance criteria of solar reflectance and thermal emittance after a roof sample has been aged (weathering tests in a variety of climates) for a specified period, often set to three years. Aged cool roofs of high quality can reflect 80% of the solar radiation compared to black roofs that reflect only 5% to 10% (IEA, 2013).

Gaffin (2012) examined the albedo performance of a number of cool roof coatings on an outdoor field site in California. They found that most of the multi-year albedo decline occurred within the first year, with an average albedo loss of 0.15, starting from an average initial albedo of 0.65. In the following years, the incremental decreases in albedo were small, and general coating maintenance returned the albedo values close to its initial value. Consequently, a periodical maintenance is recommended every 1-2 years in order to sustain the cool roof performance (Taha et al., 1992). Location can also have a large impact on the performance of cool roofs in various ways. Gaffin (2012) reported that the cool roofs membrane in a botanical garden showed evidence that leaf litter and vegetation debris from vegetation can significantly impact surface exposure and thus affect albedo and temperature performance. In addition, glare problems caused by highly reflective surfaces can lead to hazards and discomfort for people and animals. Therefore, high-albedo, darker-colored materials and low-glare colours should be considered before implementing a cool roof.

<center>HEATING PENALTIES IN WINTER</center>

The solar reflectance, emissivity, and thermal insulation are three parameters affecting roof heat flux. According to Hosseini and Akbari (2014), cool roofs can help reduce the heat flux penetration into a building, as less radiation is transformed into heat. A roof with a high infrared emittance will be cooler than a regular roof. During winter the absorption of solar radiation is lower, and a cool roof may increase the heating energy of the building. There have been many studies on this topic, with widely ranging conclusions. One study by Oleson et al. (2010) found that, in the annual average, white roofs increased winter space heating more than they decreased summer air conditioning. Another study showed that for cold climates with hot summers, a roof with high albedo and high emissivity is preferred as the heating penalty during the year is less important. The small winter heating penalties are small largely due to

<center>36</center>

high wintertime zenith angle, short days, increased cloud cover, and heating period (early in the morning and evening hours). In cold climates, the roof may be covered by snow during some months of the heating season and there would not be a significant difference in heating energy use of a building with a cool or conventional roof (Hosseini and Akbari, 2014). Most roofing materials have emissivities in the 0.85 range or higher, including many white membranes. Some research also suggests that lower emissivities can be desirable in colder climates to avoid any winter heat penalty (Gaffin et al., 2009).

In a study by Gaffin et al. (2009), the cool roof experienced a similar heat loss rate as the conventional roof. A possible reason for these unexpected results, was an emissivity difference between the two roof types at night. If the cool roof has a lower emissivity than the conventional, then the white roofs will be warmer at night when there is no sunlight and the atmospheric exposure is identical. Another contributing factor can be the underlying material of the cool roof membrane, which can have different thermal properties, resulting in a lower total emissivity of the roof.

2.6.8 GREEN ROOFS – THE SUPERIOR ALTERNATIVE?

In urban landscapes, impervious surfaces are gradually replacing green spaces as the city densifies, and few spaces remain for integration of new green areas on street level. Consequently, green roofs are being recognized as an effective urban climate resilience strategy, and many studies have established the correlation between an increase in green areas and local temperature reductions. Green roof properties like shading, evapotranspiration, absorption and insulation contribute to a reduction in transmission of heat through the roof. A conversion into green roofs on city-scale can bring about several benefits; effects on UHI, air quality, storm water management and biodiversity on urban scale; and increase in life span of building materials underneath the soil and reduction in noise (Susca et al., 2011). Another recognized benefit of greens roofs is their ability to conserve the heating and cooling energy of buildings, and thereby reduce the amount of waste heat from air conditioning. As with cool roofs, these benefits are strongest in poorly insulated buildings. Greening of urban rooftops have other benefits as well; not only can they serve social and recreational purposes as green oases and gardens, they can also be used for food production and habitat conservation to promote biodiversity and secure endangered flora (Wilkinson and Dixon, 2016).

COOLING PERFORMANCE

In a comparison between green and cool roofs, the surface temperature clearly shows that green roofs stay much cooler. In a research project by the University of Melbourne, scientists performed experiments on test buildings in order to compare the effect of different types of roofings; green, white and control roofs. When comparing the different roof types, the internal temperature conditions between

white and green roofs varied by around 3 °C on a 35 °C day. Both the green and white roof retrofit contributed to an internal temperature reduction; the white by up to 4 °C, and green up to 7 °C. Green roofs also have the tendency to keep internal temperatures higher at night because of the added thermal mass the green roof provides. This results in a reduced night-time comfort and cooling during summer but provides benefits during wintertime. Furthermore, the amount of reflected radiation is larger from the white retrofitted roof, while for green roofs radiation is being absorbed by the plants during the process of photosynthesis instead. Thus, green roofs have an increased performance of reducing the impact of roof surface on the UHI effect, whereas cool roofs have an impact by reduced heat retention and absorption of insolation (Wilkinson and Dixon, 2016).

COST AND MAINTENANCE

When comparing cost, green roofs are substantially costlier than cool roofs. Where financial matters are the major decision point, cool roofs may be preferential. Prices for green roofs varies from 108-2368 $/m^2, averaging at 173 $/m^2. For cool roofs, prices for different types of roofing will vary a lot, but the average price for the CRP alternative is 22 $/m^2. With regards to maintenance aspects, green roofs will need more tending to than a simple white roof. Green roofs also have larger structural requirements that must be considered before implementation than do white roofs. Water availability for irrigation in dry climates can also present challenges, even though low-maintenance water preserving species like *sedum* is used. In conclusion, cool roofs are generally preferred over green roofs in cases of significant aspects of cost, maintenance, water availability, structural load and roof pitch (Wilkinson and Dixon, 2016).

3. Methodology and data

In this chapter, the methodology and modelling procedures are described, along with an explanation for selection of data for the study. The majority of these procedures are conducted using MATLAB.

3.1 Methodology

3.1.1 The 1-D bulk urban canopy model

The main target was to investigate the effects of changes in rooftop albedo on the urban heat island effect in idealized, homogenous, geometrically identical big cities in different climate zones. The 1-D bulk urban canopy model (BUCM) combined with a 1-D atmospheric layer model was developed by Sorteberg (2017) which is heavily based on the urban canopy model developed by Wouters et al. (2016), where a semi-empirical urban canopy parametrization (SURY) for atmospheric modelling is described. SURY introduces an efficient dependency of bulk urban land-surface schemes on the urban canopy parameters using bulk radiative and thermal parameters. The different components of the bulk urban substrate are roofs, walls, roads, paved surfaces, bare ground and vegetation.

The urban canopy parameters that is used for input in the model include the canyon height-to-width ratio, building height, roof fraction, short-wave albedo, thermal emissivity, heat conductivity and heat capacity. The output parameters are the bulk albedo, bulk emissivity, aerodynamic and thermal roughness length and vertical profiles of the bulk heat conductivity and heat capacity. The methodology delivers theoretical and empirically verified robustness based on detailed urban observational and modelling experiments. The translation of urban canopy parameters into bulk parameters is based on the physical processes like heat transfer from the ground, the surface radiation exchanges and the surface layer turbulent transport for momentum, heat and moisture (Wouters et al., 2016)

The radiative bulk parameters accounts for the albedo reduction factor, which results from the trapping of radiation by the urban canopy. Below the surface, the urban substrate layer with a thickness equal to the building height is considered for representing the thermal mass of the urban canopy in contact with the natural soil below. The urban heat islands in this method occur at the scale of the cities and magnitude increases with city size. Excess conversion of solar radiation into sensible heat is taking place in cities at daytime. The excess heat is partly stored into the urban canopy, which leads to day-time excess land-surface temperatures (Wouters et al., 2016).

Figure 3-1 illustrates the layout of the urban canopy model and provides an overview of the components and programs involved in the process. A complete description of the urban canopy model and associated

equations along with a list of model input, boundary conditions and output can be found in Appendix A1-A3.

The canopy layers describe the temperature changes into the idealized bulk urban canopy substrate (consisting of the thermal properties of the roofs, walls roads, paved surfaces, bare ground and vegetation), and not the air temperature as the layers move down into the canopy. Due to this idealized bulk urban canopy substrate approach it is the first canopy layer is the one that will provide implications for the urban temperature. Consequently, this is the layer of interest in this study. Below the canopy layers are the ground layers, which is the bulk soil temperature under the roads, houses and vegetated areas in the urban environment (Sorteberg, 2017). The atmospheric layer that is considered in this thesis stretches from the canopy surface and 40 meters up. Under the atmospheric levels are the canopy and urban layers, that stretches 0.015 meters from the canopy surface and down into the idealized canopy substrate. By making the first canopy substrate layer very thin, we can assume that the temperature of the canopy surface is given by the temperature of the first canopy layer. The canopy layer differs from the urban layer in the fact that a slight mixing with the rural air have been accounted for in the urban layer.
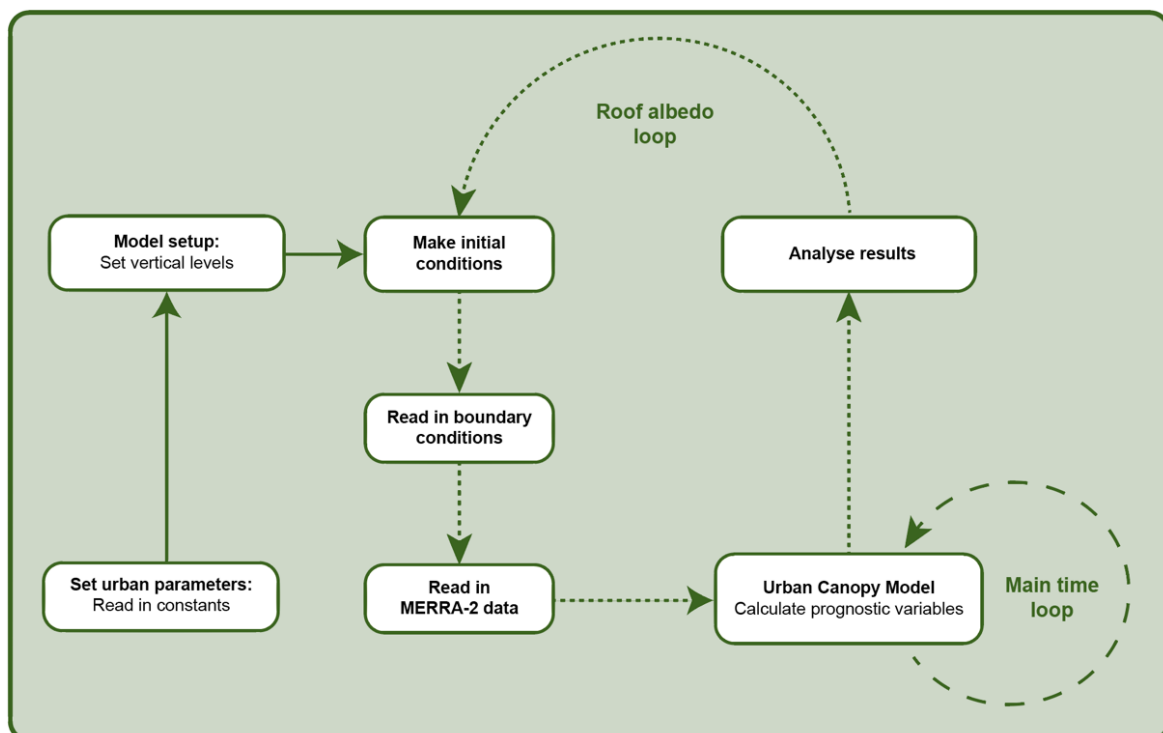
Figure 3-1*: Flow chart illustrating how the urban canopy model works by showing the connection between the different programs used to build the urban canopy model in MATLAB. Under initial conditions, the albedo for conventional and white roofs are given, and the program loops through the entire program with the two given albedos.*
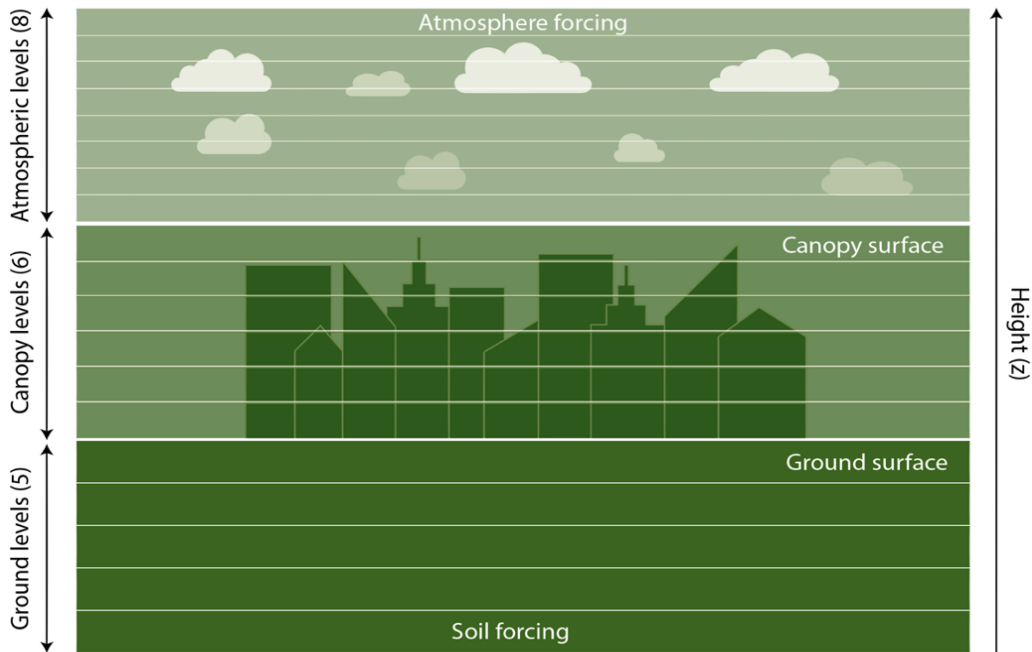
Figure 3-2*: The three main vertical levels of the urban canopy model: atmosphere, canopy and ground, divided into 8, 6 and 5 layers, respectively. The model setup is given by the boundary values at the top (atmosphere forcing) and bottom (soil forcing). The surface of the canopy and ground levels are also indicated on the figure.*

The urban canopy model is divided into three main vertical sections, as illustrated in Figure 3-2; atmospheric, canopy and ground, which in turn is divided into eight, six and five layers, respectively. The model setup is given by the boundary values at the top (atmosphere forcing) and bottom (soil forcing). The model is forced with prescribed atmospheric winds and temperatures at the top and prescribed soil temperatures at the bottom.
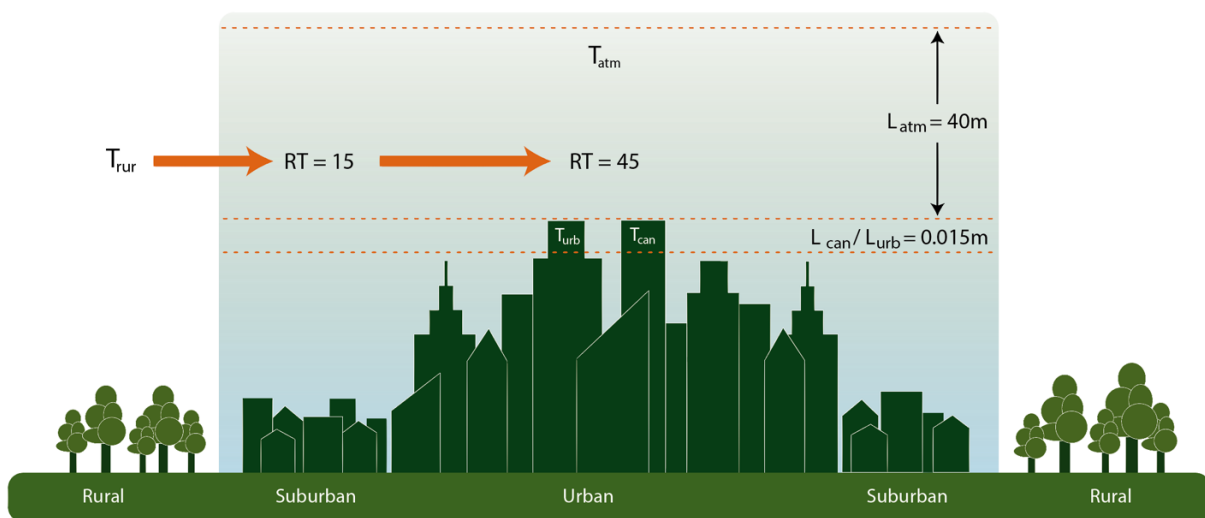
Figure 3-3: *Schematic of how the different layers in the urban and suburban areas respond to influence from the rural areas, which is modelled through relaxation time of 15 and 45 minutes. The three layers considered are the canopy (L_{can}), urban (L_{urb}) and atmospheric (L_{atm}). The corresponding temperatures are marked as T_{can}, T_{urb} and T_{atm}.*

41

The atmospheric model is a turbulence model assuming similarity theory and an advection term where the urban temperature is relaxed toward the rural temperature with a fixed time scale, as illustrated in Figure 3-3 (Krayenhoff and Voogt, 2010). The relaxation time depends on the local wind speed and distance to the urban-rural boundary that is being modelled. In this study, two different relaxation times are considered (15 and 45 minutes), corresponding to the outer urban areas (suburbs) and the central urban area. For a more comprehensive description, see Appendix 1, section A1.10.

The temperature at the top of the substrate is calculated using the energy balance with an effective volumetric heat capacity (C_{can}). Consequently, the heat flow into the canopy substrate is given by conduction, which is the heat flow into buildings and other urban surfaces. By calculating the temperature for a thin slab of the canopy with thickness $d_{can,1}$, the urban canopy surface temperature can be obtained. The following statement of urban canopy energy balance is expressed in terms of seven energy fluxes and the effective volumetric heat capacity:

$$C_{can,1} d_{can,1} \frac{\partial T_{can,1}}{\partial t} = (1 - \alpha_{can}) SW_{sky}^{\downarrow} + LW_{sky}^{\downarrow} - LW_{can}^{\uparrow} - H_{can} - LE_{can} - G_{can,1,2} + Q_{ant} \qquad [\text{Eq. } 3-1]$$

The term on the left-hand side of the equation is the rate of change of the heat content of the upper urban canopy layer (layer 1), while the right-hand term states the energy balance. The seven energy flux terms needed to describe the surface energy balance of urban areas are: net shortwave radiation ($(1 - \alpha) SW_{sky}^{\uparrow}$) (downwards and reflected upwards expressed in same term by the albedo, α), longwave radiation downwards ($LW_{sky}^{\downarrow}$), longwave radiation emitted upwards ($LW_{can}^{\uparrow}$), sensible heat (H_{can}), latent heat (LE_{can}), conduction of heat from the upper canopy layer to the layers below ($G_{can1,2}$), and anthropogenic heat (Q_{ant}). If the right-hand side is positive, the roof layer is gaining more energy per time unit than it is losing.

3.1.2 MODELLING ENERGY DEMAND OF BUILDINGS

For modelling the weather-related energy demand and consumption of buildings, a simple degree-days approach was chosen, based on mean degree-hours. The model was set up according to Figure 3-3.
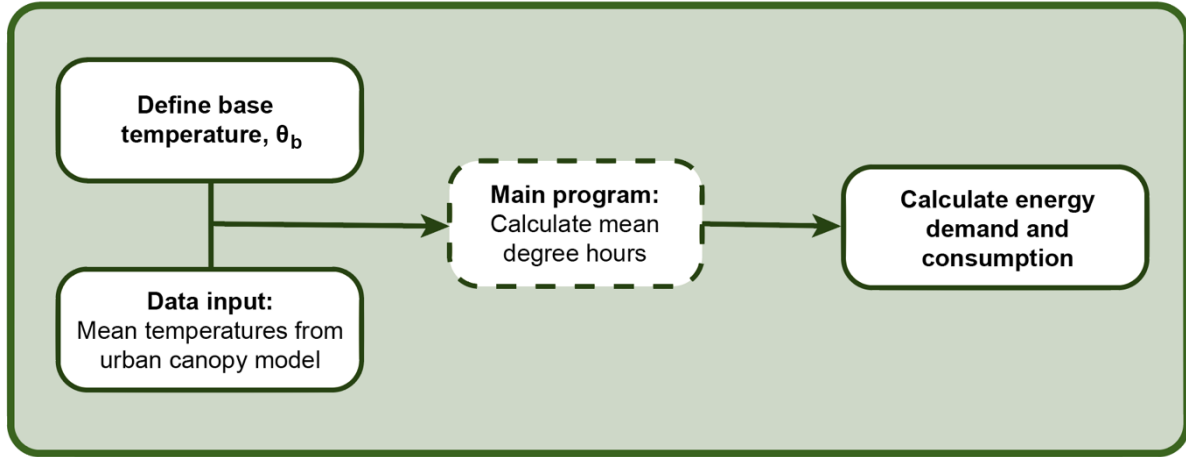
Figure 3-4*: Program for calculating cooling degree-days and the associated energy demand and consumption.*

COOLING DEGREE-DAYS

A simple degree-days approach was chosen for energy estimation purposes in this thesis. The most accurate method for estimating cooling degree-days (CDD) is the use of mean degree-hours, and as the MERRA-2 data provides hourly temperatures, this is the method that was utilized. According to the mean degree-hours method in CIBSE (2006), CDDs can be estimated according to three simple steps:

1. Subtract the base temperature from hourly outdoor temperature
2. If the hourly outdoor temperature is lower than the base temperature, the value is set to 0.
3. Sum up all positive values

The general formula for calculating cooling degree-days are given by (CIBSE, 2006):

$$DD = \frac{\sum_{j=1}^{24}(\theta_b - \theta_{o,j})}{24} \qquad if\ (\theta_b - \theta_{o,j}) > 0 \qquad [Eq.\,3-2]$$

Where DD is the degree-days for each day, θ_b is the base temperature and $\theta_{o,j}$ is the outdoor temperature for hour j. Only positive values should be summed as the only values of interest are those that lead to cooling requirements.

The daily cooling degree-days (CDD) were summed over the entire summer period of 92 days according to the equation:

$$CDD = \sum_{i=1}^{92} DD \qquad [Eq.\,3-3]$$

IMPLICATIONS FOR ENERGY DEMAND AND CONSUMPTION

For determining the building cooling load and energy consumption, the calculation depends on the cooling system used. An all-air air-conditioning system is assumed, and the energy demand can be calculated by multiplying the CDD with the mass flow and specific heat of the air, and then dividing by the coefficient of performance (COP) of the AC unit. According to CIBSE (2006), the energy demand (Q_C, kW) can be calculated according to this equation:

$$Q_{C_{kW}} = \frac{\dot{m} \cdot C_p \cdot CDD}{COP} \qquad [Eq.\,3-4]$$

$\dot{m}$ denotes the mass flow rate of air that is cooled per second (kg/s) given by the cooling capacity of the AC unit, and C_p is the specific heat of air (kJ/kg K). The equation indicates that the cooling energy consumption is proportional to the CDD.

For calculating the energy consumption (kWh), the demand should be multiplied by time t (the number of hours a day the cooling system needs to operate). Then the equation becomes:

$$Q_{C_{kWh}} = \frac{\dot{m} \cdot C_p \cdot CDD \cdot t}{COP} \qquad [Eq.\,3-5]$$

The mass flow rate ($\dot{m}$) was determined based on the following equation (CIBSE, 2006):

$$\dot{m} = \frac{Cooling\ capacity}{C_p \cdot \Delta T_{design}} \qquad [Eq.\,3-6]$$

Where the cooling capacity (kW) of the AC unit is divided by the product of specific heat of air (kJ/kg K) and the number of degrees (K) cooling reduction required for thermal comfort. The temperature difference (ΔT_{design}) is the cooling reduction required for thermal comfort, and for calculation purposes this usually ranges between 4-10 K, and $\Delta T_{design} = 8$ K will be used for the purpose of this thesis (CIBSE, 2006).

The temperature dependent coefficient of performance (COP) for cooling was determined by digitalizing Figure 14 in (Winkler, 2011), which can be found in Appendix 5, Figure A5-1. The resulting equation was

$$COP = -0.0756\,\bar{T}_{urb} + 6.18 \qquad\qquad [Eq.\,3-7]$$

Where $\bar{T}_{urb}$ is the mean temperature of the urban layer over the entire period for each city, and four different values of $\bar{T}_{urb}$ was used for conventional and cool roofs with RT15 and RT45.

For calculating costs of the energy consumption, the following equation was used

$$Cost = Q_c \cdot cost\ of\ electricity\ (\$) \qquad\qquad [Eq.\,3-8]$$

The implications for electricity costs relative to the purchasing power parity (cost percentage of GDP/capita) was calculated according to:

$$Cost_\% = \frac{Cost}{GDP/Capita} * 100 \qquad\qquad [Eq.\,3-9]$$

3.2 Data selection

3.2.1 The 1-D bulk urban canopy model

MERRA-2, also known as the Modern-Era Retrospective analysis for Research and Applications, is an atmospheric reanalysis data product by NASA. The data set, which originates from 1980, has a resolution of 0.5° x 0.625° longitude-by-latitude grid, and a vertical grid of 72 model layers, or 42 standard pressure levels. It provides an enhanced use of satellite observations from MERRA, and includes more aspects of the earth system, providing a broader spectrum of the assimilation system. All collections of MERRA-2 contains variables that define the dimensions of longitude, latitude and time (Bosilovich, 2016).

As global warming intensifies, average year-round temperatures will increase, and both winter-time and summer-time temperatures is predicted to increase. Many studies have shown the potential impacts of changing climate on heating and cooling energy demands, and Meng et al. (2017) found that the dry bulb temperature (DBT) is the dominant climatic factor affecting office building heating and cooling loads in all of the climate zones studied. While the summer cooling demand increase significantly with the warming climate, heating loads have shown a decreasing trend under continuous warming over the past 50 years (Meng et al., 2017). Therefore, I have chosen to only focus on the three summer months for each of the selected cities; June, July and August (JJA), as these are likely to experience high temperatures and increase in energy demand.

1-hourly time-averaged single-level data was downloaded from the NASA Earthdata website for a five-year time period, covering the years from 2013 to 2017. The three summer months, June, July and August, were selected, and an hourly average was taken over the three months of the five years. The variables downloaded for each of the selected cities is listed in Table A1-1 in Appendix 1 and was used as input for the urban canopy model described in section 3.1.

Cool roof material

Gaffin (2006) estimated the 'equivalent albedo' – the albedo needed on a cool roof to reproduce the cooling effect observed on a green roof. The model calculated an equivalent albedo in the range 0.7–0.85. The Cool Roof Rating Council have defined typical values for albedo and emissivity for standard black and white roofs as can be seen in Table 3-1 (Hao et al.). The values for the standard white roof are also within the range of the equivalent albedo, and as a result, these are the input values used in the urban canopy model.

Table 3-1: Standard roofing materials for buildings, with the two types of membrane and their associated albedo and emissivity. Both membranes have high emissivities, while the black membrane have a significantly higher albedo than the white (Hao et al.)

ROOF MEMBRANE	ALBEDO (α)	EMISSIVITY (ε)
Standard black	0.05	0.9
Standard white	0.8	0.9

RELAXATION TIME

As previously stated, the relaxation time of 15 minutes corresponds to the outer areas of the city column, often characterized by suburbs. These areas are slightly more affected by the surrounding rurals than are the central city area, with a relaxation time set to 45 minutes. This is illustrated more comprehensively in Figure 3-3.

CLIMATE ZONES

Cities in different climate zones were selected based on the Köppen-Geiger climate classification system, illustrated in Table A4-1, Appendix 4, with a geographical distribution of the climate zones illustrated in Figure A4-2. It should be noted that climate zones are dynamical and evolve over time as local, regional and global climates change.
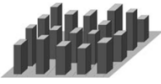
The heaviest populated and densest cities chosen for this study is located in climate zones that have the greatest potential to benefit from cool roofs, based on the literature reviewed in chapter 2. I have chosen cities from four of the five main climate groups: A (tropical), B (arid), C (warm temperate) and D (snow). Although warm, arid regions might have the greatest cooling potential from this kind of retrofit, it will also be interesting to compare these regions with areas that have colder and more humid summers.

LOCAL CLIMATE ZONES (CLZ)

A local climate zone system was developed by Stewart and Oke (2012) due to the lack of a universal definition of physical structure, surface properties or thermal climate for urban areas. They defined different local climate zones (LCZ) based on measured and estimated values of geometric, thermal, radiative, metabolic, and surface cover properties that were gathered from urban and rural field sites

worldwide. Local climate zones were formally defined as regions of uniform surface cover, structure, material, and human activity that span hundreds of meters to several kilometers in horizontal scale. Each LCZ is named and ordered by one or more distinguishing surface properties, which in most cases is the height/packing of roughness objects or the dominant land cover. The landscape universe consists of 17 standard LCZs, where 15 are defined by surface structure and cover and two by construction materials and anthropogenic heat emissions. The standard set is divided into "built types" and "land cover types". For this study, *LCZ 1: compact high-rise* was chosen as it best covers the characteristics of densely built urban areas. Tables 3-2 and 3-3 summarizes the characteristics and input values of a compact high-rise city.

Table 3-2: Characteristics of the compact high-rise local climate zone, and the input values of thermal, radiative and metabolic properties. All values are representative of the local scale (Stewart and Oke, 2012)..

LOCAL CLIMATE ZONE (LCZ)	BUILT TYPE	DEFINITION	SURFACE ADMITTANCE[A]	SURFACE ALBEDO[B]	ANTHROPOGENIC HEAT OUTPUT[C]
1. Compact high-rise		Dense mix of tall buildings to tens of stories. Few or no trees. Land cover mostly paved. Concrete, steel, stone, and glass construction materials.	2620	0.22	150

[A] Ability of surface to accept or release heat ($Jm^{-2} s^{-1/2} K^{-1}$). Varies with soil wetness and material density.
[B] Ratio of the amount of solar radiation reflected by a surface to the amount received by it. Varies with surface color, wetness, and roughness.
[C] Mean annual heat flux density (Wm^{-2}) from fuel combustion and human activity (transportation, space cooling/heating, industrial processing, human metabolism). Varies significantly with latitude, season, and population density.

Table 3-3: Values of geometric and surface cover properties for the compact high-rise local climate zones. All properties are unitless except height of roughness elements (m) (Stewart and Oke, 2012).

SKY VIEW FACTOR[A]	ASPECT RATIO[B]	BUILDING SURFACE FRACTION[C]	HEIGHT OF ROUGHNESS ELEMENTS[D]
0.22	2.5	0.6	25

[A] Ratio of the amount of sky hemisphere visible from ground level to that of an unobstructed hemisphere
[B] Mean height-to-width ratio of street canyons (LCZs 1–7), building spacing (LCZs 8–10), and tree spacing (LCZs A–G)
[C] Ratio of building plan area to total plan area
[D] Geometric average of building heights (LCZs 1–10) and tree/plant heights (LCZs A–F) (m)

In order to determine the response of cool roofs to different climates, heavily populated cities in climate zones located in the northern hemisphere were selected. A high population density has been important in the selection process, as denser cities tend to have a higher intensity of anthropogenic heat and consequently the urban heat island effect can be more prominent (Yang et al., 2017). I have chosen to work with the cities listed in Table 3-4, as these are big, dense cities located in climate zones with potential to benefit from cool roofs. The geographic distribution of the cities is depicted in Figure 3-5.

Table 3-4: Selected cities and main geographic and demographic characteristics. For simplicity, values have been rounded to the nearest 10. (Data collected from Köppen-Geiger (, WPR (2018) and Geoplaner (2018)).

CITY (COUNTRY)	CLIMATE ZONE (GEOGRAPHY)	LOCATION (LAT/LON)	ELEVATION (m)	POPULATION (MILLION)	AREA (km²)	POPULATION DENSITY (/km²)
Cairo (Egypt)	BWh (inland)	30°2' N, 31°14' E	18	19.8	610	32,600
Chicago (USA)	Dfa (inland)	41°50' N, 87°41' E	240	2.7	230	11,700
Delhi (India)	BSh (inland)	28°36' N, 77°13' E	229	18.6	1,480	12,500
Rome (Italy)	Csa (inland)	41°54' N, 12°30' E	64	3.8	1,290	2,900
Singapore (Singapore)	Af (coastal)	1°17' N, 103°50' E	58	5.6	720	7,800
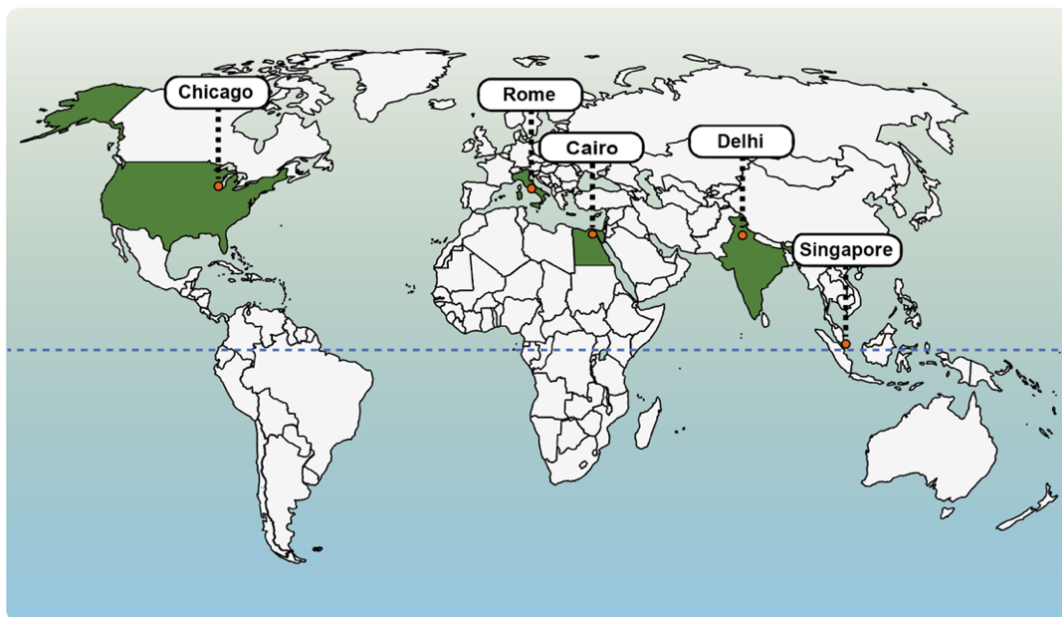
Figure 3-5: The geographic distribution of the cities in this study.

3.2.2 ENERGY DEMAND

SELECTION OF BASE TEMPERATURE

Antunes et al. (2015) lists a wide range of base temperatures used for calculation of CDD, ranging from 18 °C and 28 °C. The median of these values of 22 °C was chosen as the base temperature for this study. The same base temperature has been used for all cities, in order to compare the energy demand response to temperature in cities of each climate zone.

INPUT DATA FOR ENERGY CALCULATIONS

The urban canopy model does not calculate the near-surface temperature, but rather the temperature 40 meters above the urban canopy and the temperature in a thin layer below the canopy surface. Due to the small thickness (0.015 meters) of this layer, the temperature is very close to the canopy surface temperature. The temperature of the urban layer (T_{urb}) has been utilized for the degree-days calculation, as this accounts for a small amount of mixing with the atmospheric air.

The COP is temperature dependent and was calculated using the mean urban layer temperature for each of the energy calculations. An electrical all air air-conditioning unit of about 12,000 BTU (3,517W) is assumed, which is a typical cooling capacity value for a standardized AC unit (CIBSE, 2006). For determining energy consumption, an occupancy period of 12 hours was assumed. The input values for all energy calculations are given in Table 3-5. An overview of the electricity prices used for the calculations are provided in Table 3-6.

Table 3-5*: The input values for the energy calculations*

INPUT	SYMBOL	VALUE
Base temperature (θ_b)	°C	22
Outdoor temperature	°C	T_{urb}
Cooling capacity	W	3,517
Mass flow rate of air ($\dot{m}$)	kg/s	Calculated (Eq. 3-6)
Specific heat of air (C_p)	(kJ/kg K)	1.006
Coefficient of performance (COP)	-	Calculated (Eq. 3-7)
Occupancy period	h	12
ΔT_{design}	°C	8
$\bar{T}_{urb}$	°C	See mean T_{URB} in Table 4-1 and 4-2

Table 3-6: Overview of the electricity prices (US$/kWh) for each city/country (Statista, 2018, Ceicdata, 2016).

CITY/COUNTRY	US $ / kWh
Cairo / Egypt	0.02
Chicago / USA	0.21
Delhi / India	0.08
Rome / Italy	0.29
Singapore / Singapore	0.22

Table 3-7: Overview of GDP/capita (US $) for each city/country in 2016 (Worldbank, 2016)

CITY / COUNTRY	GDP / CAPITA (US $)
Cairo / Egypt	3,478
Chicago / USA	57,638
Delhi / India	1,710
Rome / Italy	30,669
Singapore / Singapore	52,963

4. RESULTS AND DISCUSSION

In the following chapter, the results and discussion are presented together for the convenience of the reader. The chapter is divided into two main parts; the first part considers the results and their significance for the urban heat island effect, while the second part examines the associated implications for cooling energy demand. An overview of general trends will be provided before the results of each individual city is presented and discussed more comprehensively. A comparison and interpretation of the similarities and differences between cities will ultimately be described. As a reminder, all results are based on the assumption that the summer months (JJA) are treated as one period. Therefore, the entire summer period is accounted for in the results and discussion presented in this chapter.

4.1 EFFECT OF COOL ROOFS ON URBAN HEAT ISLANDS

Note that the timeline for the mean 24-hour plots are in coordinated universal time (UTC) times and not local time. I therefore base the time of mid-day of each city on the time for peak incoming solar radiation. The other variables will be discussed relative to the time of the solar noon. Since the temperature of the canopy layer and urban layer are nearly identical, only the urban layer will be considered for discussion purposes.

4.1.1 GENERAL TRENDS IN COOL ROOF RESPONSE

Table 4-1: *The temperatures before and after implementation of cool roofs for the urban canopy layer (T_{urb}) and the first atmospheric layer (T_{atm}) for each city in °C. The relaxation time set to 15 minutes.*

CITY	α_{roof}	T_{URB} (°C)			T_{ATM} (°C)		
		Max	Min	Mean	Max	Min	Mean
Cairo	0.05	46.2	22.8	34.0	44.7	22.3	33.1
	0.80	42.5	22.7	32.6	41.7	22.3	32.0
Chicago	0.05	35.0	16.2	26.1	34.0	15.7	25.4
	0.80	31.4	16.1	24.9	31.0	15.6	24.4
Delhi	0.05	51.9	28.8	36.7	50.4	28.2	35.9
	0.80	48.2	28.7	35.5	47.3	28.1	34.9
Rome	0.05	42.6	16.5	29.4	41.1	16.2	28.6
	0.80	38.6	16.5	28.0	37.8	16.2	27.4
Singapore	0.05	35.7	27.4	31.2	34.7	27.1	30.6
	0.80	32.8	27.3	30.4	32.3	27.1	29.9

Table 4-2: The temperatures before and after implementation of cool roofs for the urban canopy layer (T_{urb}) and the first atmospheric layer (T_{atm}) for each city in °C. The relaxation time set to 45 minutes.

CITY	α_{roof}	T_{URB} (°C)			T_{ATM} (°C)		
		Max	Min	Mean	Max	Min	Mean
Cairo	0.05	52.5	24.8	38.1	51.2	24.4	37.3
	0.80	46.3	24.7	35.6	45.5	24.3	35.0
Chicago	0.05	39.4	19.1	29.4	38.4	18.6	28.6
	0.80	33.3	18.8	27.2	32.8	18.3	26.7
Delhi	0.05	58.6	31.7	40.2	57.2	31.3	39.5
	0.80	52.2	31.4	38.1	51.4	30.9	37.5
Rome	0.05	48.7	16.7	33.1	47.4	16.5	32.4
	0.80	42.0	16.7	30.6	41.3	16.5	30.1
Singapore	0.05	39.9	27.3	34.0	39.0	27.0	33.4
	0.80	35.1	27.1	32.7	34.6	26.9	32.2

Table 4-3: The mean temperatures differences for the urban and atmospheric layers, calculated by subtracting the cool roof temperature from the from conventional roofs temperature ($T\alpha_{roof=0.80}$ - $T\alpha_{roof=0.05}$) for each city.

CITY	ΔT_{URB} (°C)		ΔT_{ATM} (°C)	
	RT15	RT45	RT15	RT45
Cairo	-1.4	-2.5	-1.1	-2.3
Chicago	-1.2	-2.2	-1.0	-1.9
Delhi	-1.2	-2.1	-1.0	-2.0
Rome	-1.4	-2.5	-1.2	-2.3
Singapore	-0.8	-1.3	-0.7	-1.2

The resulting temperature output for each city from the BUCM is shown in Table 4-1 and Table 4-2, for relaxation times of 15 (RT15) and 45 minutes (RT45), respectively. The relaxation time of 15 minutes corresponds to the outer areas of the city column often characterized by suburbs, which are slightly more affected by the temperature of the surrounding rural areas compared to the central city area with a relaxation time of 45 minutes. The layers discussed in this section are the urban layer and atmospheric layer, which have previously been defined in section 3.1.1.

According to Table 4-3, the model calculated a significant temperature difference between the two roof albedos (α_{roof}). In general, the greatest temperature difference occurs when the temperature reaches a maximum for all cities in both layers (T_{urb} and T_{atm}). The mean temperature differences are smaller, while the minimum temperatures only differ slightly and are for most cities close to zero. The temperature change in both layers are greatest for RT45, as the city core is less affected by the air surrounding the city. Consequently, the city core is more sensitive to changes in absorbed solar radiation that follows the implementation of cool roofs, and the cooling potential is therefore greater.

Furthermore, for all cities and both relaxation times, the temperature of the atmospheric layer (T_{atm}) has a slightly weaker response to the change in albedo than does the urban layer. The temperature of the urban layer is more immediately affected by the heat from solar radiation absorbed at the surface. The atmospheric temperature, on the other hand, experiences more mixing with the surrounding air, which is largely caused by convection of sensible heat from the surface.

Table 4-4: *The incoming (SW$\downarrow$) and outgoing (SW$\uparrow$) solar radiation in W/m^2 for each city. The SW$\uparrow$ is strictly dependent on the surface albedo as shown in Equation 3-1. Note that all values are listed as absolute values, such that the SW$\downarrow$ is usually positive, while the SW$\uparrow$ is usually a negative term.*

	SW$\downarrow$ (W/m^2)			SW$\uparrow\alpha_{roof=0.05}$ (W/m^2)			SW$\uparrow\alpha_{roof=0.80}$ (W/m^2)		
CITY	Max	Min	Mean	Max	Min	Mean	Max	Min	Mean
Cairo	769	0	253	38	0	13	384	0	127
Chicago	829	0	223	41	0	11	414	0	111
Delhi	775	0	219	39	0	11	387	0	109
Rome	810	0	257	40	0	13	405	0	128
Singapore	604	0	140	30	0	7	302	0	70

Although variations occur between the different climate zones in which the cities are located, all cities receive a lot of solar radiation during the summer months, as shown in Table 4-4. The amount of total solar radiation reflected in each city for the different albedos is significantly different. Before the implementation of the cool roofs the cities reflected only about 5% of all incoming sunlight, whereas for cool roofs, a net total of 50% of all sunlight of the cities is reflected. This large difference is mainly induced by the bulk radiative parameters, where the urban canopy albedo (α_{can}) is given by the weighted reflectivity of the roof albedo and the canyon albedo (walls and roads) (Equation A1-26 in

Appendix A1). The diurnal cycle of all significant output variables will be presented and discussed in more detail in the following sections for each individual city.

Table 4-5: *The outgoing longwave radiation (OLR) from the canopy surface in W/m² for each city. The table contains information on OLR for relaxation times set to 15 and 45 minutes, as well as for albedo set to α_{roof} = 0.05 and α_{roof} = 0.8. Note that the values are listed as absolute values, and the OLR term is usually negative.*

CITY	α_{roof}	LW↑$_{RT=15}$ (W/m²)			LW↑$_{RT=45}$ (W/m²)		
		Max	Min	Mean	Max	Min	Mean
Cairo	0.05	364	268	312	394	276	330
	0.80	348	268	306	365	276	319
Chicago	0.05	316	245	281	334	255	294
	0.80	301	245	276	309	254	285
Delhi	0.05	391	291	323	424	302	338
	0.80	373	290	317	392	301	329
Rome	0.05	348	246	294	376	247	309
	0.80	331	246	288	345	247	298
Singapore	0.05	318	286	300	336	285	312
	0.80	307	285	297	315	285	306

The longwave radiation emitted upwards from the urban canopy is listed in table 4-5. The outgoing longwave radiation represents the primary means of planetary cooling and is a powerful diagnostic of the surface and atmospheric response to the diurnal solar forcing and mirrors the temperature of the various roof types and relaxation times to a large extent. As the OLR is temperature dependent, the OLR will vary with both the albedos and relaxation times: the higher the surface temperature, the greater the magnitude of the OLR. The maximum and mean OLR is slightly reduced after the implementation of cool roofs in each city, while the minimum remains unchanged. As the emissivity of both roofing materials is set to 0.9, the heat loss from thermal longwave emission will be nearly equal.

Table 4-6: The sensible heat flux from turbulence from the canopy surface in W/m² for each city. The table contains information on sensible heat for relaxation times set to 15 and 45 minutes, as well as for albedos set to 0.05 and 0.8. Note that the values are listed as absolute values, and the sensible heat flux term is usually negative.

City	α_{roof}	$H_{RT=15}$ (W/m²)			$H_{RT=45}$ (W/m²)		
		Max	Min	Mean	Max	Min	Mean
Cairo	0.05	782	196	419	725	159	398
	0.80	486	185	312	457	159	297
Chicago	0.05	583	170	337	541	161	321
	0.80	296	122	243	282	120	232
Delhi	0.05	774	179	364	713	152	345
	0.80	483	176	272	452	150	259
Rome	0.05	710	145	380	657	130	361
	0.80	417	145	271	391	130	258
Singapore	0.05	497	286	295	462	285	280
	0.80	262	285	235	249	285	224

Table 4-7: The latent heat flux from turbulence from the canopy surface in W/m² for each city. Note that the values are listed as absolute values, and the latent heat flux term is usually negative.

City	LATENT HEAT FLUX (W/m²)		
	Max	Min	Mean
Cairo	17	2	5
Chicago	363	3	101
Delhi	380	1	85
Rome	246	4	62
Singapore	294	28	99

The sensible and latent heat fluxes are given in Table 4-6 and Table 4-7, respectively. The sensible heat flux depends on temperature and will vary with albedo and relaxation time. As stated in section 2.3.3, both sensible and latent heat fluxes respond to temperature differences between the surface and the air; when chilled air from the rural areas flows across the warm urban surfaces, strong sensible and latent heat fluxes warm and moisten the air, and turbulent motions mix the air as it rises up. As can be seen for all cities, this sensible heat flux decreases with increasing albedo due to the fact that the surface temperature experiences a greater temperature reduction than the atmosphere. This contributes to a reduction of the temperature difference between the surface and the air, and therefore the sensible heat flux decreases. The opposite yields for relaxation time, where the sensible heat flux is higher for RT15 minutes than for RT45. This can be explained by the very nature of sensible heat flux: as the urban

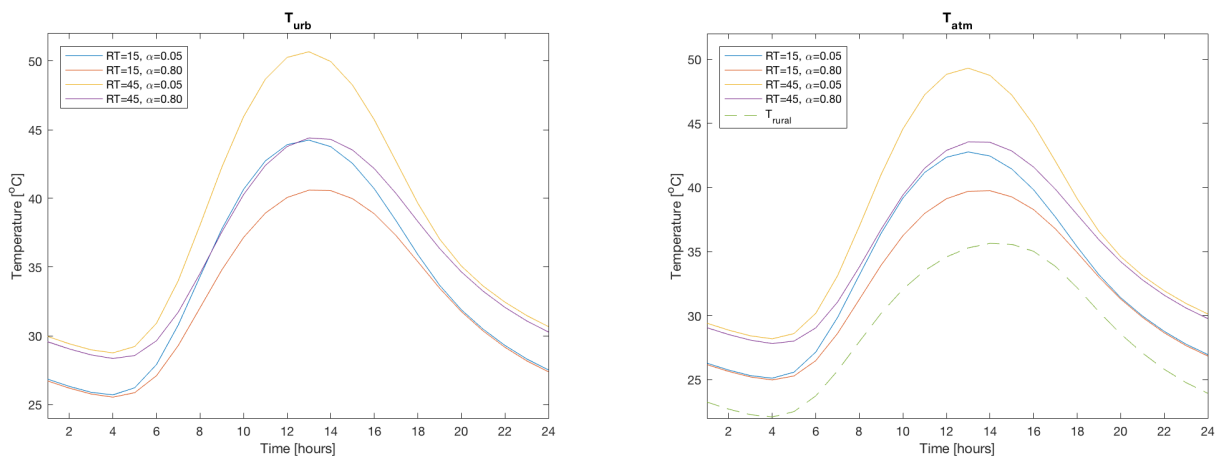surfaces are more affected by cooler air from the rural areas for a RT15, the temperature differences between surface and atmosphere increase, such that the sensible heat flux term also becomes larger in this area. The wind profile for the cities are assumed to be logarithmic (see Appendix 1, Equation A1.33), and wind speeds will vary temporally and spatially from one city to the next. High wind speeds will contribute to cool the urban surfaces, as the sensible heat flux is proportional to wind speed; the maximum sensible heat flux will occur when the temperature differences between the surface and the air is large and wind speeds are high (Appendix A, Equation A1-3). It should also be noted that cities with a higher mean latent heat flux, generally have a lower sensible heat flux. As more of the radiation goes into evaporating water from the surface, less heat is available to warm the air. However, a prerequisite for the increase in latent heat flux is that surface water must be available, and the availability of surface water is mostly related to the amount of precipitation.

4.1.2 CAIRO

Cairo is characterized by a hot desert climate (BWh) and is located in northern Egypt, 165 km south of the Mediterranean Sea and 120 km west of the Gulf of Suez. At an elevation of 18 meters, the city is concentrated along the river banks of the Nile, and the metropolitan area extends away from the river in all directions, covering an area of 610 km^2. The metropolitan area has a population of 19.8 million people, corresponding to a density of 37,600 people/km^2, making it the densest city in this study. During summer, air temperatures usually lie between 20 and 40 °C. The relative humidity is high due to the coastal proximity, averages ranging from 49-61% during the summer months. Precipitation is extremely rare, estimated to an average of about 0 mm during the summer in Cairo (WMO, 2018, Geoplaner, 2018).
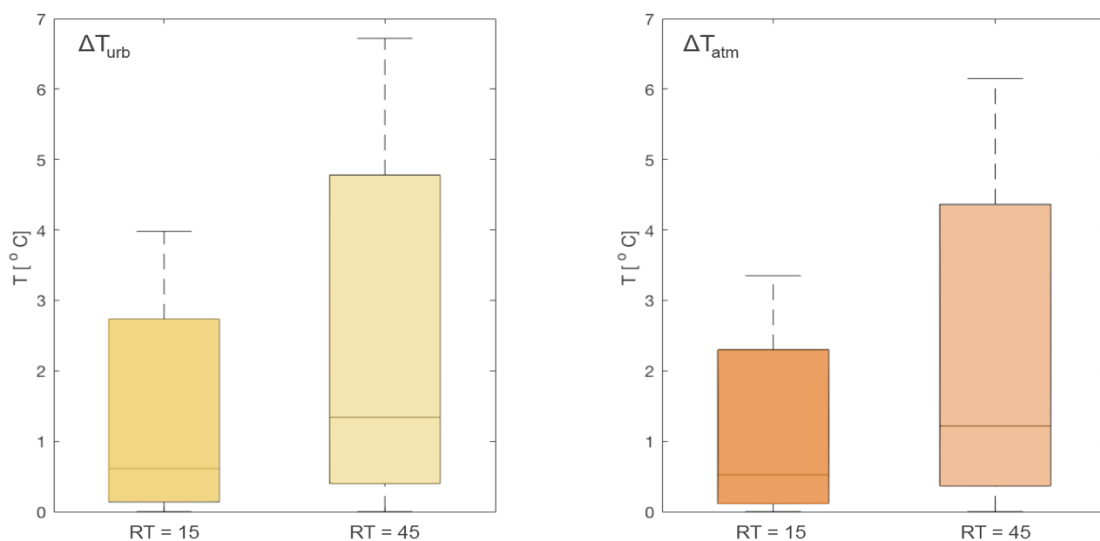
Figure 4-1: *The temperature differences (ΔT) for Cairo before and after implementation of cool roofs are presented in boxplots for relaxation times of 15 and 45 minutes. The yellow boxes represent the temperature of the urban layer (T$_{urb}$) and the orange ones represent the temperature of the atmospheric layer (T$_{atm}$).*

Figure 4-2*: The graphs depicts the mean 24-hour temperature of the urban (left) and atmospheric (right) layers for Cairo over the three summer months (JJA) for the different albedos and relaxation times: α = 0.05, RT15(blue), α = 0.80, RT15 (red), α = 0.05, RT45 (yellow), α = 0.80, RT45 (purple). The temperature of the corresponding rural atmospheric layer (from canopy surface to 40 meters) is also indicated in the figure to the right.*

Figure 4-3: *Cairo's diurnal cycle of **a)** shortwave radiation, showing incoming (blue) and reflected solar radiation for α = 0.05 (orange) and α = 0.8 (yellow). **b)** Diurnal cycle of outgoing longwave radiation for α = 0.05, RT15(blue), α = 0.80, RT15 (red), α = 0.05, RT45 (yellow), α = 0.80, RT45 (purple). **c)** Diurnal cycle of sensible heat flux for α = 0.05, RT15(blue), α = 0.80, RT15 (red), α = 0.05, RT45 (yellow), α = 0.80, RT45 (purple).*

As can be seen for the temperature in both the urban and atmospheric layers, the temperature change is greatest for relaxation time of 45 minutes, where the mean changes (Table 4-3) indicates a temperature reduction of 1.4°C and a maximum change close to 7°C as shown in Figure 4-1. The changes are somewhat lower for the atmospheric layer, although this layer also experience a significant change in temperature. For RT15 the results are modest in comparison, but it still shows a significant potential for temperature reductions. The incoming shortwave radiation in Cairo peaks at 11:00 according to Figure 4-3a. This is also the time when the temperature differences reach their maxima, which is modelled to about 4 °C for RT15 and close for 7 °C for RT45 (somewhat lower for the atmospheric layer). The

minimum difference between conventional and white roofs are close to zero, which takes place during night-time.

For all layers, the diurnal mean temperature is highest for conventional roof with R45, peaking at over 50°C for the canopy layers, and just below 50°C for the atmospheric layer, as shown in Figure 4-2. The time lag is about one hour after the solar noon for the conventional roofs, and two hours for the cool roofs. Generally, for all temperature plots for both layers, the two roof types have identically shaped curves but are shifted along the y-axis due to different temperatures for the two relaxation times. Consequently, the conventional roof has the same curve, but peaks just below 45°C. The cool roof curves are also identical at different temperatures, the highest with RT45, reaching the same temperature as the conventional roof with RT15. The lowest daily temperature is for the cool roofs with RT15, which peaks at about 41°C. As the day progresses, the curves of the conventional roofs are steeper and reaches lower night-time temperatures than the cool roof because of the significantly higher sensible heat fluxes according the findings in Figure 4-3c. As can be seen in Figure 4-3b, the temperature dependent OLR mirrors the diurnal temperatures very closely.

In Figure 4-2 for the atmospheric urban layer, the corresponding atmospheric rural temperature of the same height is plotted as the green stapled line. It illustrates how the atmospheric UHI (AUHI) develops throughout the day. The rural temperature follows diurnal patterns of the cool roofs very closely, only the peak temperature occurs slightly later in the day for the rural area. Generally, the rural temperatures are 3-4°C below that of the urban atmosphere for RT15, and about 6-7°C lower than for RT45 at night. The difference reaches a maximum when the daily temperature peaks, and the atmospheric temperatures above conventional roofs of RT45 reaches temperatures of about 13-14°C above the rural. Cool roofs bring the urban atmospheric temperatures much closer to rural temperatures, contributing to a reduction in the UHI effect, especially during daytime. The night-time temperatures of the conventional and cool roofs of same RT is nearly unchanged. This indicates that the night-time UHIs does not experience any significant effect from the cool roofs.

4.1.3 CHICAGO

Chicago is characterized by a hot-summer humid continental climate (Dfa), located in northern Illinois along the western shore of Lake Michigan. At an elevation of 240 meters, the city of 230 km² lies beside two rivers. The metropolitan area has a population of 2.7 million people, corresponding to a density of 11,700 people/km². The Chicago summer months are characterized by hot and humid weather with temperatures ranging from 26 to 28 °C on average, although temperatures of 52 °C was recorded during the 1995 heatwave. Mean monthly precipitation peaks at around 90-110 mm during summer, reaching

an annual maximum in August. Relative humidity is also high, at around 70 % on average for this period (WMO, 2018, Geoplaner, 2018).
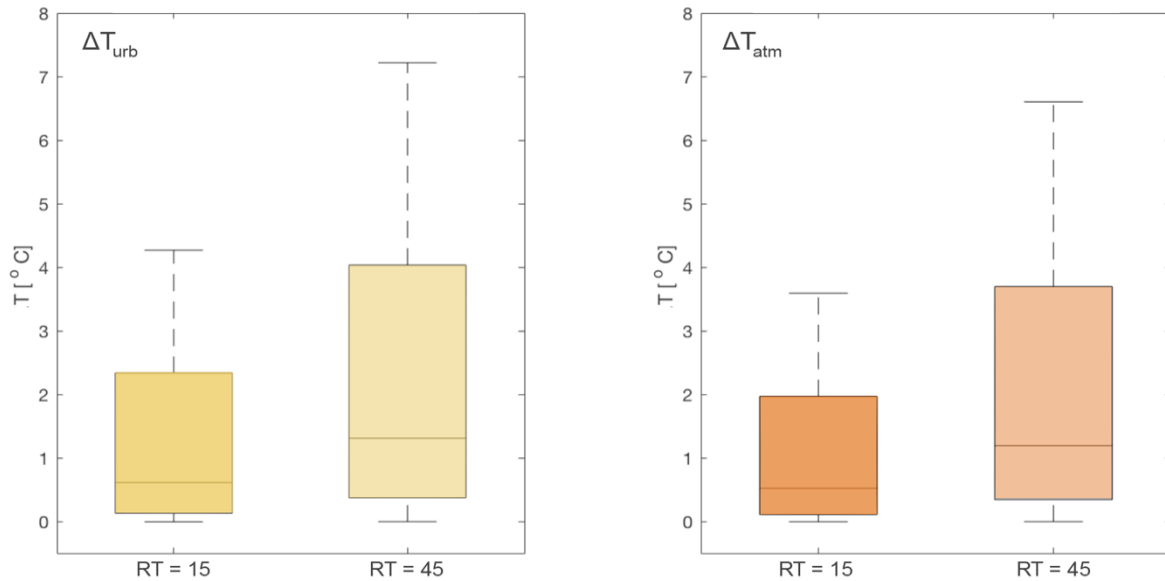
Figure 4-4: *The temperature differences (ΔT) for Chicago before and after implementation of cool roofs are presented in boxplots for relaxation times of 15 and 45 minutes. The yellow boxes represent the temperature of the urban layer (T_urb) and the orange ones represent the temperature of the atmospheric layer (T_atm).*
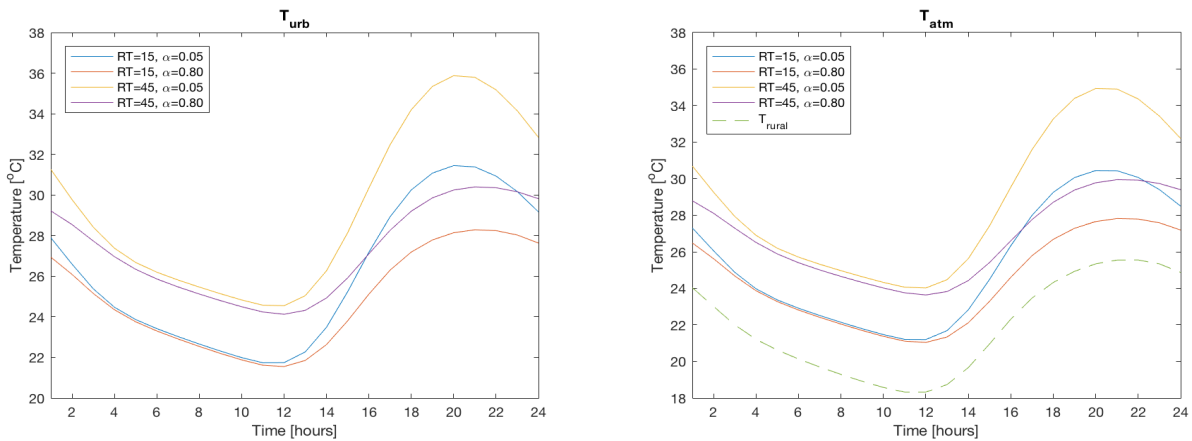
Figure 4-5: *The graphs depicts the mean 24-hour temperature of the urban (left) and atmospheric layers (right) for Chicago over the three summer months (JJA) for the different albedos and relaxation times: α = 0.05, RT15(blue), α = 0.80, RT15 (red), α = 0.05, RT45 (yellow), α = 0.80, RT45 (purple). The temperature of the corresponding rural atmospheric layer (from canopy surface to 40 meters) is also indicated in the figure to the right.*

Figure 4-6: *Chicago's diurnal cycle of **a)** shortwave radiation, showing incoming (blue) and reflected solar radiation for α = 0.05 (orange) and α = 0.8 (yellow). **b)** Diurnal cycle of outgoing longwave radiation for α = 0.05, RT15(blue), α = 0.80, RT15 (red), α = 0.05, RT45 (yellow), α = 0.80, RT45 (purple). **c)** Diurnal cycle of sensible heat flux for α = 0.05, RT15(blue), α = 0.80, RT15 (red), α = 0.05, RT45 (yellow), α = 0.80, RT45 (purple).*

According to Figure 4-4, for both layers in the model the temperature response to the cool roofs is greatest for RT45, resulting in mean temperature changes of about 2.2°C for the urban layer and 1.9°C for the atmospheric layer according to Table 4-3. The greatest change in temperature exceeds 7°C for the canopy layers, while the result for the atmospheric layer was just below this point. The maximum temperature change occurs at solar noon, which for Chicago is at 19:00 with a peak of 642 W/m^2 and average of 223 W/m^2, as illustrated in Figure 4-6a. The minimum temperature change is approximately zero, as the night-time temperatures for cool and conventional roofs are about the same.

According to Figure 4-5, the diurnal mean temperature for both layers is highest for conventional roofs with RT45, peaking at about 36°C and 32°C for the urban layer with RT45 and RT15, respectively. Both cool roofs display a significantly lower temperature than their corresponding conventional roof, with maxima at just above 32°C and 28°C for RT45 and RT15. In general, the temperatures of the atmospheric layer are about 1°C lower than the canopy surface layers. The temperatures rise quickly at sunrise, peaks with a lag of 1-2 hours (somewhat later for cool roofs), and rapidly decline as the day progresses due to the sensible heat fluxes in Figure 4-6c. Although the cool roofs do not display the same extreme diurnal variations as the conventional, the temperature variation still has a significant peak a few hours past mid-day. Additionally, Figure 4-6b illustrates how the temperature dependent OLR mirrors the diurnal temperatures very closely.

As can be seen in Figure 4-5 for the atmospheric layer, the rural night-time temperatures are generally 3°C below that of the urban atmosphere for RT15, and about 5-7°C lower than for RT45. The difference reaches a maximum at peak daily temperatures. The rural temperature peaks at just below 26°C, while atmospheric temperatures above conventional roofs of RT45 reach temperatures of about 11°C above

this. Cool roofs have a significant effect on the AUHI during daytime, while it is limited at night due to the insignificant temperature differences between conventional and cool roofs for same RT.

4.1.4 DELHI

Delhi is located in the north of India and borders between a humid subtropical climate (Cwa) and a hot semi-arid climate (BSh) which introduces significant seasonal variations within the city. The city is located at an elevation of 229 meters, and the Yamuna river runs through it. The metropolitan area of Delhi has a population of 18.6 million people, corresponding to a density of 12,500 people/km^2. Although the warm season lasts from March to June, the mean daily temperatures from June to August ranges between 28 and 34 °C. The mean precipitation peaks at 70-180 mm during the summer months (JJA), and so does the relative humidity at 40-80 % (WMO, 2018, Geoplaner, 2018).
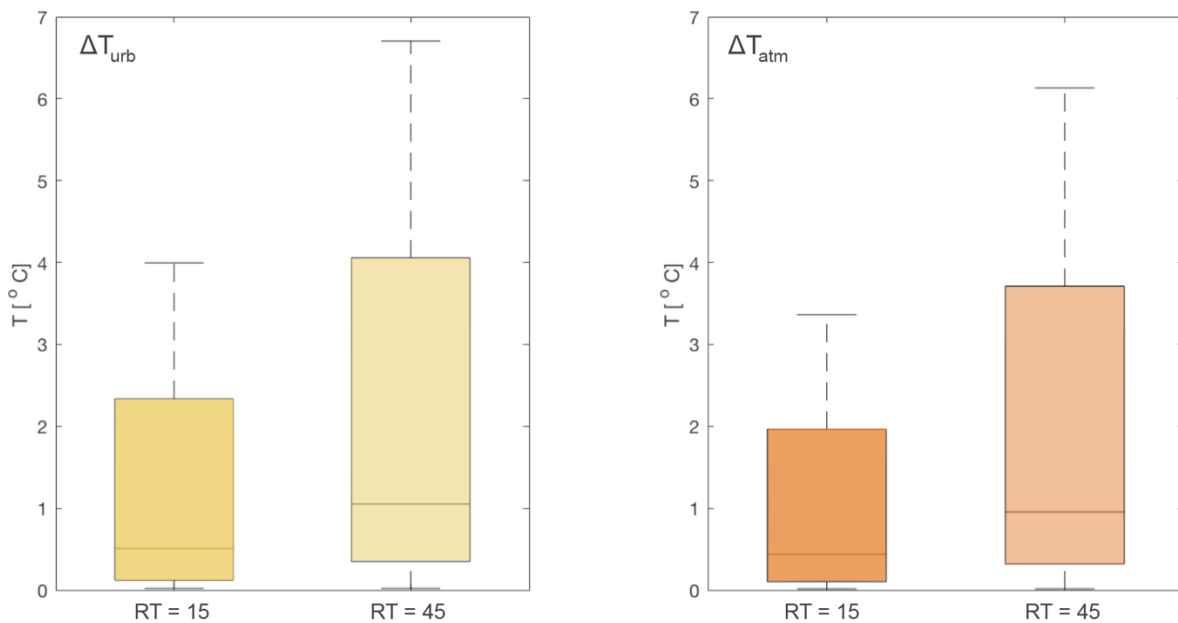
Figure 4-7*: The temperature differences (ΔT) for Delhi before and after implementation of cool roofs are presented in boxplots for relaxation times of 15 and 45 minutes. The yellow boxes represent the temperature of the urban layer (T$_{urb}$) and the orange ones represent the temperature of the atmospheric layer (T$_{atm}$).*
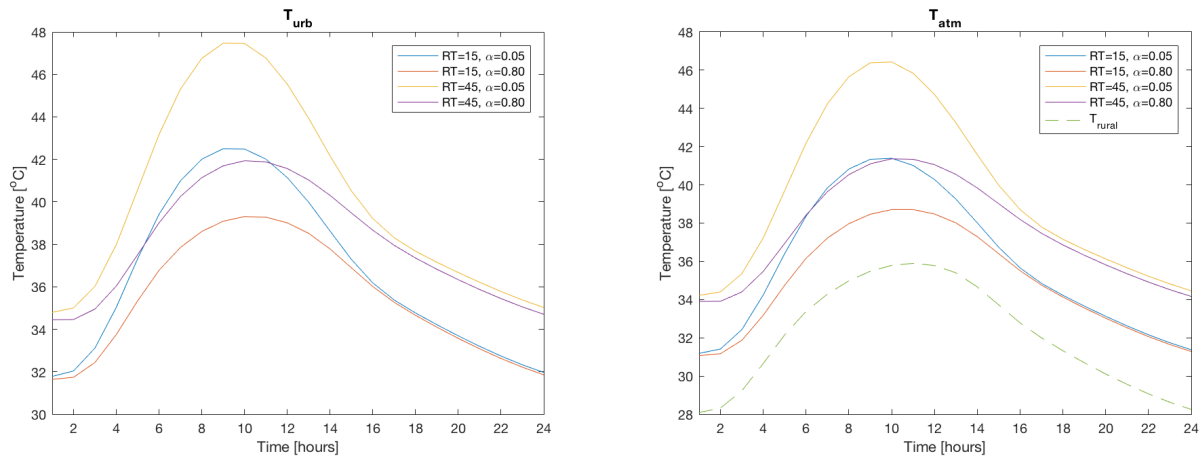
Figure 4-8*: The graphs depicts the mean 24-hour temperature of the urban (left) and atmospheric layers (right) for Delhi over the three summer months (JJA) for the two different albedos and relaxation times: α = 0.05, RT15(blue), α = 0.80, RT15 (red), α = 0.05, RT45 (yellow), α = 0.80, RT45 (purple). The temperature of the corresponding rural atmospheric layer (from canopy surface to 40 meters) is also indicated in the figure to the right.*
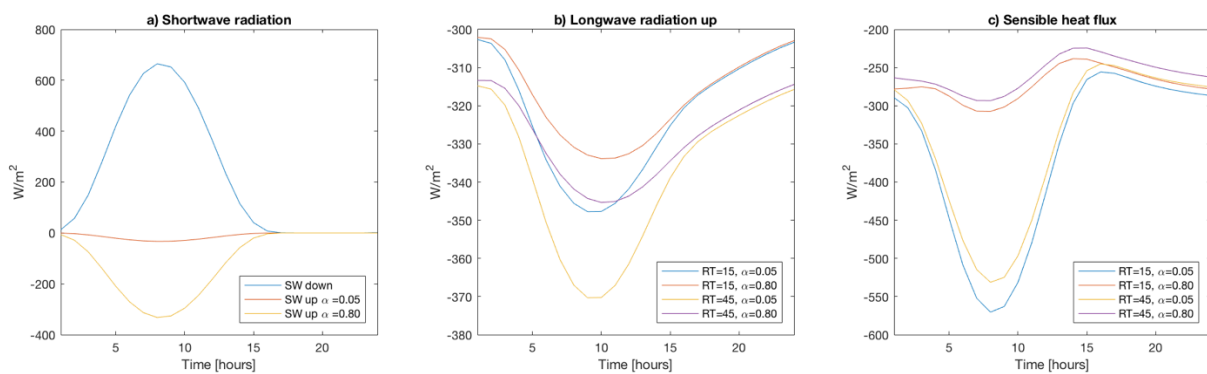
Figure 4-9: *Delhi's diurnal cycle of **a)** shortwave radiation, showing incoming (blue) and reflected solar radiation for α = 0.05 (orange) and α = 0.8 (yellow). **b)** Diurnal cycle of outgoing longwave radiation for α = 0.05, RT15(blue), α = 0.80, RT15 (red), α = 0.05, RT45 (yellow), α = 0.80, RT45 (purple). **c)** Diurnal cycle of sensible heat flux for α = 0.05, RT15(blue), α = 0.80, RT15 (red), α = 0.05, RT45 (yellow), α = 0.80, RT45 (purple).*

In the case of Delhi, Figure 4-7 indicates that the temperature change is greatest for relaxation time set to 45 minutes for both layers, with the greatest change for RT45 where the temperature displays a maximum change of just below 7°C for the urban layer and closer to 6°C for the atmospheric layer. The mean change of 2.1°C and 2.0°C for the urban and atmospheric layers, respectively (Table 4-3). The values are significantly lower for RT15. According to Figure 4-8, the maximum change in both layers are modelled to about 4 °C for RT15 and close for 7 °C for RT45 (somewhat lower for the atmospheric layer). The minimum occurs at night, when the difference between conventional and white roofs are close to zero.

As shown in Figure 4-7, the maximum temperature change occurs approximately one hours past solar noon at 08:00 (Figure 4-9a). At the Delhi solar noon, the incoming solar radiation peaks at 664 W/m^2, as compared to the summer period at 219 W/m^2. At this point, the conventional roof with RT45 reaches temperatures close to 48°C for T_{urb}, while T_{atm} peaks at approximately 47°C. The conventional roof for RT15 also reaches quite high peak temperatures, while both cool roofs hold the lowest temperature. As expected, the cool roof for RT15 displays the lowest temperature, peaking at about 39°C for T_{urb}, while T_{atm} reaches temperatures similar to that of the cool roof of RT15. As can be seen from Figure 4-9c, the diurnal sensible heat fluxes are strong for the conventional roofs, which results in a steeper temperature decline. For T_{urb}, both roofs of RT15 experience the coldest night-time temperatures at just below 32°C where the cool roof is observed as somewhat colder than the conventional roofs. The same yields for both RT45 roofs, but they only reach a minimum 24-hour mean temperature of about 35°C. The behavior of the atmospheric layer is similar to that of the urban, but the atmospheric temperatures are generally about one degree Celsius lower compare to the estimated urban temperatures. Figure 4-9b demonstrates the temperature-dependent relationship of OLR, which to a large extent mirrors the surface temperatures.

For Delhi, Figure 4-8 also shows that the rural night-time temperatures are generally 3°C below that of the urban atmosphere for RT15, and about 6°C lower than for RT45. The rural temperature reaches maximum values at about 36°C, while atmospheric temperatures above conventional roofs of RT45 goes as high as 47°C. Clearly, it is evident that cool roofs greatly affect the urban environment through mitigation of the AUHI, with the highest level of temperature reduction occurring during daytime at peak temperatures.

4.1.5 ROME

Rome is characterized by hot-summer Mediterranean climate and is located about 24 km from the Tyrrhenian Sea. in the north of India and borders between a humid subtropical climate (Cwa) and a hot semi-arid climate (BSh). At an average elevation of 64 meters, the city covers an area of 1,290 km^2. The roman population of 3.8 million corresponds to a density of 2,900 people/km^2, the lowest of this study. June, July and August are the warmest month of the year, and daily mean temperatures range between 21 and 25 °C. The mean precipitation reaches minimum values during the summer period of 20-35 mm. So does the relative humidity, although the mean values exceed 70% (WMO, 2018, Geoplaner, 2018).
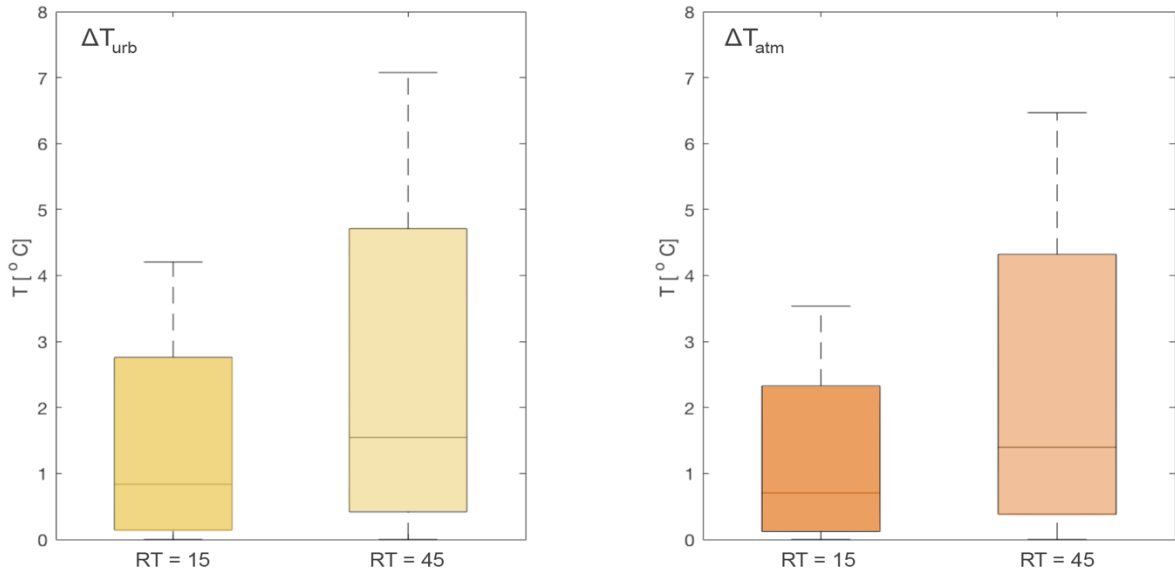
Figure 4-10: *The temperature differences (ΔT) for Rome before and after implementation of cool roofs are presented in boxplots for relaxation times of 15 and 45 minutes. The yellow boxes represent the temperature of the urban layer (T_{urb}) and the orange ones represent the temperature of the atmospheric layer (T_{atm}).*
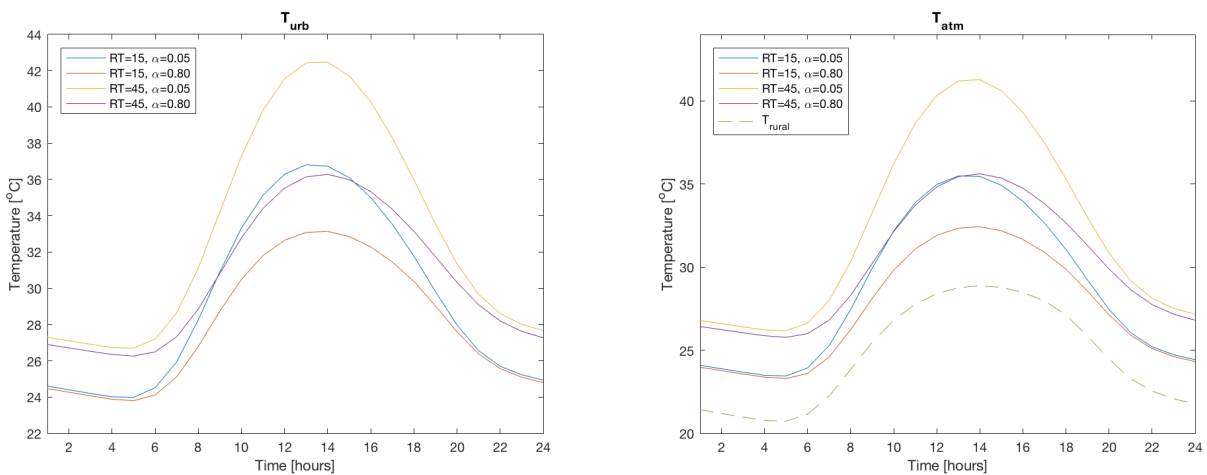
Figure 4-11*: The graphs depicts the mean 24-hour temperature of the urban (left) and atmospheric (right) layers for Rome over the three summer months (JJA) for the different albedos and relaxation times: $\alpha = 0.05$, RT15(blue), $\alpha = 0.80$, RT15 (red), $\alpha = 0.05$, RT45 (yellow), $\alpha = 0.80$, RT45 (purple). The temperature of the corresponding rural atmospheric layer (from canopy surface to 40 meters) is also indicated in the figure to the right.*
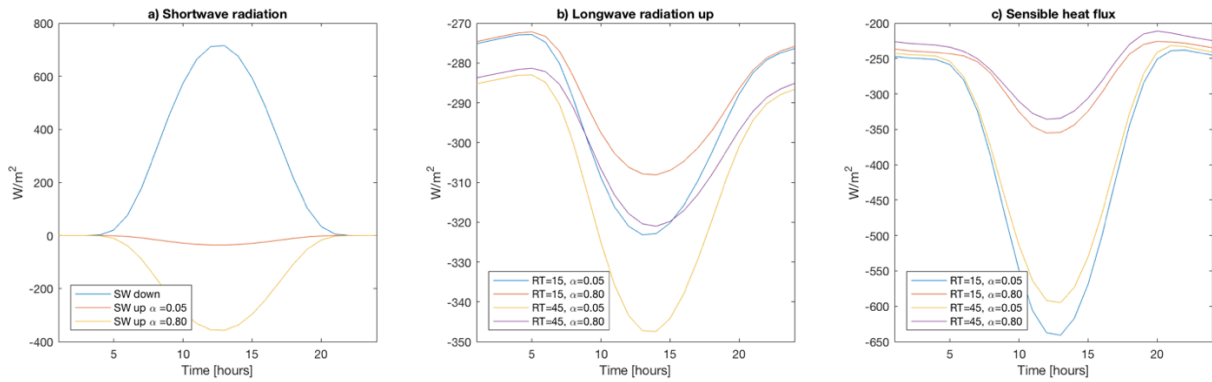
Figure 4-12: *Rome's diurnal cycle of **a)** shortwave radiation, showing incoming (blue) and reflected solar radiation for α = 0.05 (orange) and α = 0.8 (yellow). **b)** Diurnal cycle of outgoing longwave radiation for α = 0.05, RT15(blue), α = 0.80, RT15 (red), α = 0.05, RT45 (yellow), α = 0.80, RT45 (purple). **c)** Diurnal cycle of sensible heat flux for α = 0.05, RT15(blue), α = 0.80, RT15 (red), α = 0.05, RT45 (yellow), α = 0.80, RT45 (purple).*

By considering Figure 4-10, it is evident that the temperature response to cool roofs in Rome is good, especially for RT 45, where the temperature displays a mean change of 2.5°C and 2.3°C for the urban and atmospheric layers, respectively. The response of the atmospheric layer for RT45 is also significant, but somewhat lower than for the urban layer, as expected. The overall response for RT15 is more modest, as these areas are more affected by the incoming rural air than RT45 and hence the alteration in absorbed radiation at the canopy surface is of less significance. The maximum temperature change is modelled to an excess of 5°C for RT15 and 7°C in the urban layer for RT45, and somewhat lower for the atmospheric layer. This occurs at mid-day, which in Rome is at 13:00 according to Figure 4-12a. The minimum occurs at night, when the difference between conventional and white roofs are close to zero. It is also noteworthy that the temperatures of both roofs in the canopy and urban layers with RT15 drops below the atmospheric temperatures during night, likely due to a combination of longwave radiative and convective cooling, as can be seen in Figure 4-12b and Figure 4-12c, respectively.

At solar noon, the incoming solar radiation peaks at 715 W/m², though the average for the summer period is 257 W/m². The mean daily peak temperature for the conventional roofs occur at the same time as the solar noon, while the cool roof temperature reaches maximum about an hour later. For the urban layer, the temperatures of the conventional roofs are the highest for both RT15 and RT45, peaking at about 37°C and 43°C, respectively. The model calculated daily maxima of 33 °C and 36 °C for cool roofs with RT15 and RT45, which is significantly lower compared to the conventional ones. The cool roof of RT15 displays the lowest temperature according to the model for both layers, although the temperature change from before and after cool roof implementation is greater for RT45. For the atmospheric layer, temperatures are generally lower than the two layers at the canopy surface. Furthermore, it can be seen that the temperature of the atmospheric layer of the conventional roof with RT15 and the cool roof with RT45 have identical maximum temperatures, but in this case the cool roof

temperature peak occurs about an hour later. Both roofs with RT15 display the lowest modelled night-time temperatures, reaching a minimum just before sunrise at about 23-24 °C, the cool roof being somewhat colder than the conventional one. This is also the case for the roofs with RT45, although minimum temperatures never go below 26 °C. According to Figure 4-12c, the diurnal sensible heat fluxes are strong for conventional roofs. However, the conventional roof with RT15 displays an elevated sensible heat flux due to the large temperature differences between the surface and air that arises from the influence of rural air flow into the city.

Figure 4-11 shows the urban and rural atmospheric temperature differences, where the rural night-time temperatures are approximately 3°C below that of the urban atmosphere for RT15 and about 5°C lower than for RT45. The rural temperature reaches maximum values at about 29°C, while atmospheric temperatures above conventional roofs of RT45 can reach temperatures above 41°C during peak hours. Evidently, cool roofs contribute to lowering the temperature differences between the rural and urban atmosphere, reducing the magnitude of the AUHI and increases the outdoor thermal comfort for the urban inhabitants.

4.1.6 SINGAPORE

At one degree north of the Equator, the city of Singapore is located at the southern tip of the Malay Peninsula, characterized by a tropical rainforest climate. The metropolis of 720 km^2 is located on the main island, surrounded by 62 smaller islets. At an average elevation of 58 meters, Singapore's population of 5.6 million corresponds to a density of 7,800 people/km^2. The annual temperature variations are small, with daily means of about 28 degrees, including the summer months (JJA). Summer precipitation ranges between 130 and 150 mm, and the mean relative humidity is above 80% all year round (WMO, 2018, Geoplaner, 2018).
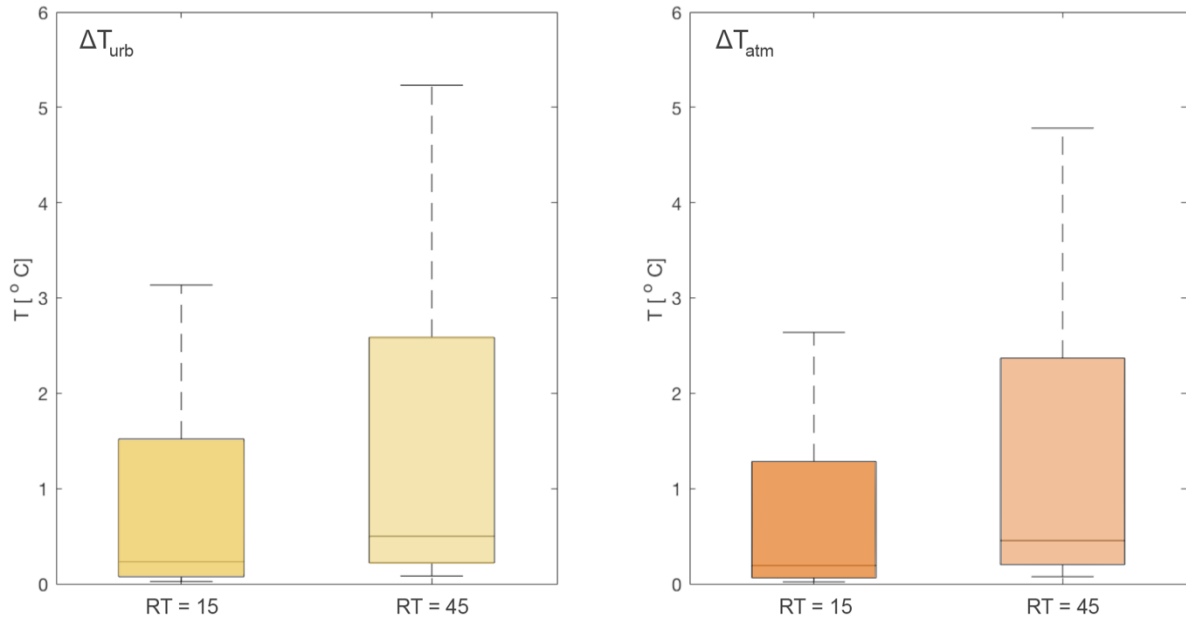
Figure 4-13: *The temperature differences (ΔT) for Singapore before and after implementation of cool roofs are presented in boxplots for relaxation times of 15 and 45 minutes. The yellow boxes represent the temperature of the urban layer (T_{urb}) and the orange ones represent the temperature of the atmospheric layer (T_{atm}).*
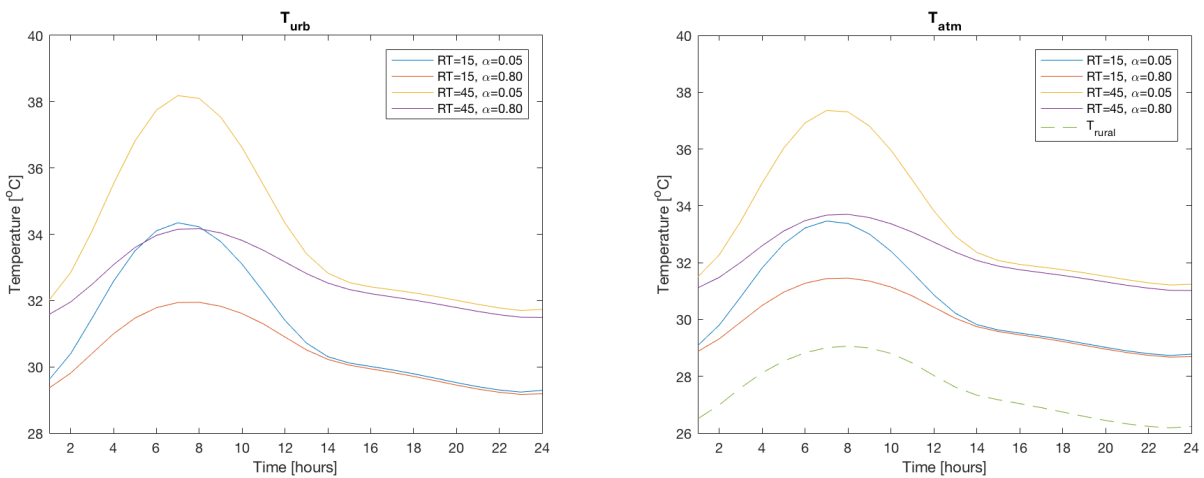
Figure 4-14: *The graphs depicts the mean 24-hour temperature of the urban (left) and atmospheric (right) layers for Singapore over the three summer months (JJA) for the different albedos and relaxation times: α = 0.05, RT15(blue), α = 0.80, RT15 (red), α = 0.05, RT45 (yellow), α = 0.80, RT45 (purple). The temperature of the corresponding rural atmospheric layer (from canopy surface to 40 meters) is also indicated in the figure to the right.*

Figure 4-15: *Singapore's diurnal cycle of a) shortwave radiation, showing incoming (blue) and reflected solar radiation for α = 0.05 (orange) and α = 0.8 (yellow). b) Diurnal cycle of outgoing longwave radiation for α = 0.05, RT15(blue), α = 0.80, RT15 (red), α = 0.05, RT45 (yellow), α = 0.80, RT45 (purple). c) Diurnal cycle of sensible heat flux for α = 0.05, RT15(blue), α = 0.80, RT15 (red), α = 0.05, RT45 (yellow), α = 0.80, RT45 (purple).*

Overall, the temperature changes of Figure 4-13 before and after the cool roof implementation displays the same trend as observed for the other countries; with the greatest change for RT45 where the temperature displays a mean change of 1.3°C and 1.2°C for the urban and atmospheric layers, respectively. The maximum temperature change occurs at solar noon in both layers are modelled close to 3 °C for RT15 and 5 °C in both layers for RT45 (somewhat higher for the canopy layers, and lower for the atmospheric layers. The minimum occurs at night, when the difference between conventional and white roofs are close to zero.

The solar noon in Singapore with a maximum incoming solar radiation of 462 W/m² occurs at 07:00 according to Figure 4-15a. The mean incoming solar radiation for the entire summer period is 140 W/m², suggesting more frequent cloud cover and precipitation, supported by the latent heat fluxes in Table 4-7. Regarding the temperature plots in Figure 4-14 for both cool roofs, it is noteworthy that the 24-hour temperature variations are very modest, compared to the conventional roofs with strong peaks close to solar noon, which is also within the timeframe of when the largest temperature differences in Figure 4-13 can be observed. For both canopy layers, both conventional roof temperatures exceed that of the cool ones, peaking at scarcely above 34 °C and 38 °C for RT15 and RT45, respectively. The highest peak temperatures achieved in the atmospheric layer are observed for the conventional and cool roof with RT45, while the lowest temperatures are detected for both roofs with RT15. It is also noteworthy that the sensible heat fluxes for the cool roofs are very weak compared to the conventional roofs in Figure 4-15c.

The urban and rural atmospheric temperatures are shown on the right side of Figure 4-14. Rural night-time temperatures are generally 3°C lower than the urban atmospheric temperature for RT15, and about 4-5°C lower than for RT45. The rural temperature in Singapore peaks at about 29°C, in strong contrast

to the conventional roof temperature for RT45 that can reach temperatures well above 37°C during peak hours. The cool roofs level out the temperature differences between conventional and cool roofs, reducing the magnitude of the AUHI. Although the night-time contributions to UHI mitigation is modest for both cases of relaxation times, there is a significant change in daytime temperatures after the cool roof implementation in the city.

4.1.7 CITY COMPARISON

In general, all cities display a significant change in temperature after cool roofs were implemented. The changes are generally greater for RT45 as areas with RT15 are more influenced by the incoming air of the surrounding rural areas, causing sensible heat to convect away from the surface due to the increased temperature differences that arises when cooler air flows across hot surfaces. This is supported by the findings in Table 4-5, which generally shows that the sensible heat flux is higher for RT15, and also higher for conventional roofs than the cool roofs because of higher temperature differences between the surface and atmosphere. Additionally, the sensible heat flux reaches a minimum around dawn and increases slightly during night. This is likely due to the slow release of heat from the thermal mass of the urban infrastructure, which causes atmospheric UHIs to become more prominent after sunset. Canopy surface- and atmospheric temperatures level out during night but is still higher for the suburbs (RT15) than the central city (RT45), which corresponds well with literature (see Figure 2-5).

As previously explained, the magnitude of the surface urban heat islands (SUHI) changes with the intensity of the sun. As shown in the 24-hour mean temperature plots for all cities in the above section, it is evident that the maximum temperature difference between conventional and cool roofs occurs one to two hours after solar noon, and somewhat later for cool roofs as they take longer to heat. This is because the sun's intensity is still high a few hours after mid-day, and the heating of the surfaces continues past this point. This lag in temperature response to solar heating is primarily due to the finite heat capacity of the surface, which can be influenced by various atmospheric and surface feedbacks to the heating (Comer et al., 2007). However, the bulk urban canopy model does not calculate surface temperatures for rural areas, and it is consequently not possible to quantify the change in SUHI after the surface albedo alteration. Nevertheless, by considering the general trend in temperature response to cool roofs in the 24-hour mean plots and the development of the rural atmospheric temperature, it is likely that the rural surface temperature will display a similar behavior to that of the rural atmosphere, only at higher temperatures.

Change in magnitude of atmospheric urban heat islands
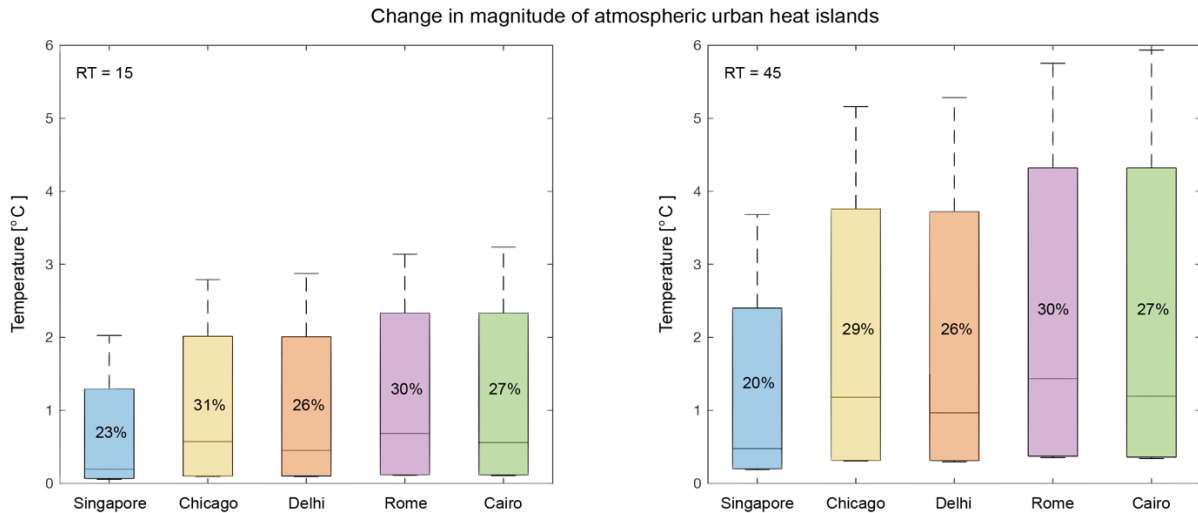
Figure 4-16: *The boxplots show the change in magnitude of the atmospheric UHIs in each city after the introduction of cool roof. The plots are based on the 24-hour mean of both the atmospheric temperature for RT15 and RT45, and the 24-hour mean of the corresponding rural atmospheric temperature layer. The rural temperature was subtracted from the urban atmospheric, before the values for cool roof temperatures were subtracted from those of conventional roofs. The boxes are also marked with mean percentage change in UHI magnitude from before and after cool roof implementation.*

Figure 4-16 shows the change in magnitude of the atmospheric UHI effect after cool roofs were introduced and emphasizes the great potential cool roofs can have on reducing the temperature differences between the rural and urban areas. Although the temperature reductions are generally smaller for RT15, the percentage change in temperature is quite similar for both relaxation times, such that the suburban areas respond just as well as the central urban areas.
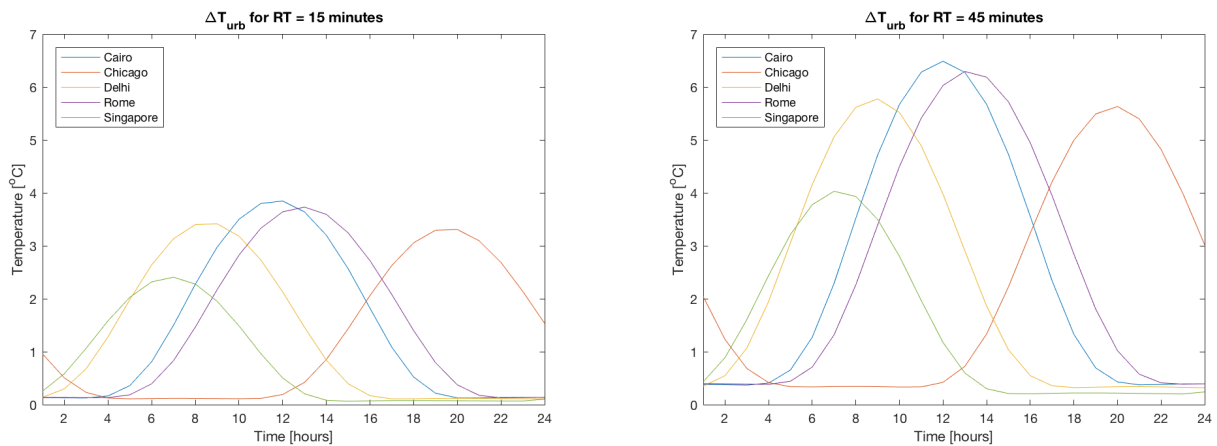
Figure 4-17: *The curves compare the 24-hour temperature difference for all cities for the urban layer. The temperature difference is based on $\Delta T = \alpha_{0.05} - \alpha_{0.80}$, in order to compare the magnitude of the changes before and after cool roof implementation for the different relaxation times. The time difference between the cities are not accounted for, hence the offset.*

71

ΔT_{atm} for RT = 15 minutes

ΔT_{atm} for RT = 45 minutes
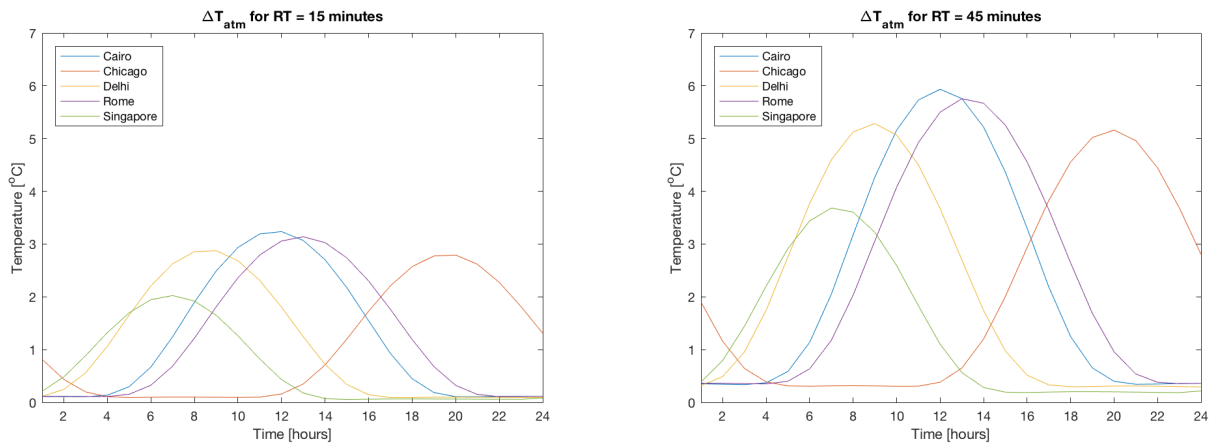
Figure 4-18: The curves compare the 24-hour temperature difference for all cities for the atmospheric layer. The temperature difference is based on $\Delta T = \alpha_{0.05} - \alpha_{0.80}$, in order to compare the magnitude of the changes before and after cool roof implementation for the different relaxation times. The time difference between the cities are not accounted for, hence the offset

Overall, the hot-summer Mediterranean climate of Rome responded best to the implementation of cool roofs, with a mean temperature reduction of approximately 1.4°C for RT15 and 2.5°C for RT45 in the urban layer and 1.2°C and 2.3°C for the atmospheric layer from Table 4-3. The city has the lowest mean latent heat flux and a general high mean sensible heat flux, which means that latent cooling is limited. Additionally, Rome receives the most incoming solar radiation during the summer period, which in turn provides Rome with an ideal climate for cool roofing. Moreover, Figure 4-16 demonstrates the magnitude of the urban heat island, which was reduced by 30% for both RT15 and RT45 in the case of Rome. Conclusively, it is evident that cool roofs had a great impact on the urban atmospheric temperatures.

Surprisingly, Chicago had the second-best response to the cool roof with its hot-summer humid continental climate. As seen in Table 4-3, the mean temperature reduction was 1.2°C for RT15 and 2.2°C for RT45 in the urban layer and just below 1.0°C and 1.9°C for the atmospheric layer. Chicago receives a lot of incoming sunlight, while the sensible heat flux is also strong. On the other hand, the latent heat flux is quite high, which can be explained by the fact that precipitation reaches peak values during summer. Despite this, and the proximity to Lake Michigan (which can also help moderate land surface temperatures), Chicago evidently is a suitable city for cool roof implementation. As Figure 4-16 demonstrates, the urban heat island mitigation potential was very high for Chicago, reaching values of 31% and 29% for RT15 and RT45.

The results in Table 4-3 for the hot desert climate of Cairo indicated a good response to the cool roofs, with mean reductions in temperature of 1.4°C for RT15 and 2.5°C and RT45 for both the urban layer, and a corresponding 1.1°C and 2.3°C for the atmosphere. According to literature, cities in arid climates

with limited latent cooling should be the best candidates for cool roofs. Although Cairo has the highest mean sensible heat flux (Table 4-5) and by far the lowest latent heat flux (Table 4-6), the response to cool roof implementation was not as high as might be expected for this desert climate. According to Figure 4-16, the urban heat island effect can be reduced by 27% for both relaxation times in Cairo, which implies a significant effect from the cool roofs on the hot desert climate.

Delhi also showed a moderate response compared to the other cities, with mean temperature changes in the urban layer of 1.2°C and 2.2°C RT15 and for RT45, and a corresponding reduction in 1.0°C and 2.0°C for the atmospheric layer from Table 4-3. As Delhi's climate borders between two different climates, it is possible that the humid subtropical climate that dominates in the summer months contributes to higher latent heat fluxes as precipitation peaks at this time as seen in Table 4-6. Delhi does, however, have a strong sensible heat flux (Table 4-5), but might be limited by the latent cooling during the summer months. Overall, Delhi would benefit from cool roofs, although the response might have been higher for Delhi if the local warm period from March to June would be considered instead. Delhi also experienced a significant reduction in the magnitude of the UHI effect from the introduction of cool roofs, with urban-to-rural temperature differences of 26% for both relaxation times.

Singapore displayed the lowest response to the cool roofs, with mean temperature reductions in the urban layer of 0.8°C and 1.3°C for RT15 and RT45, and a corresponding temperature reduction of 0.7°C and 1.2°C for the atmospheric layer according to Table 4-3. The city receives the least amount of sunlight during the day, which indicate high precipitation rates, consistent with tropical rainforest climates. Areas with significant cloud cover will experience a reduced response to the cool roofs, as the amount of radiation received and reflected by the surface will be lower than for areas with predominantly clear skies. Singapore's climate clearly contributes to moderate the urban temperature through high latent heat fluxes (Table 4-6), as the summer precipitation is high. The sensible heat flux for Singapore is the lowest of all cities, as much of the heat provided by incoming sunlight is used to evaporate water. The coastal proximity is also likely to contribute to moderate the climate, as the small country is surrounded by water. It is not likely that the response to cool roofs would be much higher other times of the year, as the annual temperature variations are small. Although considered significant, the urban-to-rural temperature response of Singapore to cool roofs was the weakest of the study, with a temperature reduction of 23% for RT15 and 20% for RT45.

4.2 EFFECT OF COOL ROOFS ON ENERGY IN BUILDINGS

In this section, the temperature dependent energy demands will be presented and discussed. The degree-days calculations are based on the temperature of the urban layer, which is nearly the same temperature as the upper canopy layer, only slightly more affected by mixing from the rural areas surrounding the city. This temperature is likely an overestimate of the real air temperatures in the city, as it is very close to the canopy surface that experience extremely high temperature. On the other hand, the temperature of the atmospheric layer 40 meters above the canopy is likely an underestimate, and the real air temperatures are likely to be found somewhere in between these values, although it is difficult to estimate with the bulk urban canopy model. The number of degree-days and the associated energy demand and consumption will naturally be affected by this and should therefore be kept in mind when evaluating the results.

4.2.1 COOLING DEGREE-DAYS
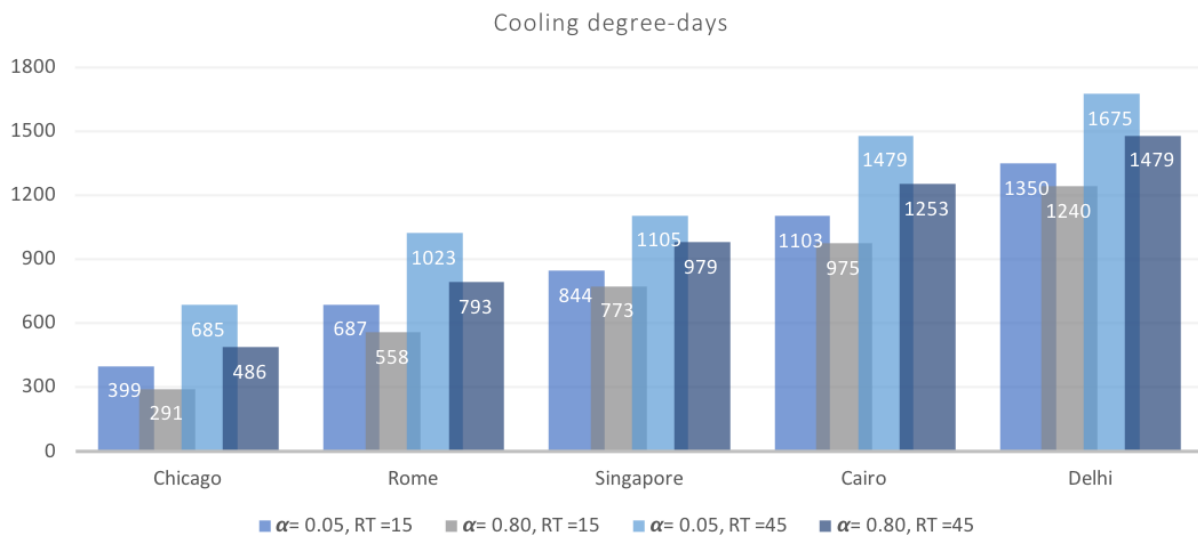
Figure 4-19: *The histogram shows the number of cooling degree-days (CDD) for each city. Conventional and cool roofs with different relaxation times are represented in the individual columns, as presented in the legend. Each column is also marked with the exact number of CDDs.*

The cooling degree-days were calculated according to Equation 3-2 and 3-3 for each city for the different roof types based on the temperature of the canopy layer that is slightly influenced by the rural air (T_{urb}), depicted in the histogram in Figure 4-19. The CDD method quantifies the weather-related energy demand for cooling in buildings, and the value represents the number of degrees over the summer months that require cooling. In general, each city experiences elevated numbers of CDDs for conventional roofs relative to the cool roofs, and the CDDs are also higher for RT15 than RT45. However, the number of CDDs differs largely between cities, with Chicago having the least number of

CDDs and Delhi having the most. This can be explained by the mean temperatures during the summer period for each city, where Delhi clearly has the highest mean temperatures and Chicago has the lowest. For an overview of all mean temperatures for both conventional and cool roofs for RT15 and RT45, see Table 4-1 and Table 4-2 in section 4.1.1.

4.2.2 COEFFICIENT OF PERFORMANCE (COP)
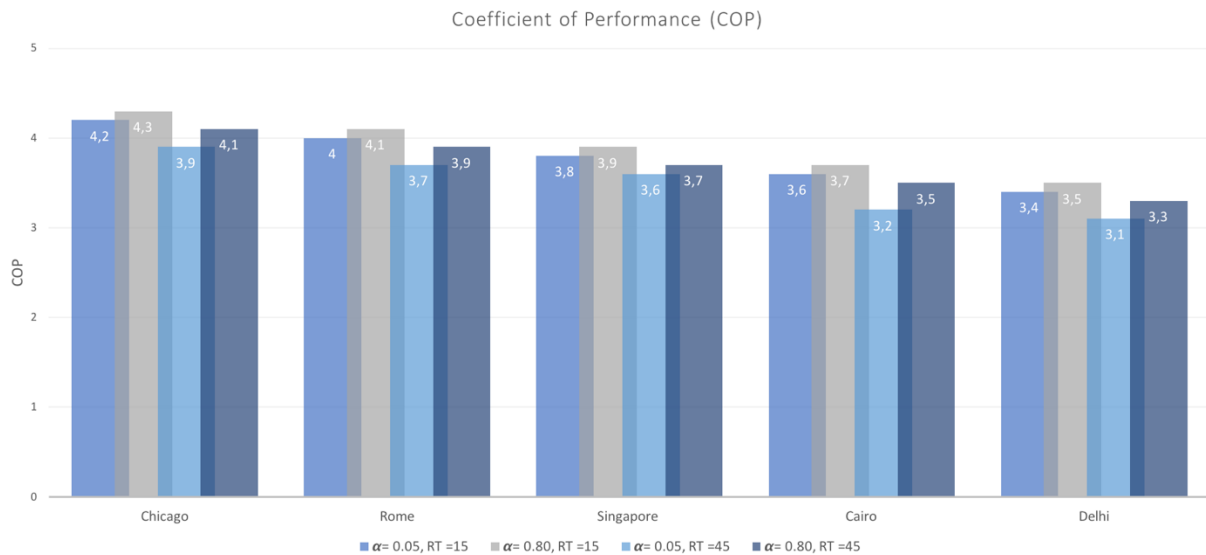
Figure 4-20: *The histogram shows the temperature dependent coefficient of performance (COP) for each city, before and after introduction of cool roofs and for RT15 and RT45 (see legend). The values were calculated from Equation 3-7. The temperature dependent COP is based on the mean temperature during the summer period for each of the four columns.*

In general, Figure 4-20 illustrates that the introduction of cool roofs resulted in an increased COP for all cities in the study. The general trend in COP of the different cities is inversed with regards to CDDs, suggesting that lower mean temperatures contributes to higher COPs, and vice versa. The cooling system is allowed to work more efficiently for a higher COP, which also lead to lower operating costs. However, it is noteworthy (although not surprising) that the mean temperature of the cool roof with RT45 exceeds that of the conventional roof with RT15, resulting in a generally higher COP for the RT15 cases. The highest COP achieved was for Chicago, with a maximum COP of 4.3 and the lowest for Delhi with a COP of 3.1.

As the temperature of the urban layer is likely an overestimate of real urban air temperatures, it is possible that the calculated COPs would be somewhat higher in reality, reducing the energy demand for all cities slightly. Furthermore, the COP will also vary throughout the day, but the diurnal variations in COP is not accounted for in this study. The highest energy consumption will likely take place when the indoor temperatures reaches max, which greatly depends on the thermal mass of the building and how

fast heat is conducted through the envelope. Generally, the need for cooling is highest in the hottest hours of the day (assuming an immediate response on indoor temperature), which also happens to be when the efficiency of the AC unit reaches a minimum. This results in an energy penalty, as the efficiency of the unit is reduced and will use more electric energy in order to maintain the cooling rates for thermal comfort.

4.2.3 COOLING ENERGY DEMAND

The energy demand (or cooling load) for a typical air conditioning unit with a cooling capacity of 12,000 Btu/h was calculated for both roof types and relaxation times. The temperature-dependent energy efficiency (COP) of the system is also considered. The calculation of energy consumption was based on the assumption that the AC unit has an operation time of 12 hours each day of the summer period, due to occupancy issues. The building occupancy will differ from one region to the next, and also from commercial to residential buildings. This depends on work hours, behavioral patterns and thermal preferences of the building users. Consequently, assumptions had to be made in order to best compare the energy use of the different cities and the corresponding change in cost of introducing cool roofs. The cooling loads of buildings are of great importance to the electricity grid, which can experience heavy strains during peak hours. From the 24-hour temperature plots, it is evident that the greatest reductions in temperature happen when temperatures peak, which in turn have implications for the temperature-dependent cooling loads. This can contribute to increase the stability of the grid and provide the urban inhabitants with improvements in power supply and energy security.
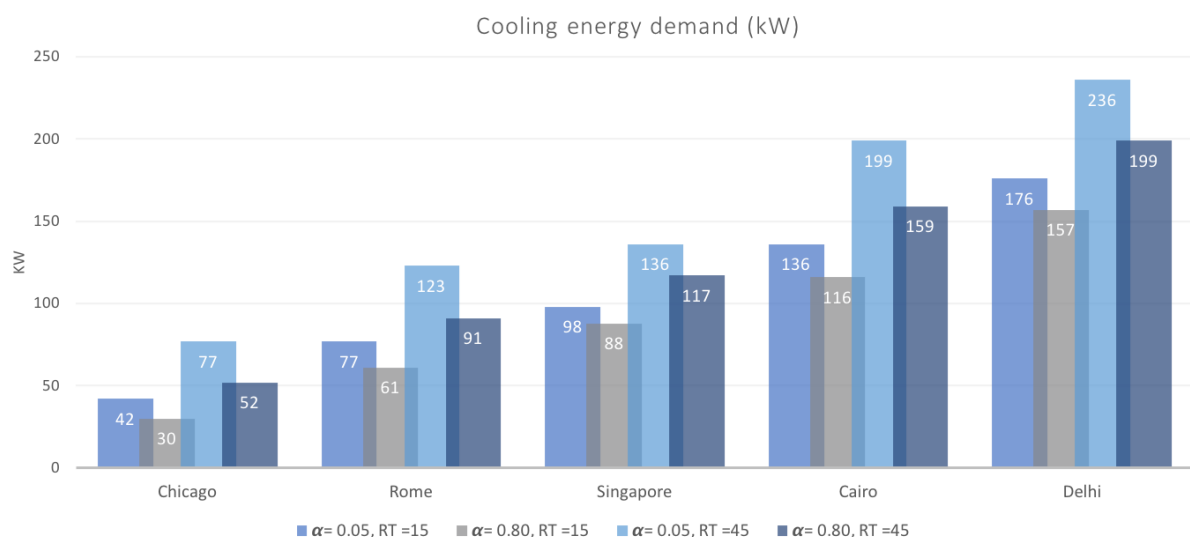
Figure 4-21*: The histogram shows the temperature-dependent cooling energy demand (kW) averaged over the summer months for the air conditioning unit of 12,000 BTU/h for each city. The values are calculated from Equation 3-4. Conventional and cool roofs with different relaxation times are represented in the individual columns, as presented in the legend. Each column is also marked with the exact amount of cooling energy demand.*
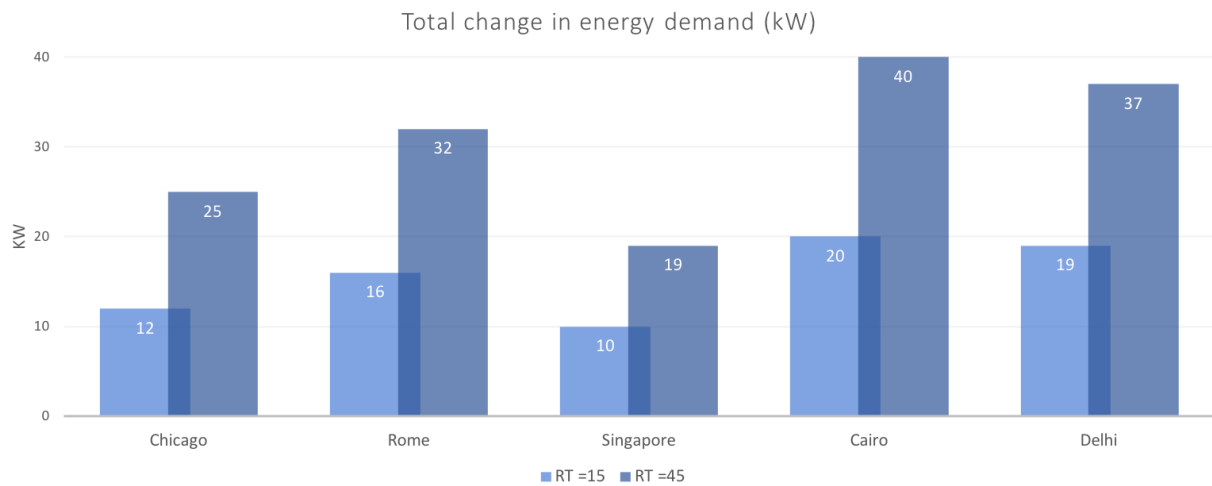
Figure 4-22: *The histogram shows the change in cooling energy demand (kW) from conventional to cool roofs ($\alpha_{0.05}$- $\alpha_{0.80}$) for the different relaxation times for the all cities. Calculated based on the values in Figure 4-21.*
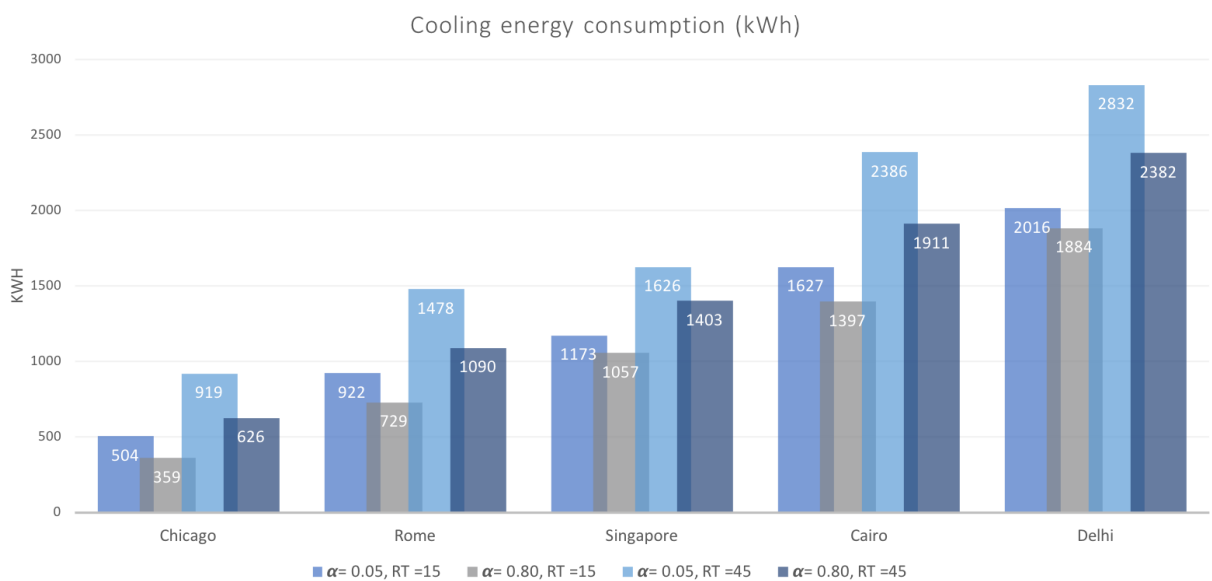
Figure 4-23: *The histogram shows the electrical cooling energy consumption averaged over the summer months for the air conditioning unit of 12,000 BTU/h during the summer period for each city. The values are calculated from Equation 3-5. An occupancy period of 12 hours was assumed for which the AC unit would operate the entire time. Conventional and cool roofs with different relaxation times are represented in the individual columns, as presented in the legend. Each column is also marked with the exact amount of energy used for space cooling.*
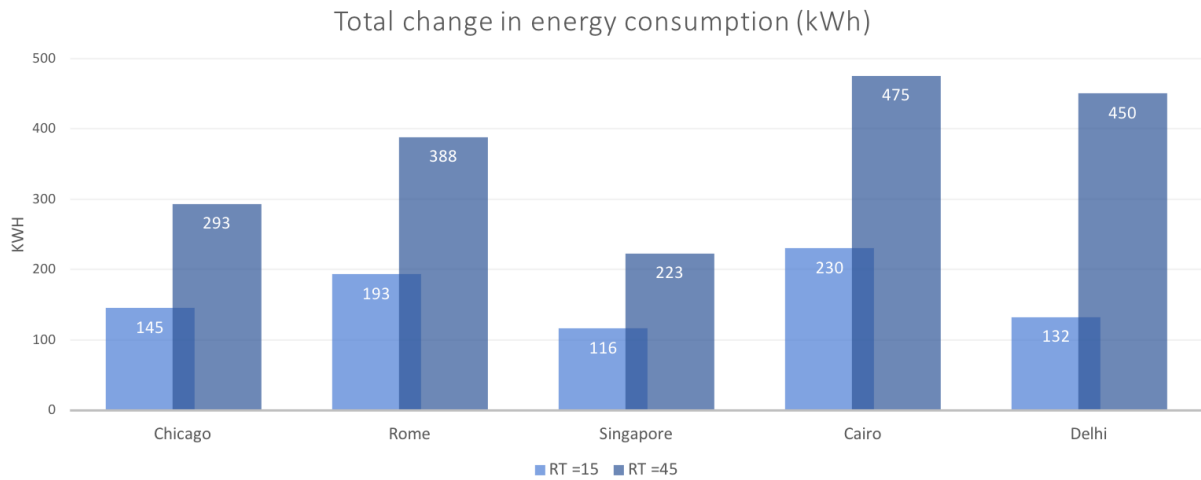
Figure 4-24: *The histogram shows the change in electrical cooling energy consumption from conventional to cool roofs ($\alpha_{0.05}$ - $\alpha_{0.80}$) for the different relaxation times for all cities (see legend). Calculated based on the values in Figure 4-23.*
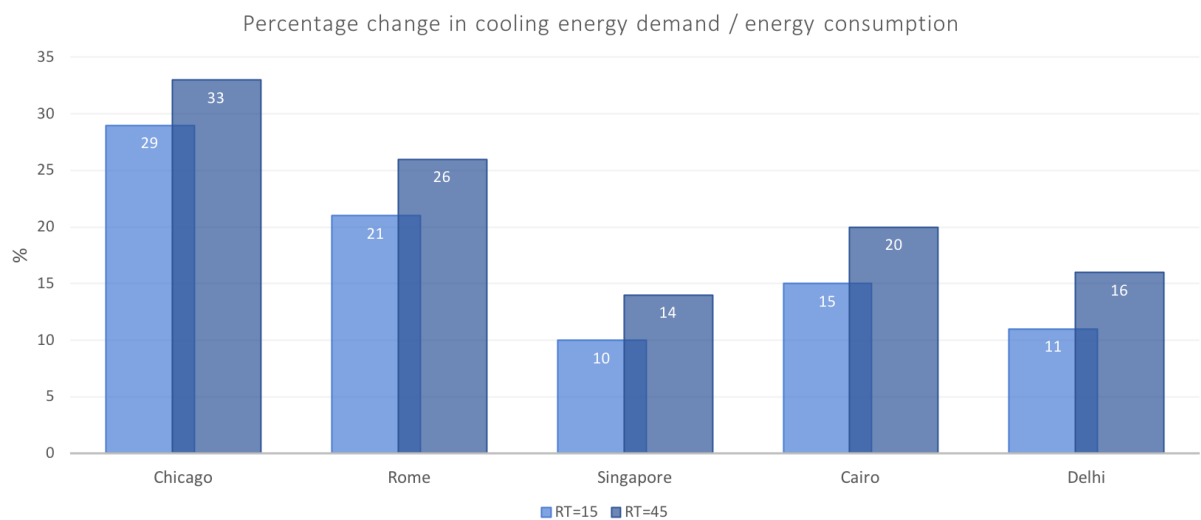
Figure 4-25: *The histogram shows the percentage change in cooling energy demand (kW) and energy consumption (kWh) averaged over the summer months for each city from conventional to cool roofs ($\alpha_{0.05}$ - $\alpha_{0.80}$) for the two relaxation times. Each column is also marked with the exact percentage of energy spared from the introduction of cool roofs.*

In general, Figure 4-21 and 4-23 shows that the cooling load and energy consumption is directly related to the number of degree-days in Figure 4-19, and it is therefore evident that energy demand for cooling strongly relies on the mean outdoor temperature. The cooling load and energy consumption for all cities is clearly lower for RT15 than for RT45, as the areas of RT15 are generally much cooler due to stronger influence from the rural air surrounding the city. It is also evident that the cool roofs have a significant effect on the cooling load and energy consumption in each city, for which lower values were achieved across location and relaxation times.

78

As depicted in Figure 4-25, the percentage change in energy demand for each city is inverse with regards to the overall energy demand and consumption. This suggests that the highest percentage reduction in energy demand is achieved for the cities with the lowest mean urban temperatures for both RT15 and RT45. The percentage change in energy demand is also greater for RT45 than RT15, suggesting that the city core will benefit more from the cool roofs with regards to energy demand than does the suburbs. This can be explained by the fact that the cool roofs have a more significant effect in the city center, where changes in absorbed solar radiation through surface albedo alteration have a greater effect, as demonstrated in Figure 4-17 and 4-18. Although the relationship between temperature and cooling energy demand is nonlinear, the lines in Figure 4-24 clearly establish a strong correlation between temperature and energy demand, which in turn depends on the temperature-dependent COP.

Figure 4-26 illustrates the temperature-load curve (TLC), a plot of cooling electricity demand against temperature. It demonstrates the temperature dependence of cooling loads, which increases for higher temperatures as the cooling requirements goes up. The figure demonstrates a strong correlation between temperature and energy demand. The additional penalty on the energy demand is accounted for due to the temperature-dependent efficiency (COP) of the AC unit, which causes the AC to operate at lower efficiencies for higher temperatures.
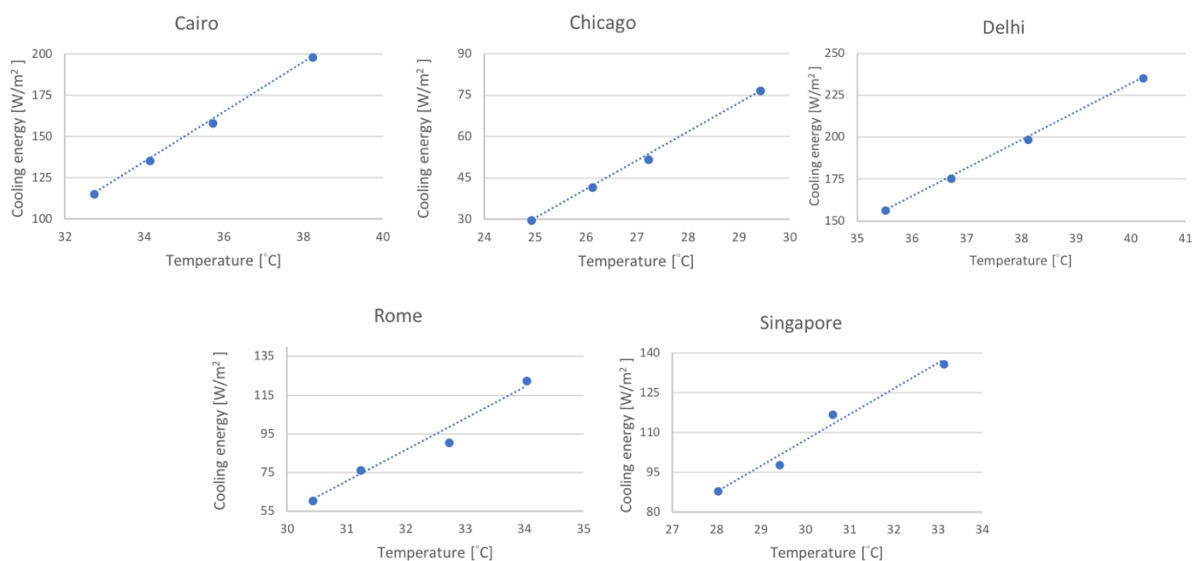
Figure 4-26: *The plots show the temperature-load curve (TLC), and the relationship between mean outdoor temperatures and the cooling energy demand (calculated based on a temperature-dependent COP). The data are presented in different plots for each city as the temperature and cooling energy varies significantly between them, and it was therefore impractical to present all data points in one plot.*

From Figure 4-25, the percentage savings in energy demand and consumption for Chicago was by far the greatest, at 29% for RT15 and 33% for RT45, but the overall energy savings was modest, as can be seen in Figures 4-22 and 4-24. The temperatures of the canopy and atmosphere was greatly reduced for

Chicago post cool roofs, as depicted in Figures 4-17 and 4-18. The humid continental climate with hot summers and lots of incoming sunlight is likely to contribute to this significant change in energy demand during the summer period. Also, the relatively low temperatures compared to the other cities contribute to higher COPs, which allow the AC system to operate more efficiently.

The second-best energy response to the cool roofs was seen for Rome, with energy savings of 21% and 26% for RT15 and RT45. Figures 4-17 and 4-18 show that the temperature reductions for Rome were significant, and the mean temperature during the summer period is also the second lowest produced by the BUCM. It is evident that Rome's Mediterranean climate with hot summers produce significant energy savings from a city-wide cool roof introduction. Figure 4-26 emphasizes the nonlinear relationship between the mean temperature and the energy demand for the cooling unit, and the intermediate temperatures of Rome allows the system to operate at relatively good COPs.

The rainforest climate of Singapore experienced a mid-level cooling load and energy consumption compared to the other cities, as depicted in Figures 4-21 and 4-23. However, the response to the introduction of cool roofs only contributed to energy savings of 10% and 14%. Figures 4-17 and 4-18 demonstrated the temperature reduction of the urban and atmospheric layer, which for Singapore was the weakest response of all cities, which can explain the relatively weak percentage change in cooling load and energy consumption. Despite the intermediate COP levels of Singapore (Figure 4-20), the energy savings was limited. The relationship between temperature and energy demand is depicted in the graph in Figure 4-23, and highlights that the temperatures deeply affect the energy demand of the region. It is worth noting that although both the UHI and energy response to cool roofs are modest, the tropical rainforest climate of Singapore has small annual variations with generally high temperatures. Consequently, the chances of heating penalties are small from the lack of a winter season, and the cool roofs could therefore provide a modest year-round contribution to the UHI effect and energy consumption.

Cairo's hot desert climate produced a response of 15% and 20% for RT15 and RT45. As Figure 4-17 and 4-18 illustrates, Cairo displayed the best temperature response to the cool roofs, likely due to the arid climate that makes the city suitable for surface albedo alterations. Cairo also produced the second-lowest COP of all cities due to the high mean temperatures, which will have a small but significant impact on the energy demand and consumption over time as the AC unit is not allowed to operate as efficiently. This is also evident from Figure 4-23, which highlights the increased energy demand of Cairo due to elevated temperatures.

Delhi had the overall highest cooling energy consumption during the period, and energy response to the cool roofs resulted in savings equal to 11% and 16%, as seen in Figure 4-23. Although the percentage

change from introducing cool roofs were the lowest of all cities, the total energy savings for cooling were still quite significant (Figures 4-21 and 4-22). From Figure 4-17 it is evident that Delhi had an intermediate temperature response to the cool roofs, and as the city produced the highest mean temperatures for the summer period, the associated COP was also the lowest. A slight energy penalty for the energy consumption is likely to have followed, which can also be seen from the high temperature-dependent cooling energy demand in Figure 4-23.

4.2.4 COST IMPLICATIONS

The cost of electricity for the energy consumption during the summer period was calculated based on the mean individual electricity prices of all countries (Equation 3-8). The energy consumption is, as previously stated, based on the assumption that the AC unit has an operation time of 12 hours each day of the period.

As previously stated in section 2.5, electricity prices are usually highest during summer and at peak demand hours because more expensive generation sources are added to meet the increased demand (EIA, 2018). Since the basis for cost calculations are mean annual electricity prices, it is likely that the electricity costs in this study might be an underestimate of the real electricity costs during the summer period.
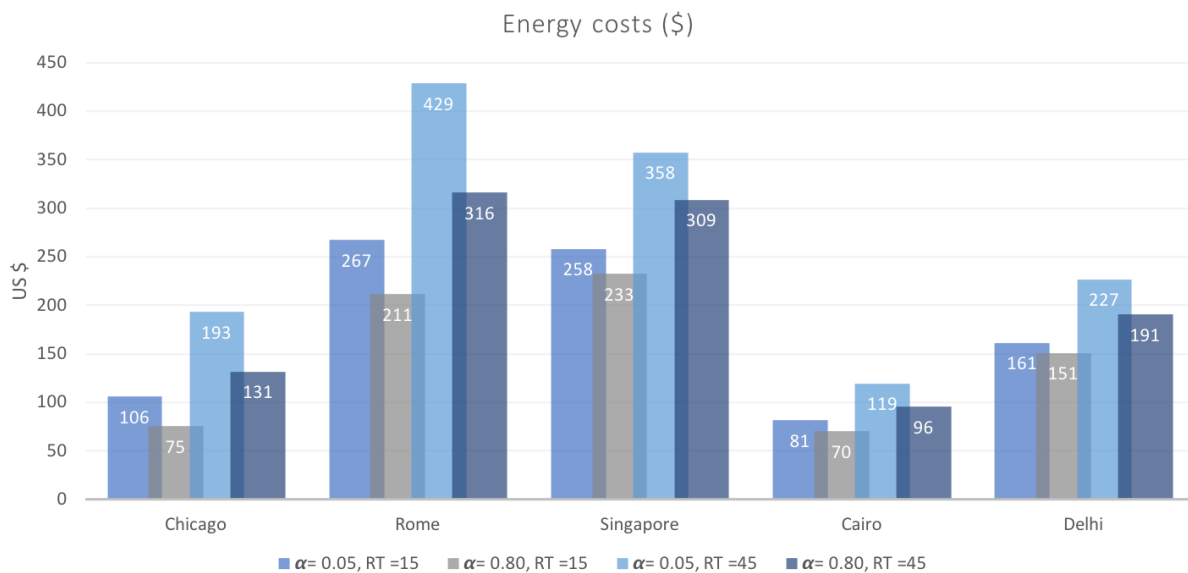
Figure 4-27: *The histogram shows the energy related costs for each city. The costs have been calculated for both roof types and relaxation times based on the average electricity cost in all countries. The resulting costs are associated with the average electricity prices within the different countries. Values have been rounded to the nearest dollar.*
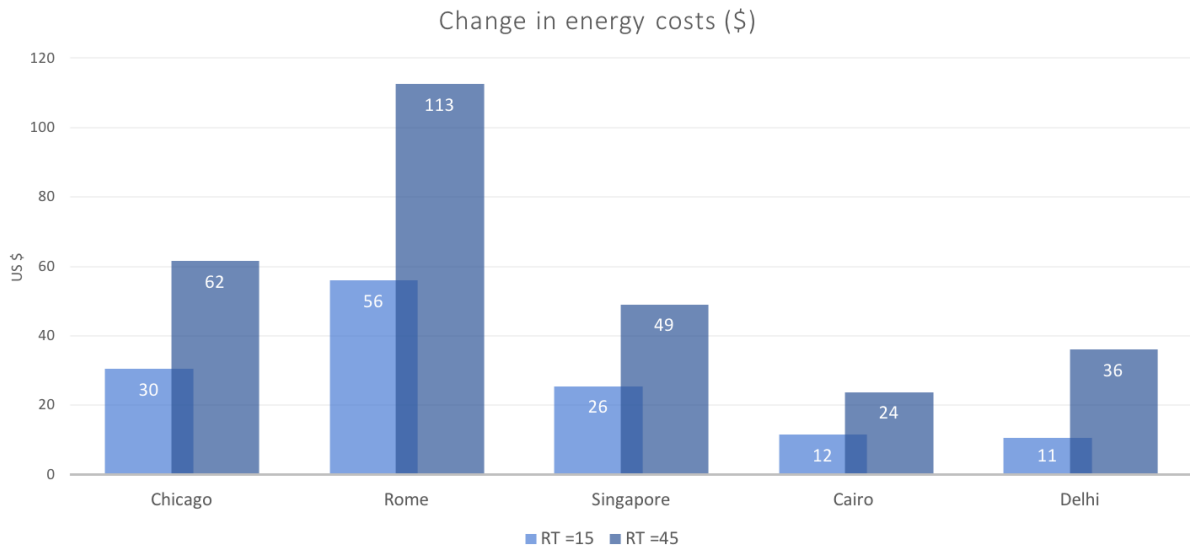
Figure 4-28: The histogram shows the savings in energy related costs for each city from introducing cool roofs. The costs have been calculated for both roof types and relaxation times based on the average electricity cost in all countries. Values have been rounded to the nearest dollar ($).

It is evident from Figure 4-27 that the cost of electric energy varies significantly from one city to another. The variations in costs translates into a significant variation for the potential savings achievable by implementing cool roof technology, as displayed in Figure 4-28. Although the energy consumption in Figure 4-21 shows that Delhi is the highest energy consumer of the cities, electricity prices in India are low, hence the savings are modest, especially for RT15. The savings were also modest due to Delhi's weak energy response to cool roofs. The findings were similar for Cairo: even though Cairo had the lowest electricity cost paired with high energy consumption, the change in costs were modest after cool roofs were installed. Singapore's intermediate electricity consumption and high electricity prices also produced high costs during the summer period, and the city achieved the second-highest savings with regards to costs. Electricity prices in the US are low, and with Chicago's low consumption during the summer, the overall costs were low. However, the city responded well to the cool roofs, which resulted in modest savings with regards to costs. Despite the low cooling energy consumption, Italy have some of the highest electricity prices in the world (Statista, 2018). The savings from cool roofs during the summer period were the highest of the study, which can have significant impacts on the electricity bill.

Electricity costs greatly affect people's energy consumption patterns: in countries with high electricity prices, people are more likely to have an interest in minimizing their electricity consumption due to financial reasons. Significant savings can be achieved through passive energy efficiency measures such as cool roofs. However, in countries where electricity prices are low, reducing electricity consumption might not be a priority because it will not affect the electricity bills notably. Moreover, as stated in section 2.5.1, electricity prices are usually highest during summer, when total demand is high because of more expensive power generation due to increased demand (EIA, 2018). Also, the electricity demand

peaks at the warmest time of the day (assuming instant response of indoor temperatures). This is also the time when the cool roof performance is at its highest, which over time can contribute to significant savings. The benefits of implementing cool roofs should therefore be considered with regards to the potential energy and cost savings that can be achieved over the lifetime of the cool roof, and deterioration and maintenance aspects should also be included in the assessment.
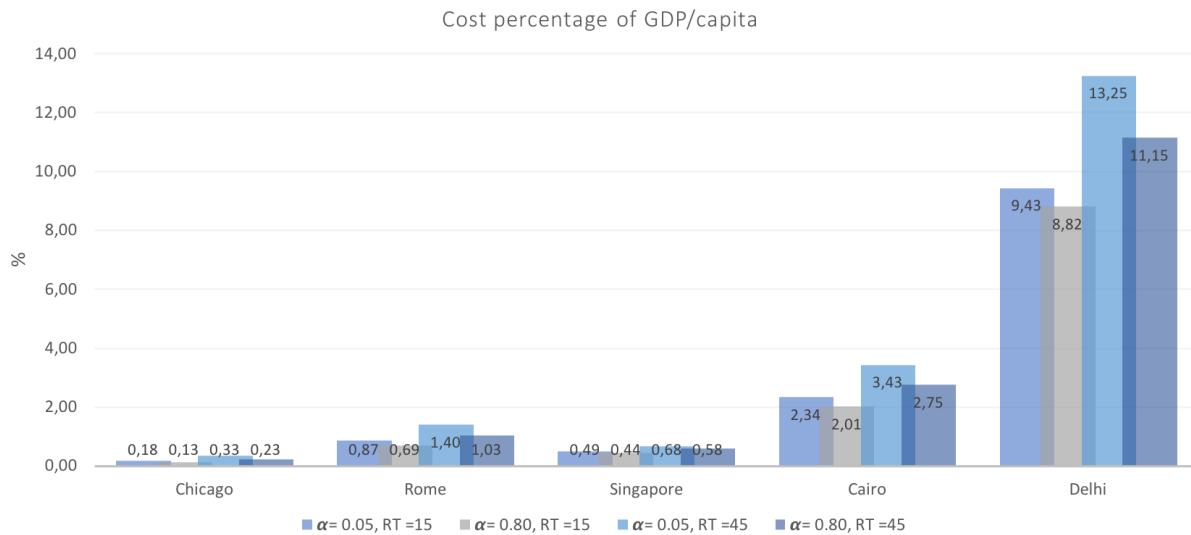
Figure 4-29: *The electricity cost percentage of each country's gross domestic product per capita (GDP/capita) was calculated according to Equation 3-9, based on the GDP values from 2016 listed in Table 3-7. Each column is marked with the percentage the electricity costs make up compared to the GDP/capita.*

By calculating the electricity costs percentage of the gross domestic product per capita for each city, the significance of the savings can be better illustrated (Figure 4-29). For cities located in countries with low purchasing power per capita, such as Cairo and Delhi, the electricity savings from introducing cool roofs can have a quite substantial influence on the economy of individuals. In contrast, for cities with high GDP/capita, like Chicago and Singapore, the cost savings might not be of significant importance compared to the purchasing power of the urban inhabitants. The electricity costs in Singapore are high, but as the GDP/capita is also high the resulting cost savings are modest in comparison. As for Rome, the high electricity prices compared with the intermediate GDP/capita shows that the savings can make up a small part of the economy. However, whether the savings are significant enough to motivate people to invest in energy efficiency measures like cool roofs remains unknown, and further research is suggested on this area.

4.2.5 Cool roofs on city-scale

In order for cool roofs to have an effect on urban temperatures and energy demand, large-scale applications are necessary to produce significant results. Although a local-scale introduction of cool roofs could influence the micro-scale climate and energy demand of small neighborhoods, this effect is likely to be modest compared to a city-wide implementation. However, the question arises of whether or not a cool roof introduction on a city scale is even possible, or likely to happen. The answer is probably no, as this would require both strong governance (top-down) and citizen-driven (bottom-up) initiatives for promoting urban sustainability.

As previously mentioned, in order to meet the 2°C target, the average building energy use per capita needs to be reduced by at least 10% by 2025. The city-wide application of cool roofs provided the various cities in this study with energy savings between 10-33%. However, an introduction of cool roofs on a city scale is unlikely to be accomplished; it is rather likely that cool roofs could be part of a larger smart urban sustainability scheme. In combination with green roofs and other (smart or passive) energy efficiency strategies that contribute to mitigate the UHI effect, cool roofs could provide a significant contribution to the overall sustainability in a well-planned urban scenario.

4.3 Methodology discussion

4.3.1 The 1-D bulk urban canopy model

As previously described in the methodology section, the 1-D bulk urban canopy model is a semi-empirical urban canopy parametrization (SURY) for atmospheric modelling, where urban canopy parameters are translated into bulk parameters. The bulk albedo approximation avoids explicit numerical computation of the complex trapping of radiation in urban canyons, and therefore reduces the computational demand compared to other canyon radiation models (Wouters et al., 2016).

The model performance strongly depends on the temperature quantity considered. Consequently, it is important to keep in mind that parameter settings that improve the UHI effects can lead to worse absolute temperatures, and the other way around. This is also the case for day-time temperatures vs. night-time temperatures, and land-surface temperatures vs. air temperatures (Wouters et al., 2016).

Wouters et al. (2016) investigated the model sensitivity of SURY for urban canopy parameter ranges in the local climate zones of compact low-rise and compact mid-rise cities in Stewart and Oke (2012). They found that the change in response and performance to alterations in urban canopy parameters are generally restricted to the urban areas and do not affect the rural areas. An intermediate sensitivity was

found for the building height and height-to-width ratio, and roof fraction displayed the lowest sensitivity. For both surface and atmospheric UHIs, the albedo sensitivity is high, although slightly lower than the sensitivity for thermal parameters during daytime. At night-time, the sensitivity is somewhat lower than for AHE, height-to-width ratio and roof fraction. Some of the model errors exceed the model sensitivity range with regard to uncertainty of the urban canopy parameters. This emphasizes that the majority of the model uncertainty may result from deficiencies in the land-surface module and other aspects of the coupled atmospheric model, and not a result of urban canopy parameter uncertainty (Wouters et al., 2016).

SURY allows for the verification of consistency between urban canopy parameters and bulk parameters, resulting in increased precision and comparison consistency in climate assessments for urban-climate research. However, the semi-explicit nature of SURY implies some limitations for complex physical urban processes. Specifically, SURY does not resolve the full heterogeneity of the urban canopy, and micro-scale dynamic and physical processes and features are therefore not represented. Instead, it assumes a homogeneous surface temperature of the urban canopy. Consequently, the model does not represent the varying temperatures among the different elements in the urban canopy resulting from shadowing and thermal and radiative properties (Wouters et al., 2016).

The 1-D atmospheric layer model is also based on many simplifications and assumptions. The temperature change with time is calculated using K-theory for turbulence and a simple relaxation time approach for advection (Krayenhoff and Voogt, 2010). For details see Appendix A1.10. The turbulent eddy diffusion coefficient for temperature is calculated assuming close to neutral atmospheric conditions and is dependent on the boundary layer height (assumed to be a time dependent input to the model) and the thermal roughness length. The assumption of near neutral conditions will possibly underestimate turbulence during strong convection. However, this simplification is in most cases of less importance than the choice of relaxation time for the advective processes. By using the displacement height and aerodynamical roughness of the city, the windspeed can be estimated using the rural wind speeds at the top of the atmospheric model (assumed to be a time dependent input to the model) and calculated for each model layer by assuming a logarithmic wind profile. Details of the calculations are given in Appendix A1.10 (Sorteberg, 2017).

4.3.2 DEGREE-DAYS

The degree-day approach is considered only as an approximation method, as many simplifying assumptions must be made. One of these assumptions is the use of average conditions of parameters such as internal temperatures, causal gains and air infiltrations rates (CIBSE, 2006). According to

Antunes et al. (2015), there are three main criticisms that should be emphasized when using degree days: 1) The use of outdoor ambient temperatures is by far the biggest limitation. With respect to this study, the temperature of the urban layer was used, which is likely an overestimate of the real temperature of the air that affects the buildings. 2) The way the degree-days methodology is calculated assumes steady state conditions, where each degree rise would result in an equal indoor temperature rise. There will also be a lot of other factors affecting the indoor temperature, such as fresh air loads and window shading. 3) Comfort levels experienced by building residents will differ from one region to the next, as buildings have varying levels of insulation and cooling technologies. Additionally, perceptions of thermal comfort are evaluated independent of age, health and activity levels, and it is false to assume that these factors will remain constant over time. As global warming drives the local urban temperatures up, the population is likely to acclimatize and adapt to the new temperature regimen. Consequently, people's perception of thermal comfort will change and thereby affect the BPT.

Additionally, calculating degree-days using hourly temperatures does not imply that the hourly energy consumption can be accurately estimated. When performing a building energy analysis, summation of degree-days over a sufficient period of time is necessary to produce outputs of any real value.

The key to a credible cooling degree-day energy assessment lies in the definition of base temperature. Base temperatures are calculated from the balance point temperature (BPT) and it considers the building size, configuration and available cooling technology for the region in question. As the base temperature is this study is not site specific, some uncertainty can be expected. Moreover, building size and configuration have not been assumed, leading to increased uncertainty. An additional problem for cooling energy calculations is that this needs to be defined specifically for each different type of cooling system. Personal preferences, acclimatization and specific building characteristics can also lead to variations in base temperatures, and these properties are likely to vary between the cities in this study. This lack of objectivity means that it is not surprising to find a wide range of base temperatures around the world (Antunes et al., 2015).

4.3.3 ENERGY CONSUMPTION

The method for calculating cooling energy loads and consumption is a simplification that is based on a lot of assumptions, and caution should therefore be exercised when interpreting results. Although the base temperatures are calculated from the balance point temperature (BPT), which take into account building size, configuration and available cooling technology, parameters such as solar gains, internal gains, fresh air loads and humidity of the indoor air are building and climate specific. As this study aims to compare the weather-related energy demands of idealized buildings in different climate zones,

building-specific parameters have been overlooked, and a more comprehensive assessment of the energy demand should therefore be applied for specific sites and buildings.

The temperature dependency of the COP has been considered, but the fact that the COP will vary with the diurnal temperature cycle is overlooked. The study does not contemplate overnight cooling effects, which in theory can be incorporated into the base temperature. Yet, the energy consumption calculations account for occupancy periods. However, as many unknown factors are related to these issues, it is hard to establish a number of hours representative for both commercial and residential buildings across cultures, regions and climates.

5. CONCLUSION AND SUGGESTIONS FOR FURTHER WORK

5.1 CONCLUSION

The main objective of this thesis was to build a framework for assessing the cool roof mitigation potential on the UHI effect and the associated response in energy demand. This framework allows for an assessment of the effects of cool roofs on the city-scale and down to the building-scale in idealized cities and buildings in different climatic zones.

In urban environments where green roofs are not the preferred option, cool roofs offer an effective and affordable strategy for mitigating the urban heat island effect and increasing building energy efficiency. Although literature suggest that cool roofs perform better in arid climates with regards to mitigating UHIs, this study has shown that this is not necessarily the case. The results displayed a general reduction in temperature after cool roofs were implemented for all cities, indicating a significant UHI mitigation potential. The magnitude of the UHI effect was reduced by 23-31% after the large-scale introduction of cool roofs. The model indicated a significant temperature response to cool roofs during daytime with peak changes in temperatures a few hours after solar noon, while it appeared to be limited at night due to the insignificant temperature differences between conventional and cool roofs.

The cool roof reduction of urban temperatures also had significant implications for energy efficiency, results ranging from 10-33% between the cities. The UHI mitigation potential proved most significant for the central urban areas, but the suburbs also achieved enhanced urban environments through alleviation of undesirable UHI consequences like increased energy consumption, reduced air and water quality and elevated levels of thermal stress. These threats will become more prominent as the temperatures rise due to climate change and addressing them at an early stage will be crucial in order to achieve future sustainability targets. As the SDG 7.3 aims to double the energy efficiency by 2030, cool roofs could play an important part in this scenario.

Cool roof implementation on a city-wide basis could help increase electricity cost savings in all cities, and at the same time reduce the demand during peak hours. The cooling loads of buildings are of great importance to the electricity grid, which can experience heavy strains during peak hours. Cool roofs can therefore contribute to increase the stability of the grid and provide the urban inhabitants with improvements in power supply and energy security, in line with SDG 7. At the same time, the energy consumption during the summer was reduced substantially, and the associated cost indicated significant savings for cities located in areas with expensive electricity. However, it should be noted that the significance of the savings greatly depends on the GDP/capita. Electricity prices are highest during summer and when the electricity demand peaks, which is also the time of the year and day when the

cool roof performance is at its highest. Although cool roofs can help solve parts of the building energy challenges, future engineers and architects should aim to improve the energy efficiency through smart, integrated design solutions to keep buildings cool during summer.

There appears to be no clear connection between the UHI mitigation potential of cool roofs and the resulting energy consumption. While the UHI largely depends on the temperature differences between the urban and rural areas, the degree-days-based energy calculations indicated that the mean temperatures during the summer period provided the main contribution to the results.

The introduction of cool roofs on a city-scale could potentially contribute to some desirable feedback effects. As the need for cooling goes down, the associated anthropogenic heat emissions (AHE) from the AC units are reduced. AHE is known to be an important contributor to the UHI, and as the urban air receive less heat input from electrical systems and devices, this can have a small positive effect on the thermal comfort and energy demand in cities. However, an introduction of cool roofs on a city scale is unlikely to be accomplished. Instead, cool roofs could be part of a larger urban sustainability scheme, and hence provide a significant contribution to the overall sustainability in a well-planned urban scenario.

As previously stated, the smart city intends to systematically incorporate mitigation and adaptation measures to enable the city to respond to climate change through a well-planned and designed urban environment. Furthermore, sustainable smart cities are cities that reduce energy demand and increase sustainability and efficiency, and such projects should include strategies for reducing urban heat islands and limit the urban energy consumption. Not only does cool roofs generate improvements in urban sustainability and environment through UHI mitigation, it also provides increased energy efficiency levels in buildings. As many technological methods and devices that are being applied in smart city schemes today consume electricity in order to operate, more passive strategies should be promoted in order to achieve higher levels of urban sustainability. Consequently, cool roofs possess the qualities required from a smart city strategy and should therefore be a natural part of any future smart city scenario where climates are cool roof-favorable.

5.2 SUGGESTIONS FOR FURTHER WORK

As the framework developed throughout this thesis was limited to investigate the UHI and energy response to cool roofs during the three summer months (June, July and August), a natural step further will be to determine the year-round effect of cool roofs in order to account for potential heating penalties during winter. Moreover, it could be useful to run the bulk urban canopy model with different parameters such as albedo, emissivity, anthropogenic heat and relaxation time for different local climate zones. It would also be interesting to further explore the cool roof mitigation potential in all climate zones globally, in order to map the response and use it as an urban planning assessment tool for various sustainability projects. Additionally, an increase in the albedo of entire buildings and the canopy floor (roads and pavements) would provide insightful information with regards to expanding the cool roof paradigm. A thorough comparison of cool and green roof performance in different climate zones could also provide beneficial information when planning for sustainable urban solutions across the globe.

APPENDIX

APPENDIX 1: THE 1-D BULK URBAN CANOPY MODEL

A1.1 THE BULK URBAN CANOPY SURFACE TEMPERATURE

The entire section is the work of Sorteberg (2017)

We calculate the urban canopy surface temperature by calculating the temperature for a thin slab of the canopy with thickness $d_{can,1}$ and an effective volumetric heat capacity C_{can}.

$$C_{can,1}d_{can,1}\frac{\partial T_{can,1}}{\partial t} = (1 - \alpha_{can})SW_{sky}^{\downarrow} + LW_{sky}^{\downarrow} - LW_{can}^{\uparrow} - H_{can} - LE_{can} - G_{can,1,2} + Q_{ant} \qquad [Eq. A1.1]$$

Using a small value for $d_{can,1}$ we assume that the canopy surface temperature equals the temperature for the 1st urban canopy layer:

$$T_{can,s} = T_{can,1} \qquad [Eq. A1.2]$$

The bulk turbulent sensible heat fluxes Q_H from the urban canopy is calculated as:

$$Q_H = c_p \rho_a k^2 \frac{u_a(z_{lowlev})}{ln\left(\frac{z_{lowlev} - d}{z_0}\right) ln\left(\frac{z_{lowlev} - d}{z_{0H}}\right)} \qquad [Eq. A1.3]$$

Where c_p is the specific heat capacity for dry air, ρ_a is the air density.

A1.2 THE BULK CANOPY TEMPERATURES BELOW THE CANOPY SURFACE

The temperatures of the other urban layers layer (layer 2 and downwards) evolve according to a simple heat conduction equation.

$$\frac{\partial T_{can}}{\partial t} = \frac{1}{C_{can}d_{can}}\frac{\partial T_{can}}{\partial z}\left(\lambda_{can}\frac{\partial T_{can}}{\partial z}\right) \qquad [Eq. A1.4]$$

Where C is the heat capacity and λ the conductivity

The text below describes a bulk urban canopy model where the different parts of the urban substrate (roofs, walls, roads, paved surfaces, bare ground, vegetation) is not treat separately but as a bulk substrate where the temperature at the top of the substrate is calculated using the energy balance with an effective volumetric heat capacity C_{can}. The flow of heat into the substrate (envision this as the flow into the buildings, roads etc.) is given by conduction.

A1.3 THE BULK CANOPY TEMPERATURES BELOW THE CANOPY SURFACE

The temperatures of the other urban layers layer (layer 2 and downwards) evolve according to a simple heat conduction equation

$$\frac{\partial T_{can}}{\partial t} = \frac{1}{C_{can}} \frac{\partial T_{can}}{\partial z}\left(\lambda_{can}\frac{\partial T_{can}}{\partial z}\right) \tag{Eq. A1.5}$$

Where C is the heat capacity and λ the conductivity. This can be approximated as

$$\frac{\partial T_{can,k}}{\partial t} = \frac{1}{\bar{C}_{can,k,k+1}d_{can,k}}\left(G_{can,k-1,k} - G_{can,k,k+1}\right) \tag{Eq. A1.6}$$

k goes from 2 to N where N is the number of canopy layers. $\bar{C}_{can,k,k+1}$ is the average heat capacity between layers k and k+1:

$$\bar{C}_{can,k,k+1} = \frac{\left(d_{can,k} + d_{can,k+1}\right)}{\left(d_{can,k}/C_{can,k} + d_{can,k+1}/C_{can,k+1}\right)} \tag{Eq. A1.7}$$

The conduction flux between layers k and k+1 (*k=2* to N-1) is given as

$$G_{can,k,k+1} = \lambda_{can}\frac{\partial T_{can}}{\partial z} \approx \bar{\lambda}_{can,k,k+1}\frac{\left(T_{can,k} - T_{can,k+1}\right)}{0.5\cdot\left(d_{can,k} + d_{can,k+1}\right)} \tag{Eq. A1.8}$$

Where $\bar{\lambda}_{can,k,k+1}$ is the average conductivity (material property describing the ability to conduct heat) between layers k and k+1:

$$\bar{\lambda}_{can,k,k+1} = \frac{\left(d_{can,k} + d_{can,k+1}\right)}{\left(d_{can,k}/\lambda_{can,k} + d_{can,k+1}/\lambda_{can,k+1}\right)} \tag{Eq. A1.9}$$

The lower boundary condition $G_{can,N,N+1}$ should be given by the temperature difference between the lowest canopy layer and the average of the internal temperature of the buildings and the internal temperature below the roads and other surface materials that the city consist of, but since this is unknown we use the soil temperature below the urban canopy as our lower boundary condition.

$$G_{can,N} = \lambda_{can,N} \frac{(T_{can,N} - T_{bndry,low})}{0.5 \cdot (d_{can,N} + d_{soil,1})} \approx \bar{\lambda}_{can,N} \frac{(T_{can,N} - T_{soil,1})}{0.5 \cdot (d_{can,N} + d_{soil,1})} \qquad [\text{Eq. A1.10}]$$

A1.4 THE BULK URBAN CANOPY HEAT CONDUCTIVITY AND HEAT CAPACITY

The three-dimensional urban canopy results in a larger contact surface with the atmosphere than a level ground. Thus, the heat exchange between the atmosphere and the urban canopy is increased. This is enhancing the surface canopy conductivity $\lambda_{can,s}$ (surface is here the top of the urban canopy). In addition, the urban canopy increases the surface thermal heat capacity conductivity $C_{can,s}$. The increase can be expressed by the surface area index (SAI):

$$\lambda_{can,s} = SAI \cdot \lambda_s \qquad [\text{Eq. A1.11}]$$

$$C_{can,s} = SAI \cdot C_s \qquad [\text{Eq. A1.12}]$$

Where λ_s and C_s is the weighted average (surface fractions of roofs, walls and roads) surface conductivity and thermal heat capacity. The surface area index (SAI) is the ratio between the land-surface area that envelops the urban canopy and the plan area. In the case of an idealized urban canopy with parallel urban canyons, straight roads and flat roofs the SAI can be expressed as the surface area index of the street canyon plus the roof fraction:

$$SAI = \left(1 + 2\frac{h_{build}}{w_c}\right)(1 - f_{roof}) + f_{roof} \qquad [\text{Eq. A1.13}]$$

Where h_{build}/w_c is the height-to-width ratio of the street canyons and f_{roof} is the roof fraction.

The weighted average surface conductivity and thermal heat capacity is given by the conductivity/heat capacity of the urban canyon ($\lambda_{s,c}/C_{s,c}$) and the conductivity/heat capacity of the roofs ($\lambda_{s,roof}/C_{s,roof}$):

$$\lambda_s = \frac{1}{SAI}\left[(1 - f_{roof})\lambda_{s,c} + f_{roof}\lambda_{s,roof}\right] \qquad [\text{Eq. A1.14}]$$

$$C_s = \frac{1}{SAI}\left[(1 - f_{roof})C_{s,c} + f_{roof}C_{s,roof}\right] \qquad [\text{Eq. A1.15}]$$

Where by the surface conductivity/heat capacity of the urban canyon ($\lambda_{s,c}/C_{s,c}$) is given by:

$$\lambda_{s,c} = \frac{w_c \lambda_{road} + 2h_{build} \lambda_{wall}}{w_c + 2h_{build}} = \frac{\left(\lambda_{road} + 2\frac{h_{build}}{w_c}\lambda_{wall}\right)}{1 + 2\frac{h_{build}}{w_c}} \qquad \text{[Eq. A1.16]}$$

$$C_{s,c} = \frac{w_c C_{road} + 2h_{build} C_{wall}}{w_c + 2h_{build}} = \frac{\left(C_{road} + 2\frac{h_{build}}{w_c}C_{wall}\right)}{1 + 2\frac{h_{build}}{w_c}} \qquad \text{[Eq. A1.17]}$$

To ensure a smooth flux of heat to the soil beneath the urban canop*y* with a thickness h_{build} the canopy conductivity/heat capacity is changing vertically from the surface (top of canopy) and down to the ground (h_{build}) as a linear gradient between the surface value and the value of the soil below:

$$\lambda_{can,N} = \begin{array}{ll} \left(1 - \dfrac{z_N}{h_{build}}\right)\lambda_{can,s} - \dfrac{z_N}{h_{build}}\lambda_{soil} & 0 < z_N < h_{build} \\[2ex] \lambda_{soil} & z_N \geq h_{build} \end{array} \qquad \text{[Eq. A1.18]}$$

$$C_{can,N} = \begin{array}{ll} \left(1 - \dfrac{z_N}{h_{build}}\right)C_{can,s} - \dfrac{z_N}{h_{build}}C_{soil} & 0 < z_N < h_{build} \\[2ex] C_{soil} & z_N \geq h_{build} \end{array} \qquad \text{[Eq. A1.19]}$$

A1.5 THE URBAN CANOPY THERMAL ADMITTANCES

Thermal admittance is a measure of a material's ability to absorb heat and release it over time. It can be used as an indicator of the thermal storage capacity (thermal mass) of a material, absorbing heat from and releasing it to a space through cyclical temperature variations, thus evening out temperature variations and so reducing the demand on building services systems. Urban thermal admittance is expressed as $\mu_{can} = \sqrt{\lambda_{can} C_{can}}$ where the higher the admittance value, the higher the thermal storage capacity.

A1.6 THE BULK LONG WAVE RADIATION FROM THE URBAN CANOPY

The longwave radiation from the canopy is given as the long wave emission from the canopy and the reflected longwave radiation:

$$LW_{can}^{\uparrow} = \varepsilon_{can}\, \sigma T_{can,s}^{4} + (1 - \varepsilon_{can})LW_{can}^{\downarrow} \qquad \text{[Eq. A1.20]}$$

The emissivity of the urban canopy is given by the emissivity of the road, walls and roof and the sky view factor ψ_{sky} (the ratio between radiation received by a planar surface and that from the entire hemispheric radiating environment) that reduces the longwave radiation coming out from the urban canyon (walls and roads). ψ_{sky} is a dimensionless value that ranges from 0 to 1.

As it is only the urban canyon that is influenced by the sky view factor, the whole urban canopy (including the canyon and roofs) sky view factor ψ_{sky} is weighted with the roof fraction:

$$\psi_{sky} = f_{roof} + (1 - f_{roof})\psi_c \qquad \text{[Eq. A1.21]}$$

Where ψ_c is the canyon sky view factor that is depending on the canyon height-to-width ratio h_{build}/w_c

$$\psi_c = e^{\left(-0.6\frac{h_{build}}{w_c}\right)} \qquad \text{[Eq. A1.22]}$$

The urban canopy emissivity ε_{can} is given by the weighted reflectivity of the roof emissivity ε_{roof} and the canyon emissivity (walls + roads) ε_c

$$\varepsilon_{can} = \varepsilon_c\psi_c(1 - f_{roof}) + f_{roof}\varepsilon_{roof} \qquad \text{[Eq. A1.23]}$$

Where the canyon emissivity is the weighted average of the road ε_{road} and wall albedo ε_{wall} that can be calculated using the mean height-to-width ratio of the street canyons:

$$\varepsilon_c = \frac{w_c\varepsilon_{road} + 2h_{build}\varepsilon_{wall}}{w_c + 2h_{build}} = \frac{\left(\varepsilon_{road} + 2\frac{h_{build}}{w_c}\,\varepsilon_{wall}\right)}{1 + 2\frac{h_{build}}{w_c}} \qquad \text{[Eq. A1.24]}$$

A1.7 THE BULK SHORT WAVE RADIATION FROM THE URBAN CANOPY

The shortwave radiation from the canopy is given as reflected shortwave radiation:

$$SW_{can}^{\uparrow} = \alpha_{can} \, SW_{can}^{\downarrow} \qquad \text{[Eq. A1.25]}$$

The urban canopy albedo α_{can} is given by the weighted reflectivity of the roof albedo α_{roof} and the canyon albedo (walls + roads) α_c:

$$\alpha_{can} = \alpha_c \psi_c (1 - f_{roof}) + f_{roof} \alpha_{roof} \qquad \text{[Eq. A1.26]}$$

Where the canyon albedo is the weighted average of the road α_{road} and wall albedo α_{wall} that can be calculated using the mean height-to-width ratio of the street canyons:

$$\alpha_c = \frac{w_c \alpha_{road} + 2h_{build}\alpha_{wall}}{w_c + 2h_{build}} = \frac{\left(\alpha_{road} + 2\frac{h_{build}}{w_c}\,\alpha_{wall}\right)}{1 + 2\frac{h_{build}}{w_c}} \qquad \text{[Eq. A1.27]}$$

A1.8 THE BULK TURBULENT SENSIBLE HEAT FLUXES FROM THE URBAN CANOPY

The bulk turbulent sensible heat fluxes Q_H from the urban canopy is calculated as:

$$Q_H = c_p \rho_a k^2 \frac{u_a(z_{lowlev})}{ln\left(\frac{z_{lowlev} - d}{z_0}\right) ln\left(\frac{z_{lowlev} - d}{z_{0H}}\right)} (T_a(z_{lowlev}) - T_{can,s}) \qquad \text{[Eq. A1.28]}$$

Where c_p is the specific heat capacity for dry air, ρ_a is the air density.

A1.9 THE AERODYNAMIC AND THERMAL ROUGHNESS LENGTHS

The aerodynamic roughness lengths for the urban canopy is calculated as

$$z_0 = 0.75 h_{build} \qquad \text{[Eq. A1.29]}$$

In contrast to homogenously vegetated surfaces, which contain porous-rough obstacles urban areas, which are composed of bluff-rough obstacles, exhibit much smaller values of the thermal roughness length z_{0H}. This inhibit the turbulent transfer of heat from the urban substrate to the atmosphere, so that

a relatively large share of the available radiant surface energy flux is converted to storage heat rather than to turbulent sensible heating of the atmosphere.

We assume that the thermal roughness is a tenth of the aerodynamic roughness lengths:

$$z_{0H} = \frac{z_0}{10} \qquad\qquad \text{[Eq. A1.30]}$$

A1.10 THE 1-D ATMOSPHERIC PLANETARY BOUNDARY LAYER MODEL

The atmospheric boundary layer temperature is T_a calculated based on the vertical fluxes generated by turbulence and advection.

$$\frac{\partial T_a}{\partial t} + u_a \frac{\partial T_a}{\partial x} = -\frac{\partial}{\partial z}(\overline{w'T'}) \qquad\qquad \text{[Eq. A1.31]}$$

By assuming first order closure K theory for the turbulent term and assuming a simple relaxation-type advection term where the urban wind and temperature is relaxed toward the rural with a relaxation timescale τ [s] we get:

$$\frac{\partial T_a}{\partial t} = \frac{\partial}{\partial z}\left(K_h \frac{\partial T_a}{\partial z}\right) + u_a \frac{T_{a,rur} - T_{a,urb}}{\tau} \qquad\qquad \text{[Eq. A1.32]}$$

The relaxation timescale $\tau = \Delta x / u_a$ where Δx is the distance from the urban site being modeled to the rural–urban boundary. For a wind speed of 4 m/s and a 5 km distance to the rural–urban boundary this translates into a relaxation time of around 20 minutes.

The wind profile is simplified by a logarithmic wind profile as:

$$u_a(z) = u_a(z_{ref}) \frac{ln\left(\frac{z-d}{z_0}\right)}{ln\left(\frac{z_{ref}-d}{z_0}\right)} \qquad\qquad \text{[Eq. A1.33]}$$

The turbulent eddy diffusion coefficients (m^2/s) for heat (K_h) is calculated as:

$$K_h(z) = K_{h,0} + \frac{k^2 u_a(z_{lowlev})}{\left(\frac{z_{lowlev}-d}{z_{0H}}\right)}\left(1-\frac{z}{h_{PBL}}\right)^n \qquad\qquad \text{[Eq. A1.34]}$$

$K_{h,0} = 0.5$ m^2/s is a minimum value. Following Nieuwstadt, 1984 we set $n=1/4$. The above expression is only valid within the planetary boundary layer ($z < h_{PBL}$) above this $K_{h,0} = 1$ m^2/s. The planetary boundary layer h_{PBL} is taken as input to the model.

APPENDIX 2: MODEL VARIABLES FROM MERRA-2

Table A2-1: 1-hourly time-averaged single-level data downloaded from the NASA Earthdata website for each city and used as input variables in the urban canopy model.

VARIABLE	DESCRIPTION
PBLH	Planetary boundary layer height
TSTAR	Surface temperature scale
USTAR	Surface velocity scale
Z0H	Surface roughness for heat
Z0M	Surface roughness
EVAP	Evaporation from turbulence
HFLUX	Sensible heat flux from turbulence
LWGAB	Surface absorbed longwave radiation
PRECCUCORR	Liquid water convective precipitation, bias corrected
PRECLSCORR	Liquid water large scale precipitation, bias corrected
PRECSNOCORR	Snowfall, bias corrected
SWGDN	Incident shortwave land
SWLAND	Net shortwave land
DISPH	Zero plane displacement height
SLP	Sea level pressure
H850	Height at 850 hpa
Q850	Specific humidity at 850 hpa
QV10M	10-meter specific humidity
T850	Air temperature at 850 hpa
T10M	10-meter air temperature
U850	Eastward wind at 850 hpa
U50M	Eastward wind at 50 meters
V850	Northward wind at 850 hpa
V50M	Northward wind at 50 meters

APPENDIX 3: MODEL INPUT AND OUTPUT PARAMETERS AND BOUNDARY

CONDITIONS

Table A3-1: Energy, radiative, thermal and geometric input parameters for the bulk urban canopy model.

SYMBOL	DESCRIPTION	UNIT
	ENERGY INPUT PARAMETERS	
$SW^{\downarrow}_{sky}$	Short wave radiation from the sky above urban canopy	W/m^2
$LW^{\downarrow}_{sky}$	Long wave radiation from the sky above urban canopy	W/m^2
Q_{ant}	Anthropogenic heat output inside the urban canopy	W/m^2
LE_{can}	Surface latent heat flux	W/m^2
	RADIATIVE INPUT PARAMETERS	
ε_{roof}	Surface emissivity of the roof	-
ε_{road}	Surface emissivity of the road	-
ε_{wall}	Surface emissivity of the walls	-
α_{roof}	Albedo of the roof	fraction
α_{road}	Albedo of the roads	fraction
α_{wall}	Albedo of the walls	fraction
	THERMAL INPUT PARAMETERS	
$C_{roofs,s}$	Surface volumetric heat capacity for roof	J/(Km^3)
$C_{walls,s}$	Surface volumetric heat capacity for walls	J/(Km^3)
$C_{roads,s}$	Surface volumetric heat capacity for roads	J/(Km^3)
$\lambda_{roofs,s}$	Surface thermal conductivity for the roofs	W/(mK)
$\lambda_{walls,s}$	Surface thermal conductivity for the walls	W/(mK)
$\lambda_{roads,s}$	Surface thermal conductivity for the roads	W/(mK)
$d_{can,k}$	Thickness of the kth urban canopy layer	m
	GEOMETRIC INPUT PARAMETERS	
f_{roof}	roof fraction (ratio of roof plan area to total plan area)	fraction

h_{build}	Height of roughness elements (building height)	M
h_{build}/w_c	Mean height-to-width ratio of street canyons	Fraction

Table A3-2: *Upper and lower boundary conditions for the urban canopy model*

SYMBOL	DESCRIPTION	UNIT
	BOUNDARY CONDITIONS	
$T_{bndry,low}$	Average of the internal temperature of the buildings and the internal temperature below the roads and other surface materials that the city consists of.	K
$T_{bndry,up}$	Atmospheric temperature	K

Table A3-3: *Prognostic variables and radiative output parameters of the urban canopy model*

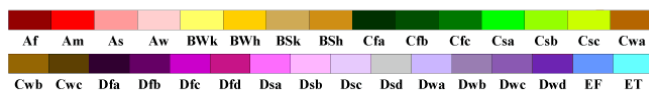| SYMBOL	DESCRIPTION	UNIT
	PROGNOSTIC VARIABLES	
$T_{can,k}$	Temperature for the kth urban canopy layer	K
$T_{can,s}$	Urban canopy surface temperature	K
	RADIATIVE OUTPUT PARAMETERS	
α_{can}	Bulk reflectivity of the urban canopy	fraction
ε_{can}	Bulk emissivity of the urban canopy	fraction
$SW_{can}^{\uparrow}$	Short wave radiation from the urban canopy	W/m²
$LW_{can}^{\uparrow}$	Long wave radiation from the urban canopy	W/m²
Q_H	Sensible heat from the urban canopy	W/m²
Q_L	Latent heat from the urban canopy	W/m²
G_{can}	The conduction flux through the urban canopy substrate	W/m²

APPENDIX 4: KÖPPEN-GEIGER CLIMATE CLASSIFICATION SYSTEM

Table A4-1: The table lists the description of the different climate zones: The first gives an overview on the five main climate groups; the second indicates seasonal precipitation and the third indicates heat levels.

1ST	2ND	3RD
A (Tropical)	f (Rainforest)	
	m (Monsoon)	
	w (Savanna, Wet)	
	s (Savanna, Dry)	
B (Arid)	W (Desert)	
	S (Steppe)	
		h (Hot)
		k (Cold)
		n (With frequent fog)
C (Temperate)	s (Dry summer)	
	w (Dry winter)	
	f (Without dry season)	
		a (Hot summer)
		b (Warm summer)
		c (Cold summer)
D (Cold continental)	s (Dry summer)	
	w (Dry winter)	
	f (Without dry season)	
		a (Hot summer)
		b (Warm summer)
		c (Cold summer)
		d (Very cold winter)
E (Polar)	T (Tundra)	
	F (Eternal winter (ice cap))	

World Map of Köppen−Geiger Climate Classification

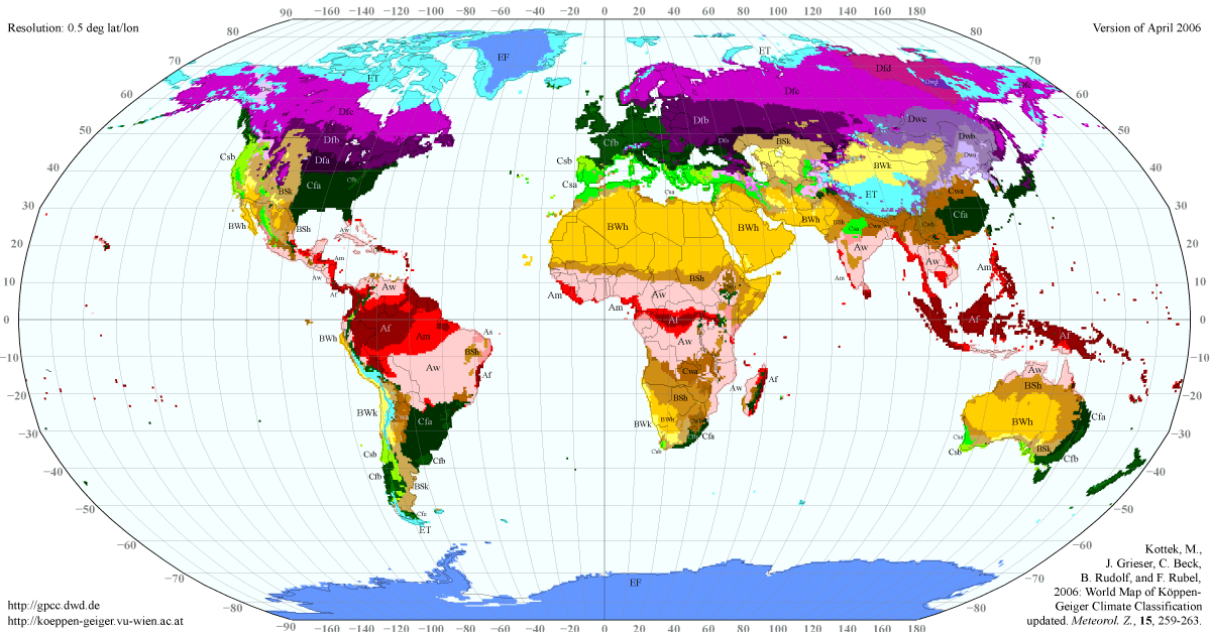updated with CRU TS 2.1 temperature and VASClimO v1.1 precipitation data 1951 to 2000

| Af | Am | As | Aw | BWk | BWh | BSk | BSh | Cfa | Cfb | Cfc | Csa | Csb | Csc | Cwa |

| Cwb | Cwc | Dfa | Dfb | Dfc | Dfd | Dsa | Dsb | Dsc | Dsd | Dwa | Dwb | Dwc | Dwd | EF | ET |

Main climates

A: equatorial
B: arid
C: warm temperate
D: snow
E: polar

Precipitation

W: desert
S: steppe
f: fully humid
s: summer dry
w: winter dry
m: monsoonal

Temperature

h: hot arid   F: polar frost
k: cold arid   T: polar tundra
a: hot summer
b: warm summer
c: cool summer
d: extremely continental

Resolution: 0.5 deg lat/lon

Version of April 2006

http://gpcc.dwd.de
http://koeppen-geiger.vu-wien.ac.at

Kottek, M.,
J. Grieser, C. Beck,
B. Rudolf, and F. Rubel,
2006: World Map of Köppen-
Geiger Climate Classification
updated. *Meteorol. Z.*, **15**, 259-263.

Figure A4-1*: World map of the Köppen-Geiger climate classification system. The system scheme divides the world into five main climate groups: A (tropical), B(arid), C (warm temperate), D (snow) and E (polar). The second and third letters indicate seasonal precipitation type and heat level, respectively.*
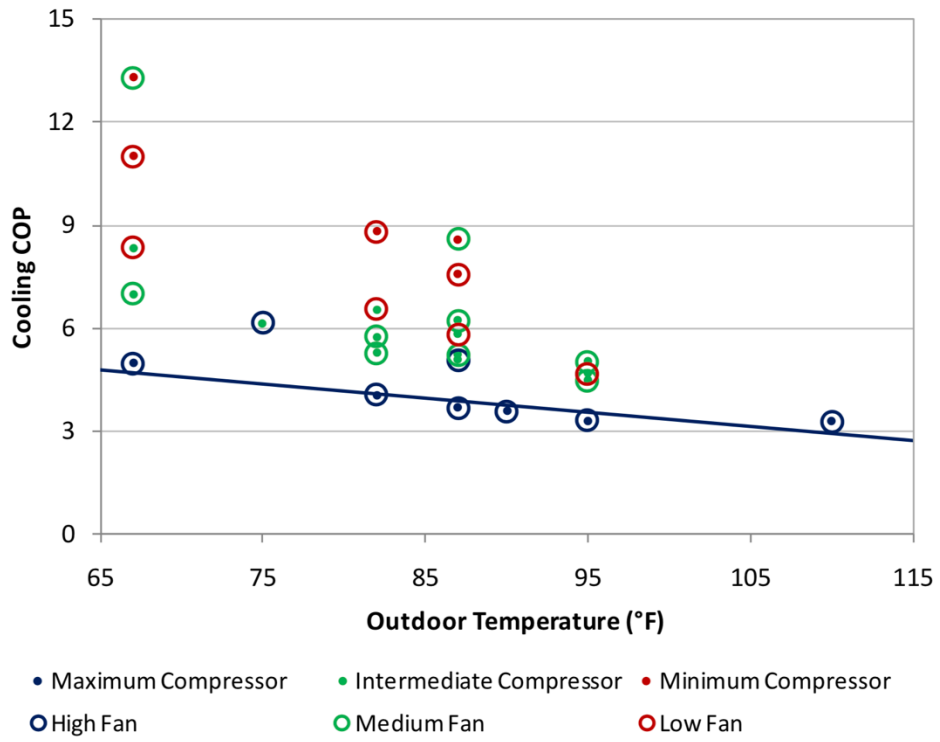
Figure A5-1: *Fujitsu 12RLS steady-state cooling COP (80°F DB, 67°F WB return condition) (Winkler, 2011)*

BIBLIOGRAPHY

1. Anand, Y., Gupta, A., Maini, A., Sharma, A., Khajuria, A., Gupta, S., Sharma, S., Anand, S. & Tyagi, S. K. 2014. Comparative Thermal Analysis of Different Cool Roof Materials for Minimizing Building Energy Consumption. *Journal of Engineering,* 2014**,** 9.
2. Anthopoulos, L. 2017. Smart utopia VS smart reality: Learning by experience from 10 smart city cases. *Cities,* 63**,** 128 - 148.
3. Antunes, A. J., Lee, C. & L., M. C. 2015. Critique and suggested modifications of the degree days methodology to enable long-term electricity consumption assessments: a case study in Birmingham, UK. *Meteorological Applications,* 22**,** 789-796.
4. Autointhebox. 2017. *Automotive Air Conditioning System* [Online]. Available: http://blog.autointhebox.com/what-you-dont-know-about-your-automotive-air-conditioning-system.html [Accessed May 27 2018].
5. Bosilovich, M., Lucchesi, R. 2016. MERRA-2: File Specification. 81.
6. Bromley, M. 2009. *Degree Days: Understanding Heating and Cooling Degree Days* [Online]. Degree Days.net. Available: http://www.degreedays.net/introduction [Accessed April 4 2018].
7. Caldeira, K., Bala, G. & Cao, L. 2013. The Science of Geoengineering. *Annual Review of Earth and Planetary Sciences,* 41**,** 56.
8. Carlowicz, M. 2014. *Measuring Earth's Albedo* [Online]. NASA Earth Observatory: NASA Earth Observatory. Available: https://earthobservatory.nasa.gov/IOTD/view.php?id=84499 [Accessed May 2018].
9. Ceicdata. 2016. *Egypt Electricity Price* [Online]. Available: https://www.ceicdata.com/en/egypt/electricity-price/electricity-price-commercial-0100-kwh [Accessed May 29 2018].
10. Cibse 2006. TM41: Degree-days: theory and application. London: The Chartered Institution of Building Services Engineers (CIBSE).
11. City-University. *Cooling Load Calculation* [Online]. City University, Hong Kong City University, Hong Kong Available: http://personal.cityu.edu.hk/~bsapplec/cooling.htm [Accessed June 3 2018].
12. Comer, R. E., Slingo, A. & Allan, R. P. 2007. Observations of the diurnal cycle of outgoing longwave radiation from the Geostationary Earth Radiation Budget instrument *Geophysical Research Letters* 34.
13. Dispenza, G., Antonucci, V., Sergi, F., Napoli, G. & Andaloro, L. 2017. Development of a multi-purpose infrastructure for sustainable mobility. A case study in a smart cities application. *Energy Procedia,* 143**,** 39-46.
14. Eia. 2018. *Factors Affecting Electricity Prices* [Online]. U.S Energu Information Administration. Available: https://www.eia.gov/energyexplained/index.php?page=electricity_factors_affecting_prices [Accessed May 27 2018].
15. Epa 2008. Reducing Urban Heat Islands: Compendium of Strategies. U.S. Environmental Protection Agency.
16. Fallman, J., Forkel, R. & Emeis, S. 2015. Secondary effects of urban heat island mitigation measures on air quality. *Atmospheric Environment,* 125**,** 12.
17. Gaffin, S., Rosenzweig, C., Parshall, L., Beattie, D., Berghage, R., O'keeffe, G. & Braman, D. 2006. *Energy Balance Modelling Applied to a Comparison of White and Green Roof Cooling Efficiency.* Columbia University.

18. *Gaffin, S. R., Rosenzweig, C., Eichenbaum-Pikser, J., Khanbilvardi, R. & Susca, T. 2009. A Temperature and Seasonal Energy Analysis of Green, White, and Black Roofs.*

19. Gaffin, S. R. E. A. 2012. Bright is the new black—multi-year performance of high-albedo roofs in an urban climate. *Environmental Research Letters,* 7.

20. Geoplaner. 2018. *Geoplaner* [Online]. Available: https://www.geoplaner.com [Accessed March 18 2018].

21. Hao, S., Clark, J., Novak, C. A. & Mantgem, S. V. Cool Roofs for Hot Projects. Continuing Education Center Cool Roof Rating Council.

22. Hartmann, D. L. 2016. *Global Physical Climatology*, Elsevier.

23. Hestnes, A. G. & Eik-Nes, N. L. 2017. *Zero Emission Buildings,* Bergen, Fagbokforlaget.

24. Hosseini, M. & Akbari, H. 2014. Heating energy penalties of cool roofs: the effect of snow accumulation on roofs. *Advances in Building Energy Research,* 8**,** 1-13.

25. Haarstad, H. 2017. Constructing the sustainable city: examining the role of sustainability in the `smart city' discourse. *Journal of Environmental Policy & Planning,* 19**,** 423-437.

26. Iea 2012. World Energy Outlook 2012 International Energy Agency (IEA).

27. Iea 2013. Transition to Sustainable Buildings: Strategies and Opportunities to 2050. Paris, France: International Energy Agency (IEA).

28. Iea 2015. World Energy Outlook 2015. International Energy Agency.

29. Iea 2017. *Energy Efficiency 2017*, International Energy Agency.

30. Ipcc 2007. Climate Change 2007, IPCC Fourth Assessment Report (AR4). Geneva, Switzerland: United Nations Intergovernmental Panel on Climate Change (IPCC).

31. Jacobson, M. Z. & Hoeve, J. E. T. 2012. Effects of Urban Surfaces and White Roofs on Global and Regional Climate. *Journal of Climate,* 25**,** 1028-1044.

32. Kim, K.-G. 2017. *Low-Carbon Smart Cities - Tools for Climate Resilience Planning,* Seoul, Springer Nature.

33. Konopacki, S. & Akbari, H. 2001. *Measured Energy Savings and Demand Reduction from a Reflective Roof Membrane on a Large Retail Store in Austin.* Berkeley, CA.

34. Krayenhoff, E. S. & Voogt, J. A. 2010. Impacts of Urban Albedo Increase on Local Air Temperature at Daily–Annual Time Scales: Model Results and Synthesis of Previous Work. *Journal of Applied Meteorology and Climatology,* 49**,** 1634-1648.

35. Köppen-Geiger. *World map of the Köppen-Geiger climate classification updated* [Online]. Available: http://koeppen-geiger.vu-wien.ac.at/present.htm [Accessed May 15 2018].

36. Lam, J. C., Wan, K. K. W., Tsang, C. L. & Yang, L. 2008. Building energy efficiency in different climates. *Energy Conversion and Management,* 49.

37. Measurequick 2017. An Overview of the Basic Refrigeration Cycle.

38. Mora, L., Bolici, R. & Deakin, M. 2017. The First Two Decades of Smart-City Research: A Bibliometric Analysis. *Journal of Urban Technology,* 24**,** 3-27.

39. Morvaj, B., Lugaric, L. & Krajcar, S. 2011. Demonstrating smart buildings and smart grid features in a smart energy city. *Proceedings of the 2011 3rd International Youth Conference on Energetics (IYCE)*.

40. Oke, T. R. 1982. The energetic basis of the urban heat island. *Quarterly Journal of the Royal Meteorological Society,* 108**,** 24.

41. Oke, T. R. 1987. *Boundary Layer Climates*, Psychology Press.

42. Oke, T. R. 1988. Street design and urban canopy layer climate. *Energy and Buildings,* 11**,** 103-113.

43. Oleson, K. W., Bonan, G. B. & Feddema, J. 2010. Effects of white roofs on urban temperature in a global climate model. *Geophysical Research Letters,* 37.

44. Roaf, S., Crichton, D. & Nicol, F. 2009. *Adapting Buildings and Cities for Climate Change: A 21st Century Survival Guide,* Oxford, Elsevier.
45. Saver, E. 2018. *Room Air Conditioners* [Online]. Available: https://www.energy.gov/energysaver/room-air-conditioners [Accessed May 16 2018].
46. Shepherd, J., Caldeira, K., Cox, P., Haigh, J. & Keith, D. 2009. Geoengineering the climate
47. Science, governance and uncertainty. The Royal Society.
48. Sorteberg, A. 2017. The 1-D Bulk Urban Canopy Model with an Atmospheric Layer Model University of Bergen
49. Statista. 2018. *Global electricity prices by select countries in 2017* [Online]. Available: https://www.statista.com/statistics/263492/electricity-prices-in-selected-countries/ [Accessed May 29 2018].
50. Stewart, I. D. & Oke, T. R. 2012. Local Climate Zones for Urban Temperature Studies. *Bulletin of the American Meteorological Society,* 93**,** 1879-1900.
51. Stewart, L. 2017. Urban Heat Island development. Bay Area Monitor.
52. Sugawara, H. & Takamura, T. 2014. Surface Albedo in Cities: Case Study in Sapporo and Tokyo, Japan. *Boundary-Layer Meteorology,* 153**,** 539--553.
53. Susca, T., Gaffin, S. R. & Dell'osso, G. R. 2011. Positive effects of vegetation: Urban heat island and green roofs. *Environmental Pollution,* 159**,** 8.
54. Taha, H. 1997. Urban climates and heat islands: albedo, evapotranspiration, and anthropogenic heat. *Energy and Buildings,* 25**,** 99-103.
55. Taha, H., Sailor, D. & Akbari, H. 1992. High-Albedo Materials for Reducing Building Cooling Energy Use. Energy and Environment Division, Lawrence Berkeley Laboratory, University of California.
56. Townsend, A. M. 2014. *Smart Cities: big data, civic hackers and the quest for a new utopia,* New York (NY), W. W. Norton & Company.
57. Un-Sdg. 2018. *Climate change affects everyone* [Online]. Available: https://www.un.org/sustainabledevelopment/climatechange/ [Accessed May 27 2018].
58. United Nations: Department of Economic and Social Affairs, P. D. 2014. World Urbanization Prospects: The 2014 Revision, Highlights
59. Voogt, J. A. & Oke, T. R. 2003. Thermal remote sensing of urban climates. *Remote Sensing of Environment,* 86**,** 370-384.
60. Waite, M., Cohen, E., Torbey, H., Piccirilli, M., Tian, Y. & Modi, V. 2017. Global trends in urban electricity demands for cooling and heating. *Energy,* 127**,** 786-802.
61. Wilkinson, S. J. & Dixon, T. 2016. *Green Roof Retrofit : Building Urban Resilience,* Chicester, UNITED KINGDOM, John Wiley & Sons, Incorporated.
62. Winkler, J. 2011. Laboratory Test Report for Fujitsu 12RLS and Mitsubishi FE12NA Mini-Split Heat Pumps. *Energy Efficiency & Renewable Energy; Building Techilogy Program.* U.S Department of Energy.
63. Wmo. 2018. *World Weather Information Service* [Online]. World Meteorological Organization. Available: http://worldweather.wmo.int/en/home.html [Accessed May 20, 2018 2018].
64. Worldbank. 2016. *GDP per capita (current US$)* [Online]. The World Bank. Available: https://data.worldbank.org/indicator/NY.GDP.PCAP.CD [Accessed May 31 2018].
65. Wouters, H., Demuzere, M., Blahak, U., Fortuniak, K., Maiheu, B., Camps, J., Tielemans, D. L. & Lipzig, N. P. M. V. 2016. The efficient urban canopy dependency parametrization (SURY) v1.0 for atmospheric modelling: description and application with the COSMO-CLM model for a Belgian summer. *European Geosciences Union.*
66. Wpr. 2018. *World Population Review* [Online]. World Population Review. Available: http://worldpopulationreview.com/ [Accessed March 22 2018].

67. Yang, J., Tham, K. W., Lee, S. E., Santamouris, M., Sekhar, C. & Cheong, D. K. W. 2017. Anthropogenic heat reduction through retrofitting strategies of campus buildings. *Energy and Buildings,* 152**,** 813-822.
68. Yigitcanlar, T. & Kamruzzaman, M. 2018. Does smart city policy lead to sustainability of cities? *Land Use Policy,* 73**,** 49-58.
69. Ürge-Vorsatz, D., Cabeza, L. F., Serrano, S., Barreneche, C. & Petrichenko, K. 2015. Heating and cooling energy trends and drivers in buildings. *Renewable and Sustainable Energy Reviews,* 41**,** 85-98.
70. Zhao, L., Lee, X., Smith, R. B. & Oleson, K. 2014. Strong contributions of local background climate to urban heat islands. *Nature,* 511**,** 216.